COMBINED DIFFUSE OPTICAL SPECTROSCOPY – MAGNETIC RESONANCE IMAGING OF HUMAN CALF MUSCLES

COMBINED DIFFUSE OPTICAL SPECTROSCOPY – MAGNETIC RESONANCE IMAGING OF HUMAN CALF MUSCLES

BY MARIA C. CHARLES, B.Sc.

A Thesis Submitted to the Department of Biomedical Engineering and the School of Graduate Studies of McMaster University in Partial Fulfilment of the Requirements for the Degree of Master of Applied Science

McMaster University MASTER OF APPLIED SCIENCE (2016) Hamilton, Ontario (Biomedical Engineering)

TITLE: Combined Diffuse Optical Spectroscopy – Magnetic Resonance Imaging of the Lower Leg

AUTHOR: Maria C. Charles, B.Sc. (Universidad de Monterrey, Mexico)

SUPERVISORS: Michael D. Noseworthy, Ph.D., Qiyin Fang, Ph.D.

NUMBER OF PAGES: vii, 137

Abstract

A magnetic resonance imaging (MRI) compatible near infrared spectrometer (NIRS) system was developed and evaluated for continuous-wave diffuse optical spectroscopy (DOS) and concurrent functional MRI measurements of human muscle. Phantom and in-vivo experiments using the system's fiber bundle suggested that an isolation distance greater than 8 mm needs to exist between adjacent illumination-detection channels. Using single and probe-pair arrangements (inter-fiber separations of 80 µm and 5 mm, respectively), in-vivo DOS point-measurements (total=20 images) were performed on 1) the antecubital vein and a reference tissue area and 2) the lower leg at the medial (MG) and lateral gastrocnemius (LG) under isokinetic exercise. Mean spectral morphological differences and relative mean intensity changes at Hemoglobin key wavelengths were found, namely reduced mean pixel intensity (~30%) for the vessel-area and a signal change of ~1-4% between the rest and the recovery condition at both muscle locations for the single-probe configuration. Subsequent work is necessary to evaluate the oxygenation assessment capabilities of this system. Lastly, experiments were performed in which two volunteers had concurrent measurement of optical and blood oxygen level dependent (BOLD) MRI, before and following exercise. The same probe arrangement was used for DOS measurements for this experiment. The BOLD signal was studied for manually-derived ROIs. BOLD recovery curves corresponding to the LG followed routine temporal progression where immediate post-exercise signal is hypointense, followed with a sigmoidal-

shaped recovery. A decrease ranging between ~0.1-20% was found in the normalized mean spectral signal (20 images) for recovery with reference to the rest condition at both muscle locations for single-probe measurements and for one probe-pair measurement (for 800,808 and 850 nm). The specific trend of the measured decrease in the mean spectral curves during recovery was not consistent among these trials. Future steps include repeatable phantom experiments, increased optical power delivery, enhanced skin contact and improved reflectance measurements.

Acknowledgements

I want to express my sincere gratitude to my supervisors, Dr. Michael Noseworthy and Dr. Qiyin Fang, for all their support along this project. Their patience, motivation and feedback was a key factor and motor for the completion of this thesis. I would also like to acknowledge Dr. Tom Farrell for the helpful discussions to introduce me to this topic. Thanks to CONACYT (Consejo Nacional de Ciencia y Tecnologia) for funding my studies. Special thanks to my labmates from the Medical Imaging Engineering and Physics Lab and the Biophotonics Lab at McMaster University. I couldn't have gotten through this without your help and encouragement. Thank you also to the many others at St. Joseph's healthcare, Hamilton, who provided me invaluable assistance during my experiments there.

Thank you to all my friends who have supported me in all ways possible during my first experiences in research. Dr. Veronika Doblhoff and Dr. Stefan Löffler, thank you for lending me a hand through this time. To my latin friends, Pedro, Melizeth, Alejandro, Oscar, Carla and all of you that made me smile all along my studies. Jacinta, Chrystal, Lety, thanks for helping me with your time, help and advice. Olga, Saurabh, Ali, Conrad, Ramy, Ian, Eric and Claudia, you were my first friends in Canada, thanks for so much! Very importantly to my friends in Monterrey: Roberto, Alberto, Brenda, Vicky, Salma, Marisa, Luisa, Faby, Fany, Jasive, Marilda, Ana Lu and Nora, for always encouraging me to be confident. And finally, many special thanks to my family, for their warm support all along this journey, I love you.

Table of Contents

List of Figures

List of Tables

Chapter 1. Introduction

Research Objective

The present thesis describes a set of exploratory experiments towards the study of combined optical and magnetic resonance imaging (MRI) signals in human muscle tissue. Specifically, the purpose of this research project was to assess the feasibility of a proposed instrumentation setup to carry out dermal diffuse optical spectroscopy (DOS) and muscle-level functional MRI (fMRI) simultaneously. This would allow further understanding of oxygenation changes in leg muscles to better understand the MRI blood oxygenation level dependent signal, which is only known to be a combination of blood flow, blood volume and metabolic changes [1].

Blood oxygenation level-dependent (BOLD) fMRI and DOS are imaging techniques that are currently applied to study hemodynamic processes of human tissues. BOLD fMRI is a method employed to evaluate functional activation based on the measurement of a change in the MRI signal that results from fluctuations of oxyhaemoglobin (HbO_2) relative to deoxyhaemoglobin (HbR) induced by metabolic changes [1]. BOLD fMRI has been extensively used in neurosciences and more recently for other areas such as skeletal muscle hemodynamics [2]. Similarly, DOS is a non-invasive technique that employs low-energy non-ionizing electromagnetic radiation, mainly in the visible or near-infrared (NIR) region of the spectrum, in order to characterize thick tissue by obtaining quantitative measurements of its main constituent components such as HbO_2, HbR, water and lipid [3],[4],[5]. DOS

has also been broadened to different fields such as breast, joints, brain [6] and skeletal muscle imaging [7],[8],[9],[10]. The combination of DOS and fMRI has been proposed with the intention of taking the most of each method, i.e., combining the higher relative spatial resolution of fMRI with the better temporal resolution of DOS [11].

The underlying motivation for this project is based on the importance of non-invasive techniques that rely on haemoglobin (Hb) as an endogenous agent for the assessment of tissue oxygenation. Moreover, optical and MRI have been used both individually and concurrently for tissue oxygenation assessment and as part of the study of human function and diseases such as peripheral vascular disease in the lower extremities [12],[13],[14]. Additionally, an MRI compatible near infrared spectroscopy (NIRS) system was available for this project and found to be advantageous due to its large number of sensors, automation capability and spectral resolution in the NIR.

Hypothesis

Based on the aforementioned applications of the two imaging techniques of interest, optical and MRI signals were collected and analysed in order to test the hypothesis that, using a proposed NIRS setup:

- oxygenation changes in the lower extremities can be assessed using DOS alone and concurrently with BOLD fMRI upon isokinetic exercise;
- dermal DOS and muscle-level fMRI time series are correlated.

Approach and results

The approach taken during this project relied on the use of optical point-measurements over the skin along with deep-muscle fMRI signals acquired at the same time. Specifically, the main research objectives and the summarized results of this project are the following:

- *System development and testing for spectral measurements*: the NIRS system was prepared to perform spectral measurements using the system's fiber bundle for simultaneous illumination and detection. The experimental results suggest that an isolation distance greater than 8 mm needs to exist between adjacent illumination-detection channels.
- *System evaluation for in-vivo DOS point-measurements over 1) the antecubital vein and a reference tissue area and 2) the lower leg at the medial (MG) and lateral (LG) gastrocnemius under isokinetic exercise*: mean spectral differences (normalized at 700 nm) at Hb-key wavelengths were found across measurement sites and experimental conditions for both single-probe trials and for the probe-pair measurements in the arm. Subsequent validations and optimizations are necessary to evaluate the oxygenation assessment capabilities of this system.
- *Concurrent optical and BOLD-fMRI measurements over the MG and LG during a foot dorsiflexion protocol*: rest and recovery spectra exhibit mean spectral differences (normalized at 700 nm) at Hb-key wavelengths across

measurement sites and experimental conditions for both single-probe trials and for one probe-pair measurement (subject #2). Optical and BOLD fMRI signals are hypointense along recovery for single-probe and one probe-pair trials.

This thesis is organized as follows: in chapter 2, a brief review on the application of DOS and BOLD fMRI for oxygenation assessment is presented. Subsequently, chapter 3 describes the instrumentation components and calibration procedures, along with the evaluation of the system's fiber bundle for multi-probe spectral measurements. Chapters 4 and 5 present the experimental results and discussion. Specifically, chapter 4 describes the in-vivo measurements using the DOS system alone whereas chapter 5 shows the combined optical-MRI approach. Finally, chapter 6 contains the conclusion as well as a discussion of the experimental limitations and an outlook on future improvements.

Chapter 2. DOS and BOLD fMRI for oxygenation measurements

DOS for oxygenation assessment

In DOS, light is delivered to different locations in the area of interest, and transmitted or back-reflected light is then measured at a specific distance along the probed surface [15],[16]. Particularly, NIRS employs excitation light in the range of 700-1000 nm in order to study changes in the spectra of diffusely-reflected light [42]. Due to the relatively low absorption of the main chromophores in tissue over the NIR range, infrared light can probe the tissue of interest within several centimeters with adequate signal-to-noise ratio (SNR) for detection [43]. Additionally, given that HbR and HbO_2 have different absorption spectra around the isosbestic point for Hb (808 nm), it is possible to distinguish the absorption characteristics of both molecules [3] (see Figure 1).

Light traveling through the tissue undergoes both absorption and scattering, which are multifactorial processes that need to be modeled as part of NIR spectroscopy quantification. Tissue optical properties, namely absorption and reduced scattering coefficients ($\mu_a(\lambda)$ and $\mu_s'(\lambda)$, respectively), depend on multiple factors such as wavelength of the excitation light and tissue composition. Therefore, a model of light transport needs to be used to derive tissue optical properties and penetration depth [17]. Regarding the oxygenation assessment with Continuous wave (CW) technology, which is described in the next paragraph, the Modified Beer-Lambert

law has been applied to account for the amount of scattering by calculating the differential path length factor from experimental data. That way, using measurements at two or more wavelengths around the isosbestic spectral point for Hb of 808 nm allows one to obtain concentration changes of Hb. This approach is applied in chapter 4 and 5 of this document. Nevertheless, there are some limitations that affect the reliability of the method such as subcutaneous fat thickness effects [13],[18],[19]. Another way to compute concentration changes with CW-DOS is the multi-distance approach, which employs a formula for the light propagation that accounts for both absorption and scattering, to calculate $\mu_a(\lambda)$ and $\mu_s'(\lambda)$ from light attenuation measurements as a function of source-detector separation distance. With this scheme, the sensors simultaneously measure light attenuation at multiple separation distances from the source, which is useful to overcome crosstalk from subcutaneous layers. InSeok, et al. proposed a method that accounts for scattering and melanin absorption under some assumptions by employing the diffuse reflectance spectra at isosbestic points and a model for quantification of HbR and HbO_2 to obtain the apparent concentrations of these parameters [20]. It is important to consider that absolute calculations of oxygenation parameters require additional techniques that can be found, e.g., in [17].

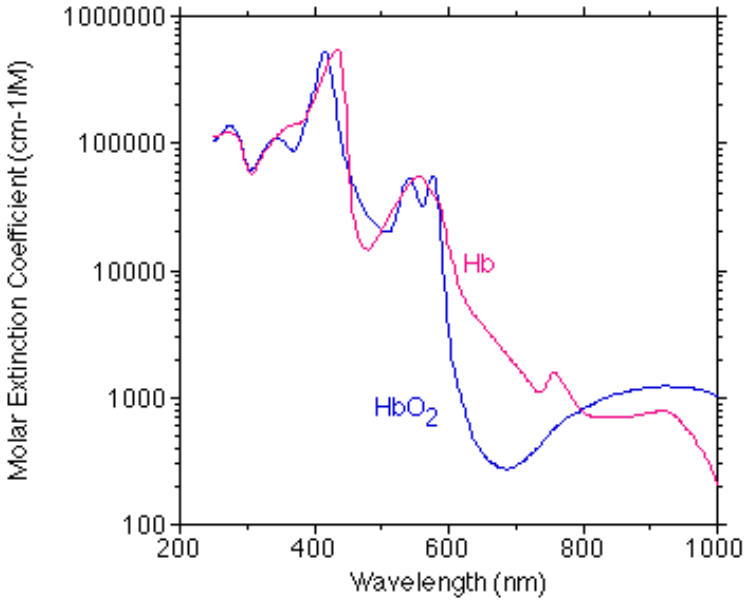

Figure 1. HbR and HbO_2 spectra taken from [21].

In general, three different NIRS imaging schemes exist: continuous-wave (CW), frequency-domain (FD) and time-domain (TD) systems. This project is based on the CW regime, where only the transmitted intensity measurements are considered. In most CW applications, fiber-coupled illumination and detection are chosen, along with white light sources or sets of narrow-band sources and different photodetectors such as photo-multiplying tubes (PMT), avalanche photo-diodes (APD) and cooled charge-coupled devices (CCD) [17].

A brief description of technical considerations to perform CW-DOS is presented in the next lines. Optical power delivered to the skin must be kept to the allowable optical safety levels and durations to avoid thermal injury. For fiber-coupled

experiments, an optical power of 0.3-3 mW was used [22] together with fiber core diameters of 1 mm and source-detector separation distances of around 2-3 cm[1] [23]. Two to four different wavelengths are usually analyzed to study one to three chromophores. A description of NIRS systems is presented in [22], where wavelengths of 690-700, 775-780, 830, and 850 nm are given as common choices in experimental NIRS systems, along with time resolutions of the order of 0.01 s.

CW-NIRS has been applied for the study of concentration changes of oxygenation chromophores in skeletal muscles during exercise. Shadgan, et al. found a comparable trend of decreasing delta HbO_2 and increasing delta HbR during isometric contraction, and a reverse tendency after exercise [25]. The same general results have been shown by Kek et al. in their study of NIRS signals on the quadriceps muscles during isometric knee extension with the novelty of detecting differences corresponding to specific muscles [26]. Koga et al. also distinguished signal variations in human quadriceps during cycling exercise [27]. Zhang et al. compared changes in the oxygenation parameters from biceps and vastus lateralis during rowing and concluded that there was a relatively higher oxidative capacity in leg muscles [28].

BOLD fMRI for oxygenation assessment

FMRI studies are based on the BOLD signal, which uses the T2* parameter as a contrast mechanism that is sensitive to small changes in blood volume and

[1] Penetration depth is usually estimated as 1/3 to 1/2 of the source-detector separation [22].

oxygenation [2]. Gradient echo MRI sequences are sensitive to the magnetic susceptibility caused by paramagnetic species if the spins are not refocused by a 180° pulse like with spin echo imaging. Therefore, changes in HbR can be represented by changes in T2* and, therefore, information about functional changes in the tissue oxygenation status can be obtained [1]. BOLD fMRI provides a temporal resolution that can be as fast as 1 slice per 70 ms, or 2 seconds for 30 slices, with a spatial resolution of the order of millimetres [29],[30].

Functional MRI studies are generally based on a “block design” experimental approach, in which a control condition block and one or more task blocks are defined and executed alternatingly with typical durations of 10-30 seconds. After motion correction and time normalization, statistical methods are applied in order to find spatially dependent activation patterns. Most frequently generalized linear models (GLMs), or model-based approaches are employed in the analysis [31]. However, model-free approaches using multivariate statistics (principle component analysis, PCA, and independent component analysis, ICA) and fractals have also been used [32].

Model-based methods can either use full correlation or simply be based on a two sample T-test for activation detection. To apply model-based approaches, a hemodynamic response function needs to be designed considering the duration and periodicity of the experiment in order to perform a general linear model statistical analysis [31]. Here the model used was a sigmoidal one [32].

Additionally, an analysis of the T2* time series is important in order to identify abnormal responses during the applied stimuli stages.

BOLD fMRI has been studied in human skeletal muscles following muscle contraction in healthy and diseased volunteers [1],[2],[33],[34],[35],[36]. In general, BOLD signal intensity changes have been found following muscle single contraction [37],[38]. Furthermore, BOLD fMRI signal changes measured in the exercising muscle have been correlated with other techniques such as venous occlusion pletismography, cardiac-gated CINE-magnetic resonance angiography, Doppler ultrasound and with optical techniques such as NIRS, showing that the BOLD signal changes depend closely on hemodynamic processes [37],[39],[40],[41].

Oxygenation assessment using Optical-MRI techniques

A correlation between superficial NIRS and fMRI muscle measurements has been proposed to further study the BOLD effect. Towse, et al. used NIRS information (in particular the muscle blood volume and the Hb saturation) to numerically predict the BOLD signal intensity, which correlated well with the actually measured BOLD signal intensity [37]. Damon et al. analyzed the influence of echo time (TE) in the post-contractile BOLD signal intensity changes by performing parallel NIRS measurements, which helped to further characterize the specificity of the BOLD signal based on this parameter (i.e. an emphasis towards blood volume was seen

using a shorter TE whereas a longer TE was found to be more descriptive for oxygenation changes [38].

In the optical imaging framework, diffuse optical tomography (DOT) has been developed as a tomographic modality that uses NIR light to provide spatial distribution of the tissue optical properties, from which oxygenation parameters can be calculated [42]. Nonetheless, this technique presents limited depth-resolution for large geometries with increasingly worse resolution in the center of the object being assessed [12].

On the other hand, MRI is useful to provide spatial prior information in order to increase the accuracy of the image reconstruction given that the DOT inverse problem is non-linear and ill-posed [43]. Therefore, combining these two methods has been proposed as DOT provides information to differentiate blood flow and oxygen consumption changes, which are not easy to understand employing BOLD fMRI without flow measurements [42]. Other researchers have incorporated the DOT-fMRI information into a single model in order to solve for the final hemodynamic values [44],[45]. To overcome their individual limitations these technologies have been integrated to acquire non-invasive brain Hb estimates for event-related [44] or resting-state [40] brain functional mapping.

Recent work has been done towards combining functional NIRS and tomography with MRI techniques. Groups at Dartmouth College have published several contributions in this field, such as MRI-guided optical spectroscopy algorithms [46]

and systems for breast cancer detection [47],[48], monitoring of breast hemodynamics [49], and assessment of peripheral vascular disease (PVD) [50]. Additionally, research groups at University College London (UCL) have contributed to the development of reconstruction software and NIR tomography systems for the functional evaluation of the infant brain and for breast applications [51].

Chapter 3. Setup, calibration and evaluation of the DOS system

Instrumentation

The Visible/NIR Spectroscopy System was composed of a grating-CCD based spectrometer (P&P Optica Inc., Waterloo Ontario, https://ppo.ca), a 144 optode bifurcated fiber bundle (Fibertech Optica, Kitchener Ontario, https://fibertech-optica.com) attached to it and a quartz halogen lamp as illumination source (Imagelite Stocker & Yale, Inc., model 20, 150W).

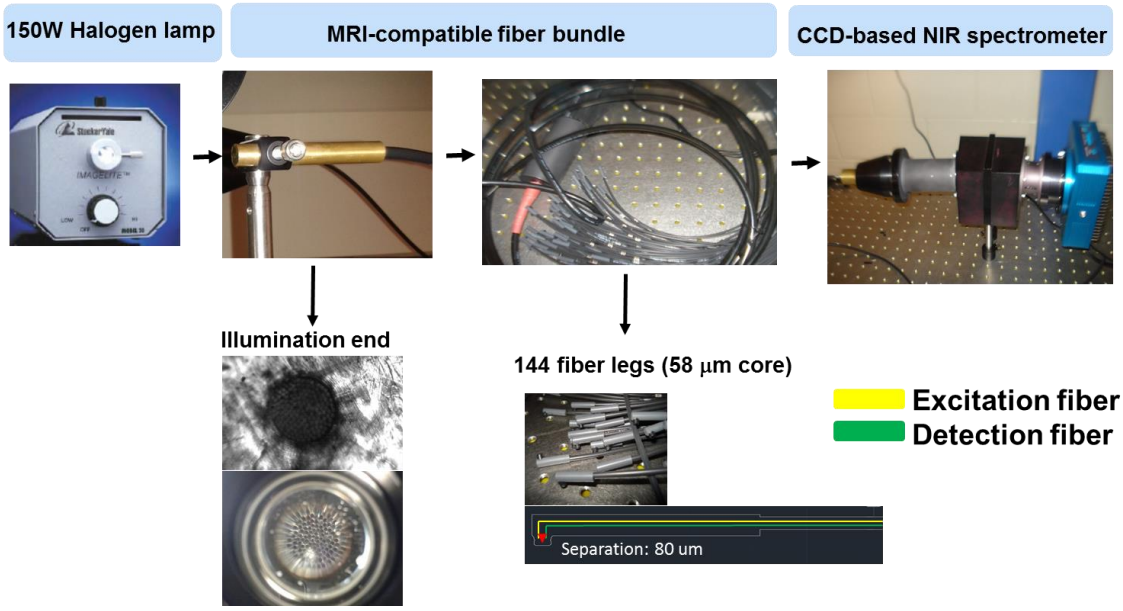

Figure 2. VIS/NIR DOS system components (P&P Optica Inc., Fibertech Optica). Light from a 150W halogen lamp (Imagelite Stocker & Yale, Inc.,) is directly coupled to the illumination end of the MRI-compatible fiber bundle. A pinhole is used to allow a narrower beam into the illumination end of the 144 fiber probes. The detector end of the fiber probes collects and transmits light into the spectrometer and the CCD (Apogee Alta F1109, Andor, Oxford Instruments, United Kingdom) for detection.

An Apogee Alta F1109 CCD camera (Andor, Oxford Instruments, United Kingdom) is connected to a PC (32 or 64-bit windows OS) via a USB interface and can be controlled through IRIS spectroscopy software (P&P Optica Inc.) or using the camera's SDK (see Figure 2 and Figure 3).

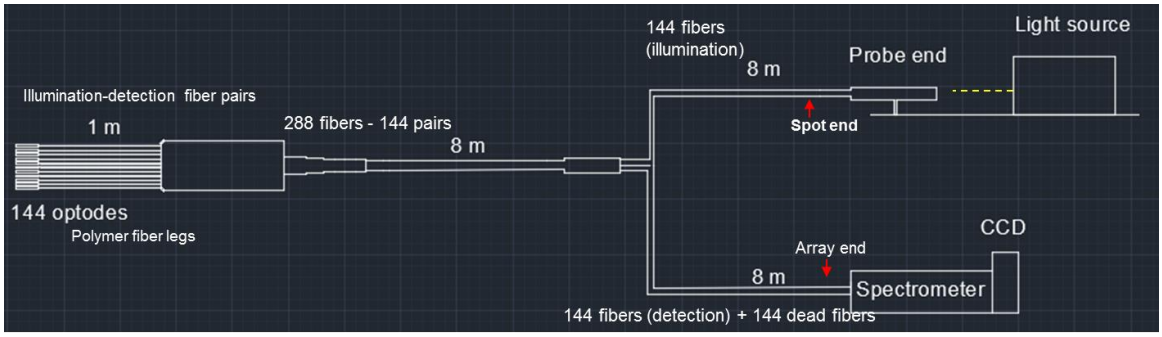

Figure 3. Schematic of the DOS system (P&P Optica Inc., Fibertech Optica) setup used for this project. The bifurcated fiber bundle consists of 144 non-metallic fiber probes, each of which contain 1 fiber from the array end and one from the illumination end. Light of a halogen lamp is coupled to the illumination end of the fiber bundle. The array end of the fiber bundle is attached to the spectrometer for light dispersion. Spectral lines are measured with a CCD detector.

Grating-CCD based spectrometer

As shown in Figure 4, the spectrometer consists of 1) the input slit (Thorlabs variable slit) which allows a thin beam of light into the spectrometer, 2) the collimating block which parallelizes the rays, 3) the grating wedge, which has an angle of 5.65° and disperses the light by wavelength content, 4) the focusing block that focuses the light onto the camera's detector, 5) the camera wedge (0.5°) that specifically opposes the grating wedge angle for optimal focus and 6) the camera mount to attach an Apogee Alta F1109 CCD camera to the system [1].

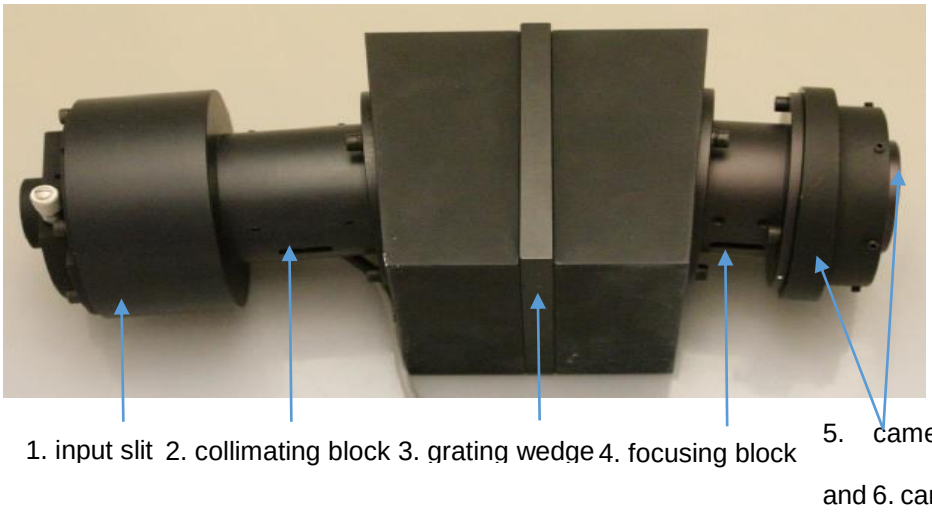

Figure 4. Spectrometer components (P&P Optica Inc., Fibertech Optica). Light entering the variable slit of the spectrometer is collimated by the lenses on the collimating block, which is then dispersed by the grating and finally focused onto the CCD sensor (Andor, Oxford Instruments, United Kingdom). [1]

A CCD camera is attached to this system. The CCD contains a Hamamatsu (Hamamatsu, Japan, http://www.hamamatsu.com/us/en/hamamatsu/index.html) S10140-1109 sensor with a 2048 x 508 array of 12 μm pixels (24.6 x 6.1 mm) and a 16-bit dynamic range [1]. The long axis of the CCD sensor is positioned such that 2048 pixels are along the fiber optic channel axis and 508 pixels are over the wavelength axis, which receives the light from different optical fibers and is described in the following section.

Fiber optic bundle

The bifurcated fiber optic bundle used in this system contains 144 non-metallic fiber probes, which will be referred to as “optodes” or “fiber probes” in the rest of this thesis (see Figure 2). Every optode contains one optical fiber from the

illumination end to transmit light and a second fiber from the array end to receive light to be transmitted to the spectrometer. The transmitting and receiving fibers are separated by 80 µm (dead-fiber spacers) and bent at 90 degrees from the optode tip. On the illumination end of the fiber bundle, the 144 transmitting optical fibers are arranged in a circle with an active area diameter of 1.06 mm to illuminate the optodes. On the detection end, the 144 receiving optical fibers are arranged in a linear array that is adapted to the spectrometer input to detect the light from the optodes. The array end is 23 mm high and 0.080 mm wide and provides the input for the pixels of the CCD sensor (spread along the channel axis). The optodes are numbered according to the position of their detector fiber over the long axis of the CCD sensor. The 244 optical fibers are 58 µm core, 0.22 NA (numerical aperture) low hydroxyl content (OH) fibers, with a 70 um cladding, 80 µm polyimide coating and a transmission range of 350 to 2400 nm.

Light source

The Imagelite broadband lamp (Oakville ON, Canada, http://www.imageliteinternational.com/home_e.html) is a fiber optic illuminator with a 150W quartz halogen EKE lamp with a manual 0-100% intensity control and a 7.6mm aperture. The lamp spectrum was measured with OSM400 Newport Spectrometer and is shown in Figure 5.

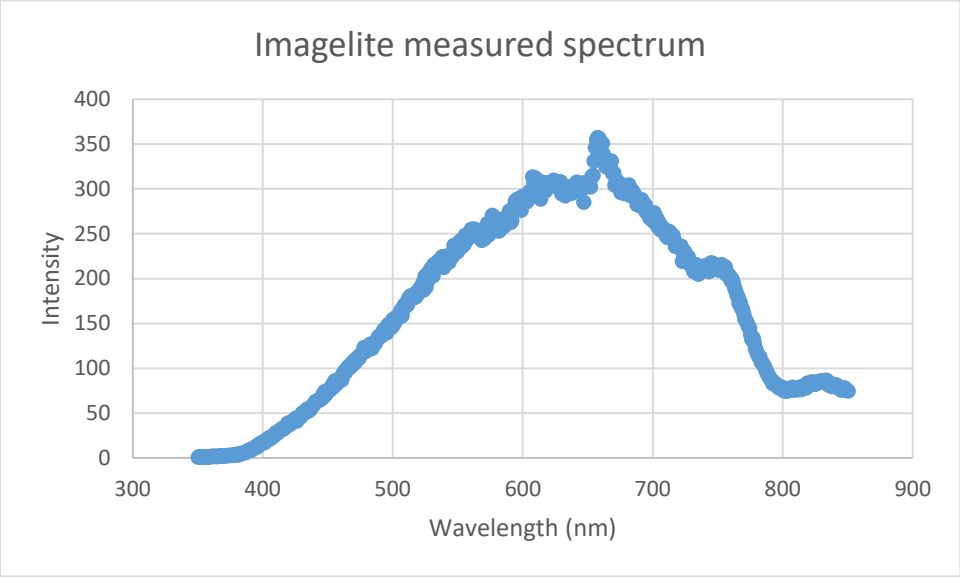

Figure 5. Imagelite Tungsten-Halogen lamp's spectrum measured with an OSM400 Newport spectrometer.

More details regarding the system's specifications can be found in the system manuals and in the P&P Optica website (https://ppo.ca) [2].

System adjustments and calibrations

To perform system adjustments, a fiber probe was continuously illuminated using a broadband lamp. The focusing and collimating blocks were alternatively and iteratively adjusted in order to obtain sharp thin straight lines across the CCD sensor. Automated image acquisition (live mode) was set during this process to monitor calibration effects over the continuously detected spectral line. The position of the CCD was also aligned during the process

Spectral calibration was done by shining light from an argon lamp into the fiber probes and comparing the detected spectrum with the National Institute of Standards and Technology (NIST) standard argon spectrum to find the pixel to wavelength relationship across the short axis (horizontal) of the CCD sensor. In summary, first each detected peak was fit with a Gaussian waveform to determine the full width half maximum (FWHM) of all the peaks. The system was found to have a spectral resolution of 2.61 nm (mean FWHM of the peaks) and a spectral range of 669-923 nm. Secondly, the pixel position of the detected peaks was correlated to the argon standard spectrum by fitting with a cubic polynomial regression. The pixel-to-wavelength relationship was found to be $y=668.93+0.504x -6.52x10^{-6}x^2 + 1.94x10^{-9}x^3$.

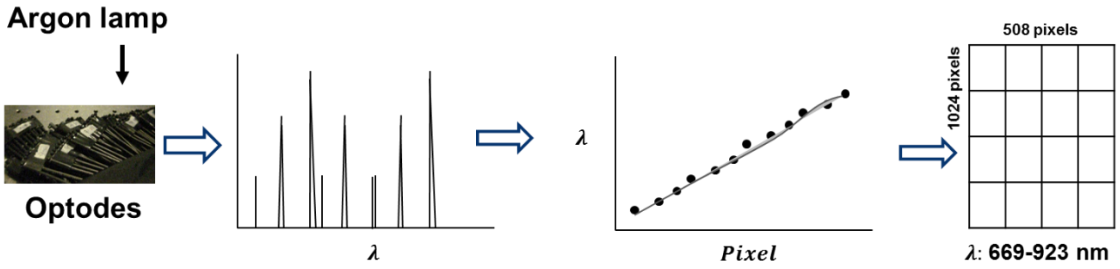

Figure 6. Process to perform spectral calibration of the VIS/NIR DOS system (P&P Optica Inc., Fibertech Optica). An argon calibration lamp was used to map the known argon peaks to the corresponding pixels along the short axis of the CCD sensor (Andor, Oxford Instruments, United Kingdom). A cubic regression was used to obtain the wavelength to pixel relationship for this system.

Channel calibration was done by illuminating each fiber probe with a halogen lamp to determine their pixel range across the long axis of the CCD sensor (vertical

direction). Region-of-interest (ROI) determination was done manually using customized IRIS system software (P&P Optica Inc.). A database of the pixel ranges corresponding to every detector number can be found in the Appendix 1 and was used on the rest of the experiments described below.

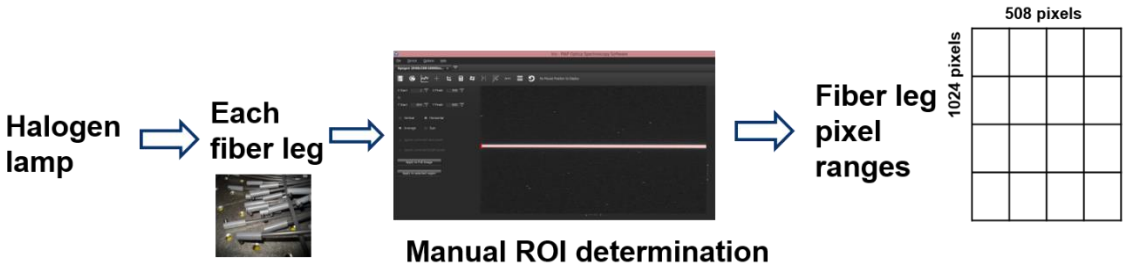

Figure 7. Process to perform channel calibration of the DOS system (P&P Optica Inc., Fibertech Optica). Each optode was secured parallel to the halogen lamp's aperture for illumination. The detected spectral line was visualized using the IRIS system software (P&P Optica Inc.) for manual region-of-interest (ROI) determination. A database with the pixel ranges along the long axis of the CCD sensor was determined for this system.

Fiber bundle evaluation

The calibrated system was tested for DOS measurements in tissue simulating phantoms and in human tissue in order to evaluate the suitability of the fiber bundle for both excitation and detection purposes and to assess the detectable signal intensity for different physical arrangements and imaging parameters. The results were analyzed over the system's spectral range and can be used as a reference point for further multi-channel measurements.

Experiment #1. Mean pixel intensity measurements in a tissue-simulating phantom

Objective: A phantom experiment was performed to characterize the scattered light intensity detected by a single fiber probe. The signal was studied as a function of emitter-detector separation and exposure time. An external optical fiber with a large core diameter was used for excitation to obtain an overview of the signal variation as a function of acquisition time and inter-fiber separation. Of particular interest were channel separation distances leading to relatively low signal intensity values as they indicate channel isolation distances.

Methods: A 200 µm core optical fiber (0.22NA) was used to illuminate a tissue-simulating phantom (Agar: 2%, Intralipid: 1.20%, India ink: 0.4%) with an optical power of ~3 mW. A single optode (optode #32) was positioned at different distances from the excitation fiber to collect the scattering signal for further evaluation. The excitation and detection probes were positioned in diffuse reflectance geometry over the phantom's surface, as seen in Figure 8. A translation stage was used to hold the fiber probes in the desired location. Given that the system's fiber tips are bent at 90º and the phantom's surface was at a level around ¾ of the Petri Dish surface, the assembly used to hold the fiber probe was positioned at an inclination in order to assure contact with the phantom's surface. Because of the way the fibers were arranged in this setup, moving the fiber probe using the translation stage affected the fiber contact angle. Therefore, the separation distance was verified using a ruler (mm precision).

Figure 8. Experimental setup for the phantom experiment. A 200µm core optical fiber was used to illuminate a tissue simulating phantom. A fiber probe from the DOS system's fiber bundle (P&P Optica Inc., Fibertech Optica) was used to measure the diffusely reflected light. The fiber tip of each optical fiber was held perpendicular to the phantom's surface and maintained a gentle touch over the surface. A translation stage was used to move the fiber probe relative to the excitation optical fiber.

Data acquisition was done in dark room conditions and at a CCD temperature of -32°C as indicated in the IRIS software.

Table 1. Integration times (ms) and optode geometrical arrangements (mm) combined for the phantom experiment (mm). A detector probe from the DOS system was positioned at different separations from the excitation fiber (4, 5, 6, 7, 8. 10 and 12 mm). Integration times of 10, 30, 50, 100, 200, 500 and 60,000 ms were used for measurements at every inter-fiber separation.

Integration times (ms)						
10	30	50	100	200	500	60,000
Source-detector separation (mm)						
4	5	6	7	8	10	12

Selected integration times and inter-fiber separations[2] were used in this experiment according to Table 1.

Results: Data were analyzed in Matlab in order to determine the mean pixel intensity (at 700 nm) as a function of integration time, channel separation and, lastly, to plot a 2-D graphical representation of the mean intensity as a function of both parameters.

According to Figure 9, for a given channel separation, the pixel mean intensity increases significantly with exposure times greater or equal to 200 ms. For large separations, a mean intensity of ~3250 is consistently measured, which suggests that that value approximates the dark noise level of the camera.

Similarly, as can be observed in Figure 10, mean pixel intensities detected at different exposure times increase rapidly within channel separations smaller than 6 mm. These results suggest that the greatest sensitivity is achieved for exposure times >200 ms and channel separations <=5 mm.

[2] Particularly, 4 mm was the minimum source-detector separation that was physically achievable

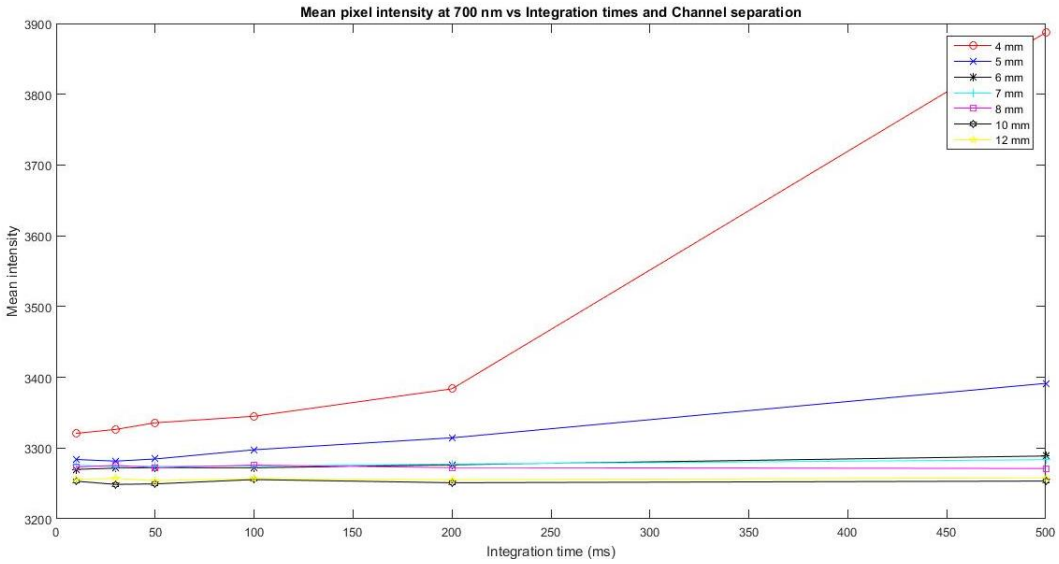

Figure 9. Mean pixel intensity (at 700 nm) measured as a function of integration time (ms) for distinct inter-fiber separations (mm) using the DOS system (P&P Optica Inc., Fibertech Optica). A tissue simulating phantom was illuminated by a 200µm optical fiber. A fiber probe from the DOS system's fiber bundle was positioned at different separations from the excitation fiber (4, 5, 6, 7, 8. 10 and 12 mm) and was used to measure the diffusely reflected light on the phantom's surface. Integration times of 10, 30, 50, 100, 200, 500 and 60,000 ms were used.

Lastly, Figure 11 provides a 2-D representation of the distribution of mean intensity values for the different channel separations and exposure times. This figure shows that, in general, longer exposure times and smaller channel separations show higher intensity values and greater sensitivity. Nevertheless, the choice of the channel separation and the integration time for the abovementioned experimental conditions would depend on the particular experiment (tissue to investigate and desired penetration depth).

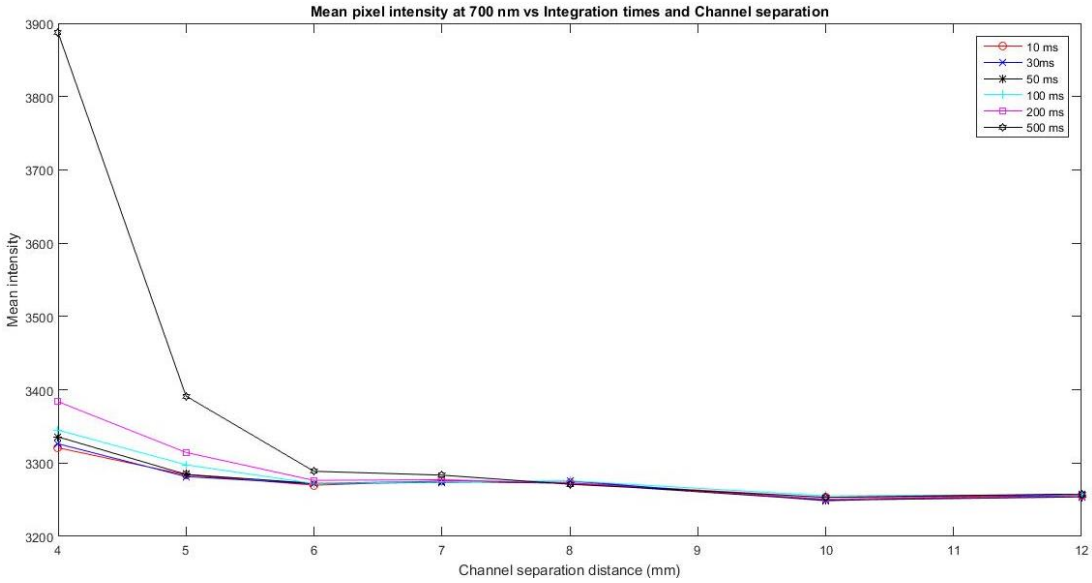

Figure 10. Mean pixel intensity (at 700 nm) measured as a function of inter-fiber separation (mm) for different exposure times (ms) using the DOS system (P&P Optica Inc., Fibertech Optica). Results are shown as a function of inter-fiber separation (mm). For this experiment, a tissue simulating phantom was illuminated by a 200µm optical fiber. A fiber probe from the DOS system's fiber bundle was positioned at different separations from the excitation fiber (4, 5, 6, 7, 8. 10 and 12 mm) and was used to measure the diffusely reflected light on the phantom's surface. Integration times of 10, 30, 50, 100, 200, 500 and 60,000 ms were used.

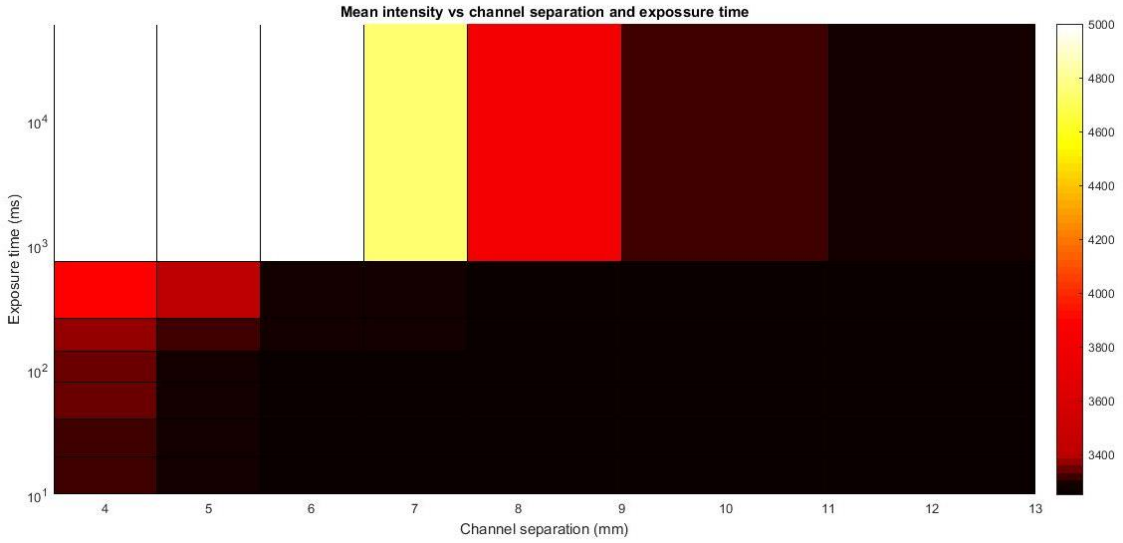

Figure 11. Figure. 2-D representation of the mean pixel intensity measured as a function of integration time (ms) and inter-fiber separation (mm) using a fiber probe of the DOS system (P&P Optica Inc., Fibertech Optica). Figure. 2-D representation of the mean pixel intensity measured as a function of integration time (ms) and inter-fiber separation (mm) using a fiber probe of the DOS system (P&P Optica Inc., Fibertech Optica). For this experiment, an external optical fiber (200 µm) was used to illuminate a tissue simulating phantom using a combination of Inter-fiber separations (4, 5, 6, 7, 8. 10 and 12 mm) and exposure times (10, 30, 50, 100, 200, 500 and 60,000 ms). A semi-logarithmic scale is used to plot the data shown in this figure.

Discussion: The aforementioned phantom experiment was performed as a means to explore the detector probe physical arrangement required to further test the system for multi-point spectral measurements using the system's customized fiber bundle for simultaneous illumination and detection. Using an excitation fiber with a higher core diameter, a safe choice for the isolation distance could be determined which was subsequently used as a reference parameter to design a probe holder

for in-vivo measurements. Based on the results at 700 nm, upon an excitation probe positioned in plane (reflectance mode) with the detector probe, an isolation distance of around 8 mm was found to assure a mean pixel intensity signal as low as the background level for integration times below 1 minute. Therefore, a detector probe corresponding to a different channel would need to be positioned at a farther distance to assure isolation. Improvements for this experiment include a) dark image acquisition for every data set during the experimental session for subsequent background subtraction and b) averaging over more acquisitions under the same conditions.

Experiment #2. In-vivo measurements using the system's fiber bundle

Objective: Evaluate the system's fiber bundle for simultaneous illumination and detection in the human arm of two subjects by 1) testing the applicability of the obtained isolation distance and 2) exploring the mean signal intensity contrast using the smallest physically possible inter-probe distance.

Methods: A probe holder concept Figure 13 evolved to the development of two probe holders. The probe holder configurations consist of two excitation probes, located at the third and sixth position of the linear array, and one detection probe next to the excitation fiber defining an illumination-detection channel. Additionally, two distant detector probes were positioned at the ends of the array (i.e., the isolation distance) (see Figure 12).

Figure 12. Schematic of the optode arrangement for both fiber holders, consisting on two excitation probes (yellow) and 4 detection probes (green). Each excitation fiber has a neighboring detector fiber located at 8 mm (H1) or at 5 mm (H2). Two extreme fibers are separated from each excitation fiber by 16 mm (Holder 1) or by 10 mm (H2).

The suction-cup based probe holder, named holder 1 (H1) in the present document, provides a probe isolation of 8 mm, whereas holder 2 (H2) was made of silicone rubber and contained the probes at a distance of around 5 mm (see Figure 14). Therefore, H1 was built to test the obtainable signal at the probe isolation distance, and H2 to assess the signal at a sensible distance.

Figure 13. Concept ideas for in-vivo experimental measurements using the system's fiber bundle. Only non-magnetic materials were considered for this experiment and for future combined optical-MRI experiments with this system.

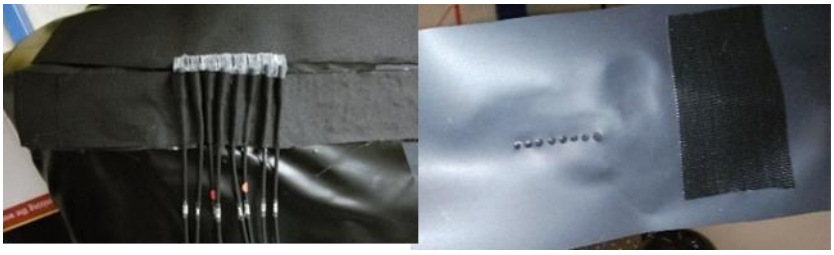

a) b)

Figure 14. The probe holder designs made of a) suction cups and polyester (H1) and b) black silicone rubber (H2). Hole patterns were done using a hole puncher (H1) and a laser cutter (H2), respectively.

For illumination, a pinhole was placed between the lamp and the illumination end of the transmitting bundle to illuminate just a select group of fibers while leaving the rest as detectors (see Figure 15). Subsequently, the illuminating and the measuring fibers were chosen and secured in the probe holders. The optical power at the excitation probes was ~5 µW (AVG).

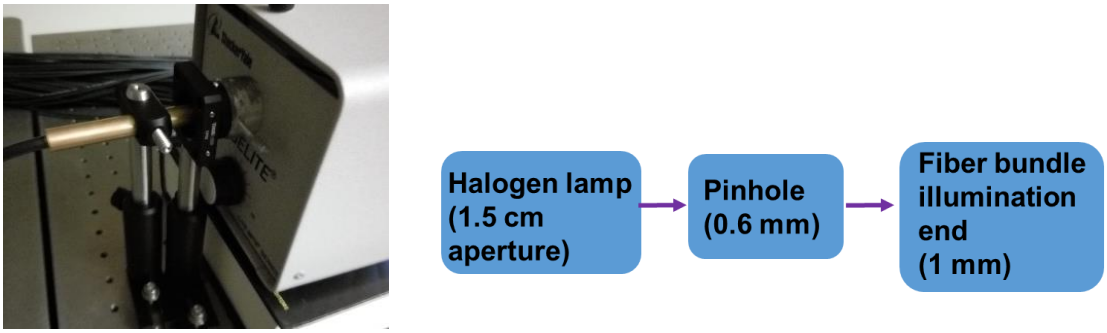

Figure 15. Setup used to couple broadband light into the illumination end of the system's fiber bundle. A 0.6 mm aperture was positioned between the illumination end of the fiber bundle and the lamp in order to target a subset of the excitation fibers.

An integration time of 250ms was used for this experiments, to explore the results using a value comparable to the MRI parameter TR. After the optical power safety calculations, the fiber holders were then positioned on the forearm of the 2 subjects. Data were acquired in dark room conditions using an integration time of 250 ms and subsequently analyzed using Matlab (see figure Figure 16).

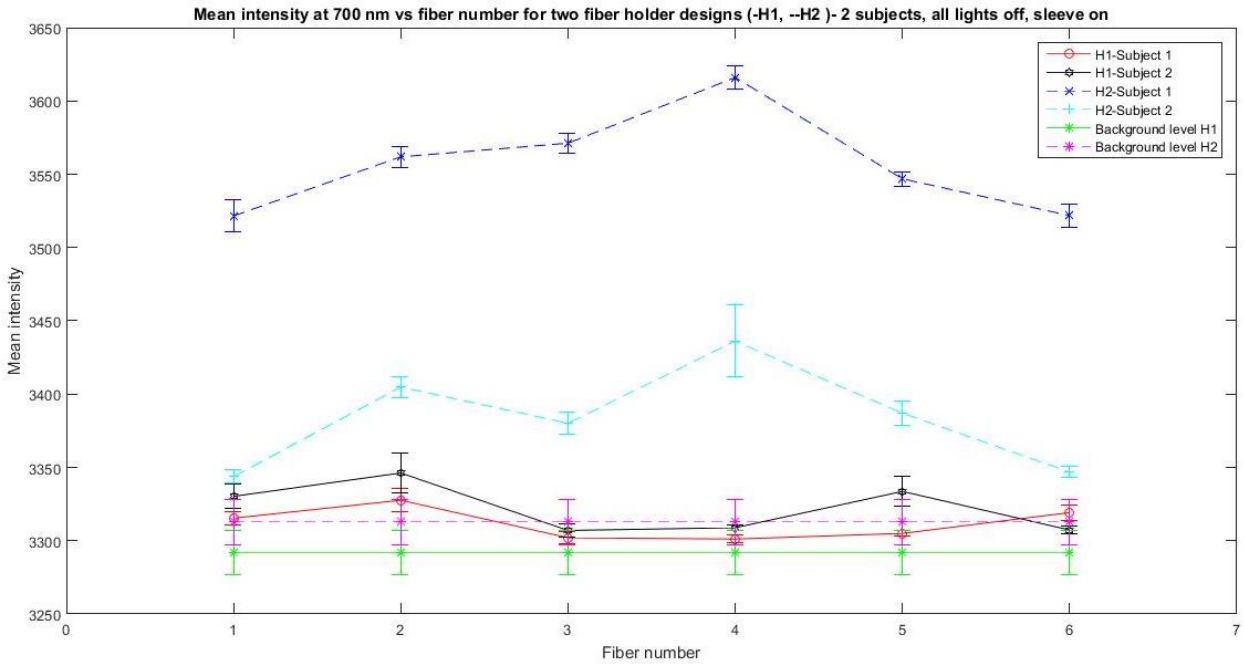

Figure 16. Mean pixel intensity (n=5 images) at 700 nm measured by six detector probes positioned on the forearm of two volunteers. The solid line represents the suction cup design (H1, 8 mm probe separation) and the dashed line represents the silicone rubber design (H2, 5 mm probe separation).

Discussion: In Figure 16, the mean pixel intensity at 700 nm is displayed for the six detectors (green line in Figure 16) measured with H2, in which the fibers were separated by only 5 mm, and the holder H1 with the larger fiber separation of 8 mm. In general, H2 presents a signal above the mean background level and higher than H1. Holder H1 shows only a very low signal, as is to be expected at such large fiber separations. Regarding H2, the mean intensity values for both subjects maintained a signal above the mean background intensity and with values higher

than the error bar sizes. The H2-curves exhibit a variation between subjects; this might only be due to experimental differences, such as contact with the subject's skin, positioning of the holder etc., or tissue differences such as skin colour and properties. Further experiments would be necessary to determine the cause.

These results also imply that fibers 2-5 are only around 2% above the two extreme fibers located at the isolation distance, therefore suggesting the need to improve imaging parameters (optical power, integration time) and skin contact (probe design) to further study multi-channel measurement capabilities in human skin with the proposed fiber holder designs and system setup. Also, there is a need to normalize with the intensity measured with a diffuse reflectance standard to compensate for non-uniform illumination from the excitation probes, as discussed in chapter 4.

Chapter 4. In-vivo DOS experiments

Objective

With the purpose of evaluating the reliability of the NIRS system to measure spectroscopy signals in human skin and to perform oxygenation assessment with the proposed setup, two sets of exploratory experiments were performed in a healthy subject, comparing relative spectral changes over 1) the antecubital vein and a reference tissue area and 2) the lower leg at the medial (MG) and lateral (LG) gastrocnemius under isokinetic exercise (see Appendix 2 for an illustration of the middle leg anatomy).

Methods

DOS signals were measured in the arm and the lower leg for study and comparison. To that end, experiment #1 involved the collection of signals from the antecubital vein and from a distal reference area where no large veins were visible. For experiment #2, sensors were located over the MG and LG of the right leg and measurements were obtained before and after 30 “calf-raises” (described below). For both experiments, every measurement site was assessed using a single measuring probe (see Figure 17) and a pair of measuring probes attached together (see Figure 18).

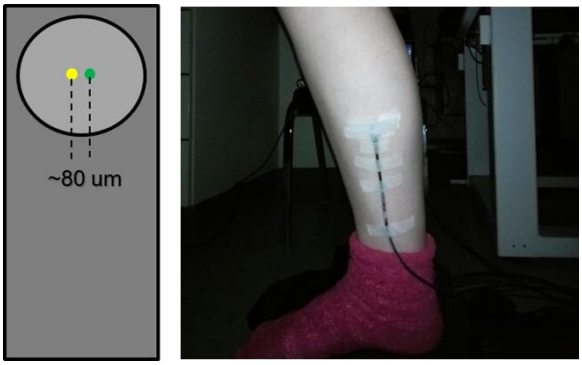

Figure 17. Schematic and photograph of a single-probe configuration for DOS measurements, where the distance between the excitation and detector fibers is 80 µm.

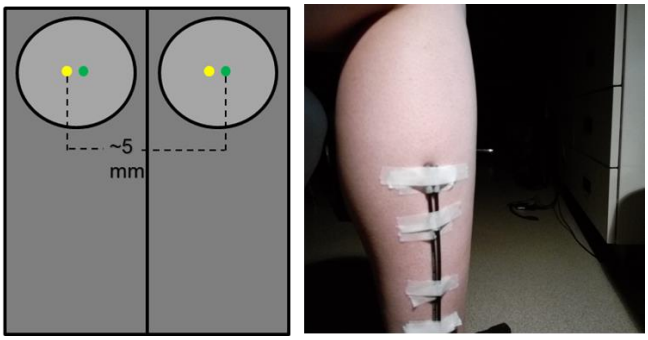

Figure 18. Schematic and photograph of a single-probe configuration for DOS measurements, where the distance between the excitation and detector fibers is 5 mm.

Repeated image acquisitions (total=20 images) were achieved in dark room conditions using the camera SDK (through Microsoft Visual C++) to study spectral changes over time corresponding to each measurement site and condition (rest and recovery for experiment #2). Time resolution for the acquisitions is 8 s, determined by the time elapsed between shutter openings. An integration time of 1 s was used for these experiments. Mean intensity spectral measurements (total=20) were acquired for each measurement site and experimental condition.

Finally, background subtraction and data processing was carried out using Matlab® (Mathworks, Natick, MA). An extract of the code routine can be found in Appendix 2.

To investigate oxygenation changes in the lower leg upon exercise, the initial intensity entering the tissue needed to be estimated. Therefore, prior to acquisitions, the initial intensity was estimated by illuminating a diffuse reflectance standard (Labsphere, Inc., NH, USA) with an excitation probe and measuring the diffusely reflected light reaching the neighbouring detector fiber present in the same probe (80 µm separation). Subsequently, the reflectance signal (R) was calculated using:

Equation 1:

$$R = \frac{I_m - B}{I_S - B}$$ [26]

where I_m represents the reflectance signal measured from the subject, I_S corresponds to the reflectance signal measured from the diffuse reflectance standard and B is the background signal intensity. In order to avoid over- or under-exposure of pixels, the standard spectra were measured using different lamp intensity levels and different separations between the standard surface and the probe sensitive surface[3]. Lastly, the detected pixel intensity and the calculated reflectance signal were studied across wavelength and acquisition time, with a

[3] The P&P Optica spectrometer manual included a recommendation to prevent pixel saturation by avoiding pixel intensities higher than 16,000. (https://ppo.ca/)

special interest in wavelengths before and after the isosbestic point of hemoglobin (at 808 nm), in this case, 750, and 850 nm.

Results

Experiment #1. Measurements over cubital vessel area

1. Results using a pair of measurement probes

Spectral images were acquired and analyzed to compare the mean signal intensity as a function of wavelength detected at each measurement site in a probe-pair arrangement. Along this project, a mean spectral image was calculated for all series of 20 acquisitions, as seen in Figure 19. The previously developed channel calibration table for this system (described in chapter 3) was used to identify the pixels of interest corresponding to the detector probe number used in this experiment (see Table 2). A complete set of channel ranges and mean spectral images corresponding to each of the other experiments can be found in Appendix 1.

Table 2. Fiber probe number used at each measurement location (MG and LG) and their corresponding pixel range over the channel direction of the spectral images.

Fiber Probe numbers and locations in the channel axis			
Location	Emitters	Detectors	Range (x-pixel number)
Vessel area	62	118	1613: 1630
Reference tissue area	143	126	1751: 1772

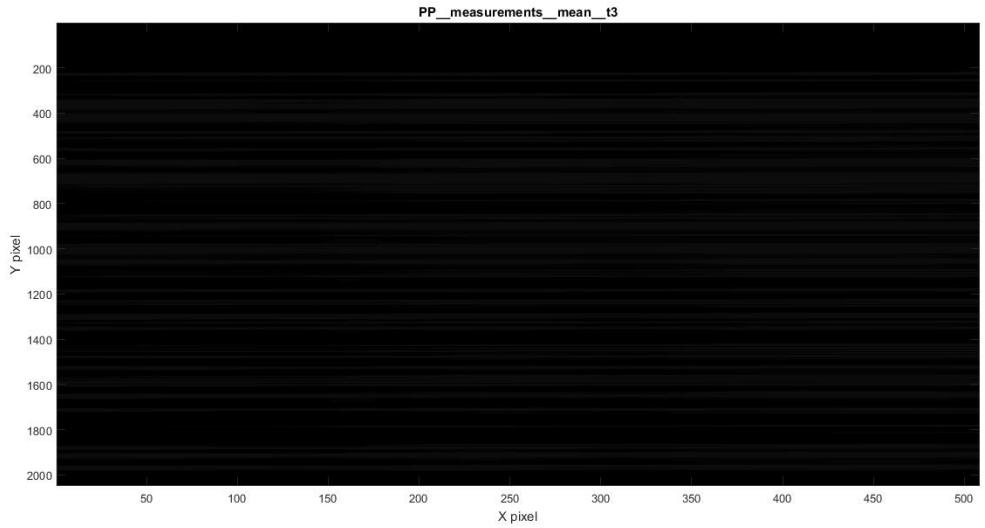

Figure 19. Figure showing the mean spectral image computed by averaging 20 images for the probe-pair measurements (integration time: 1s). The horizontal axis corresponds to the spectral axis and the vertical axis corresponds to each of the detectors. Spectral calibration database was used to selectively analyze the pixels corresponding to the detector probes used for the experimental measurements.

For every acquisition, the spectrum for each detector's range was normalized to the signal intensity at 700 nm. Figure 20 shows the mean of the normalized signal intensity values across the 20 images, as a function of wavelength. Table 3 shows the percent decrease at key wavelengths, where values at 850 nm present the higher decrease (around 39%).

Table 3. Normalized mean pixel intensity values (total=20) and relative magnitude changes for vessel and reference measurement sites (Probe-probe arrangement).

Wavelength [nm]	Vessel	Reference	Relative change
750	0.83	1.15	-0.28
800	0.87	1.4	-0.38
808	0.87	1.29	-0.33
850	1.1	1.8	-0.39

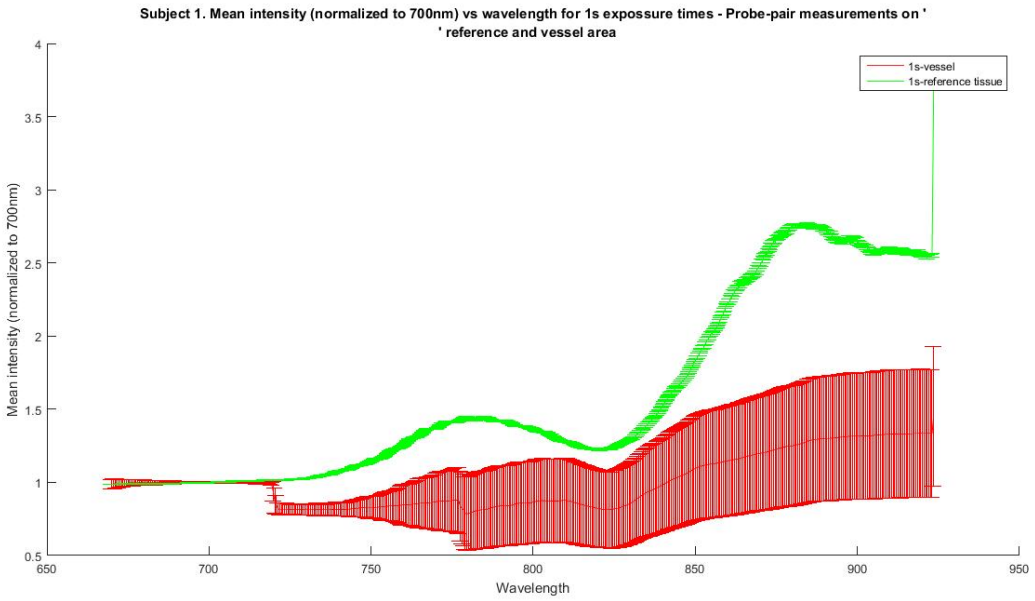

Figure 20. Mean pixel intensity (total=20 images) across wavelength (nm) for detectors located at vessel and reference areas (1s exposure time). Measurements were done with a pair of probes (inter-fiber separation of 5 mm). The green curve was obtained at the reference tissue, whereas the red curve corresponds to the vessel measurements. Error bars for each wavelength are calculated as the standard deviation of the intensity over the 20 images. The intensity reflected from the vessel area shows a reduced normalized mean pixel intensity over the whole spectrum, when comparing to the reference tissue intensity.

In Figure 20, the mean over all wavelengths of the normalized intensity is shown as a function of acquisition time (i.e. the order at which each of the 20 images was acquired). As shown in Figure 21, the time courses corresponding to the vessel measurements depict a mean magnitude decrease of around 30% from the reference signal along the whole spectral range.

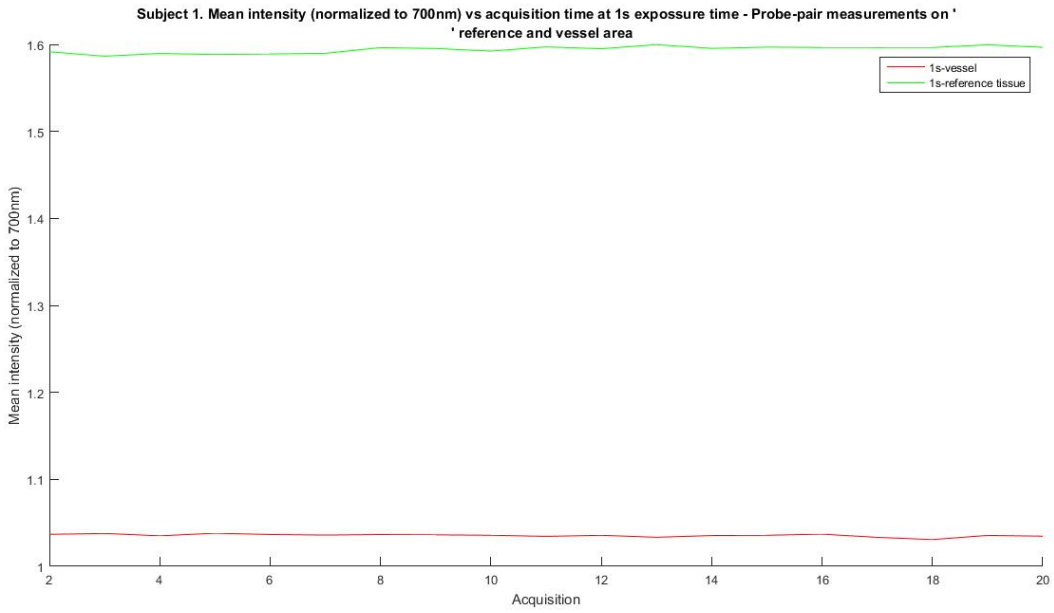

Figure 21. Mean pixel intensity vs. image acquisition order for vessel and reference areas (1s exposure time). Measurements were done with a pair of probes (inter-fiber separation of 5 mm). Time courses corresponding to the vessel measurements depict a mean magnitude decrease of around 30% from the reference signal along the whole spectral range.

2. Results using a single measurement probe

Figure 21 and Figure 22 show the normalized mean intensity spectral measurements as a function of wavelength and the time-series depiction for each

measurement position using a single probe. Differences in the spectral morphology and mean intensity for vessel and reference tissue areas are apparent in this figure. The shape of the spectra shows similar features to the measurements for the probe-pair experiment (Figure 20).

Table 4. Normalized mean pixel intensity values (total=20) and relative magnitude changes for vessel and reference measurement sites (Single-probe arrangement). This shows the relative decrease at 800, 808 and 850 nm between the vessel and the reference areas, where values at 850 nm exhibit the strongest decrease (around 65%) and there is no change at 750 nm.

Wavelength [nm]	**Vessel data**	**Reference data**	**Relative change**
750	0.87	0.87	0.00
800	0.9	1.87	-0.52
808	0.86	1.7	-0.49
850	0.84	2.4	-0.65

As shown in Figure 23, the time series corresponding to measurements on the vessel area exhibit an overall mean magnitude decrease of around 50% compared to the reference signal.

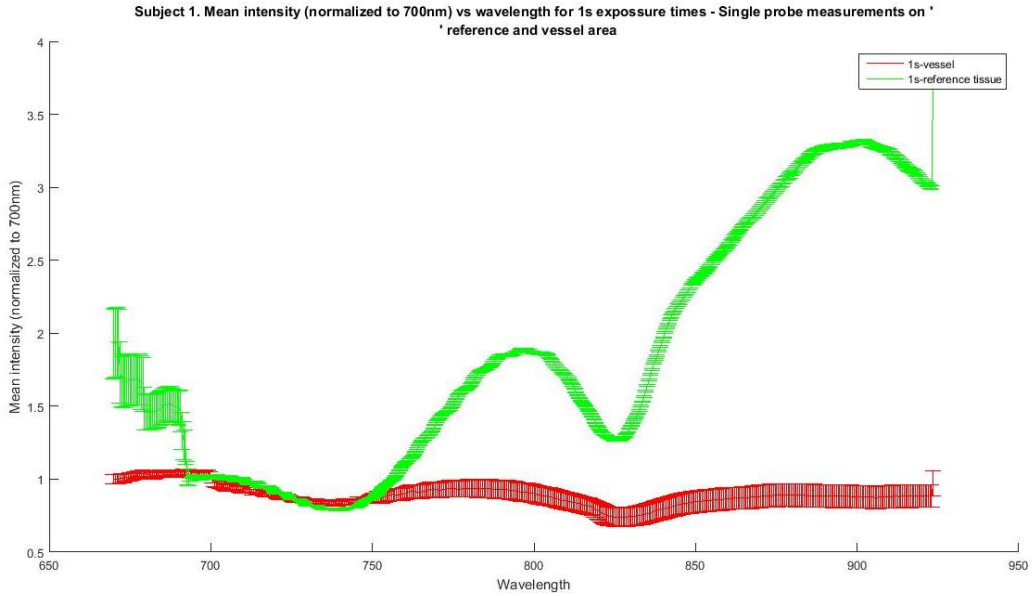

Figure 22. Mean pixel intensity (total=20 images) across wavelength (nm) for detectors located at vessel and reference areas (1s exposure time). Measurements were done with a single probe (inter-fiber separation of 80 µm). The green curve was obtained at the reference tissue, whereas the red curve corresponds to the vessel measurements. The intensity reflected from the vessel area shows a reduced normalized mean pixel intensity over the whole spectrum, when comparing to the reference tissue intensity.

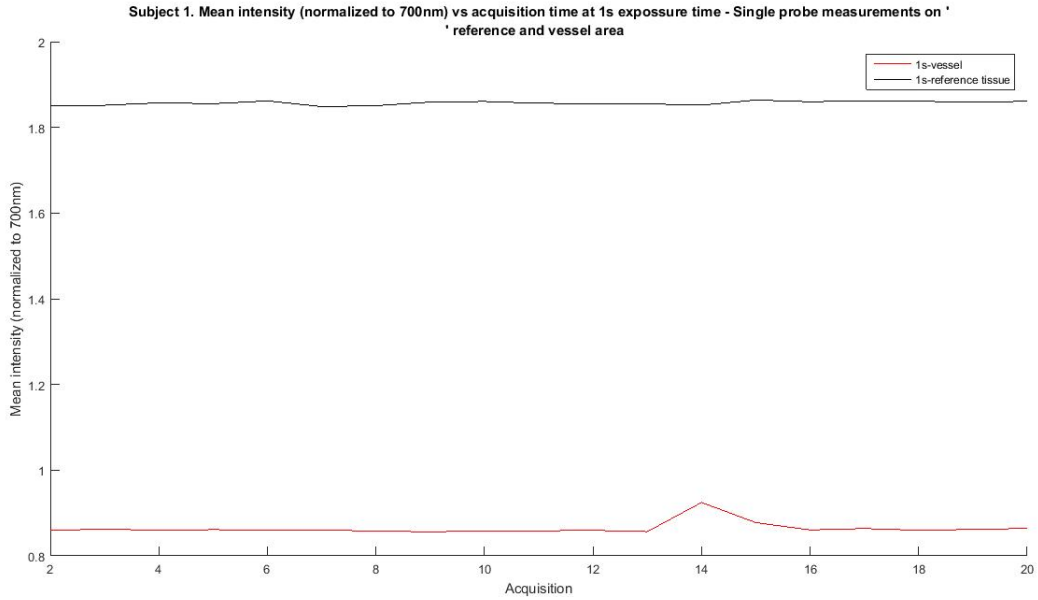

Figure 23. Mean pixel intensity vs. image acquisition order for vessel and reference areas (1s exposure time). Measurements were done with a single probe (inter-fiber separation of 80 µm). Time courses corresponding to the vessel measurements depict a mean magnitude decrease of around 50% from the reference signal along the whole spectral range

Experiment #2. Lower leg measurements upon foot dorsiflexion

1. Results using a pair of measurement probes

Figure 24 shows the normalized mean intensity spectral measurements across images as a function of wavelength for the MG and LG at rest and in recovery condition. Differences in the morphology and mean intensity for the MG and LG spectra are apparent in this figure. Changes between the rest and the recovery spectra within each muscle group may be negligible or below the instrument's accuracy in this figure.

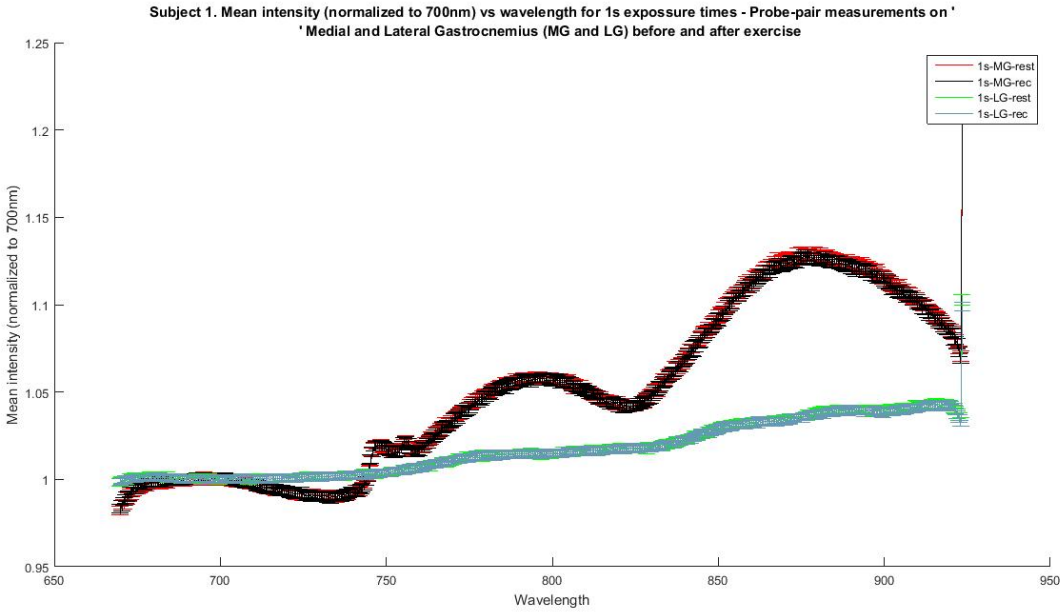

Figure 24. Mean pixel intensity (total=20 images) across wavelength (nm) for detectors located in the MG and LG at rest and recovery conditions (1s exposure time). Measurements were done with a pair of probes (inter-fiber separation of 5 mm). Changes between the rest and the recovery spectra within each muscle group may be negligible or below the instrument's accuracy in this experiment.

The normalized mean intensity spectrum measured on the diffuse reflectance standard (standard spectralon®, Labsphere) is shown in Figure 25 for the two excitation probes. The shape of the spectra shows similar features as the measured halogen lamp's spectra presented in the Figure 5 found in the previous chapter.

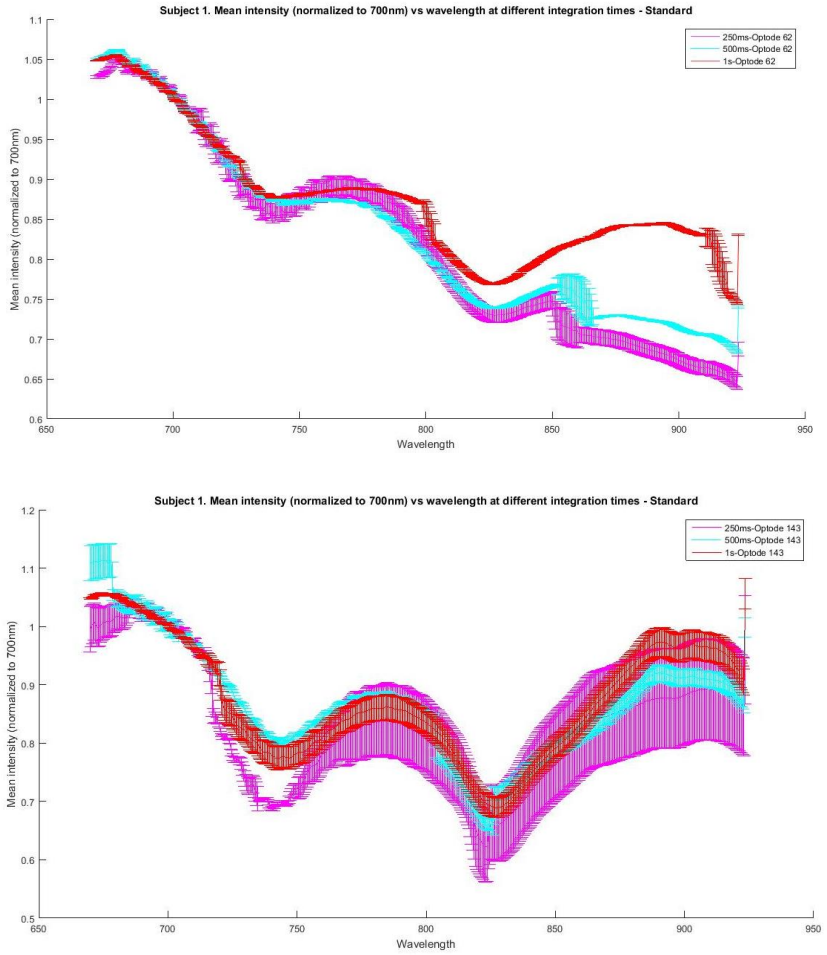

Figure 25. Mean pixel intensity (total=20 images) across wavelength (nm) measured on the diffuse reflectance standard with probe #62 – MG and #143 - LG position (250ms, 500ms and 1s exposure times). The normalized mean intensity spectrum was measured on a diffuse reflectance standard (standard spectralon®, Labsphere).

The normalization of the measurement and standard spectra is shown in Figure 26. As with the mean intensity data, changes in the reflectance data between the rest and the recovery condition seem to be below the instrument's accuracy in this figure.

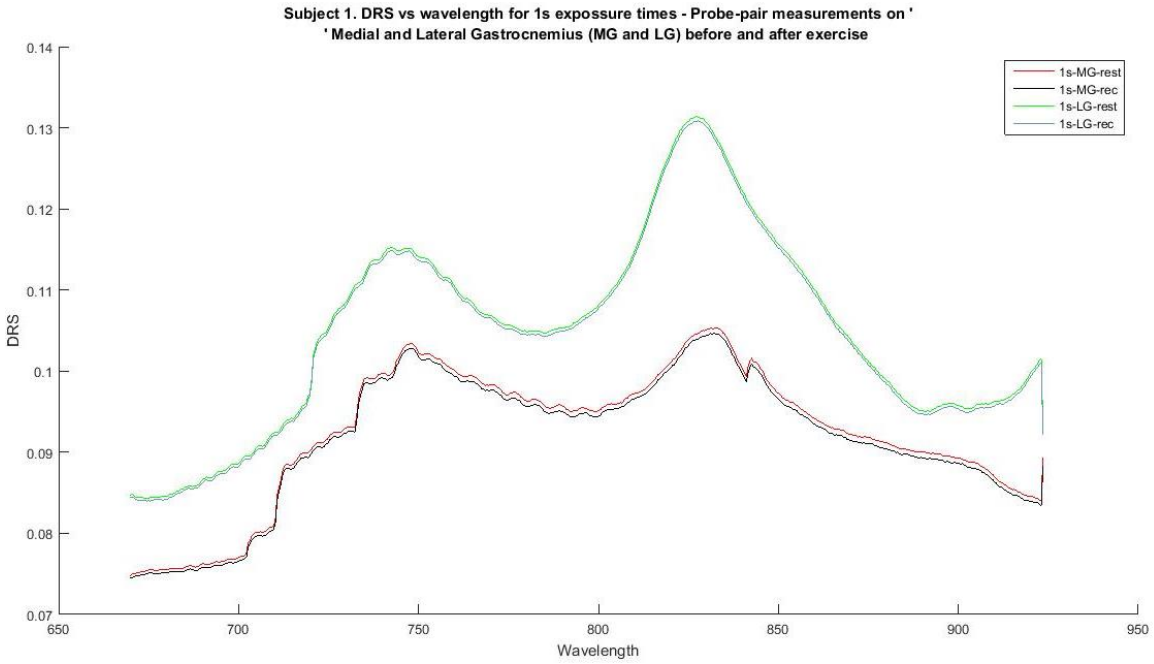

Figure 26. Reflectance signal across wavelength (nm) measured in the MG and LG at rest and under recovery condition (1s exposure time). Measurements were done with a pair of probes (inter-fiber separation of 5 mm). As with the mean intensity data, changes in the reflectance data between the rest and the recovery condition seem to be below the instrument's accuracy in this figure.

Time-series depictions of the mean signal intensity across wavelength is shown for each acquisition taken on the MG and LG using a probe-pair configuration (see Figure 27). Overall, the mean signal intensities acquired during recovery over the whole spectral range do not present a clear change from the rest signals.

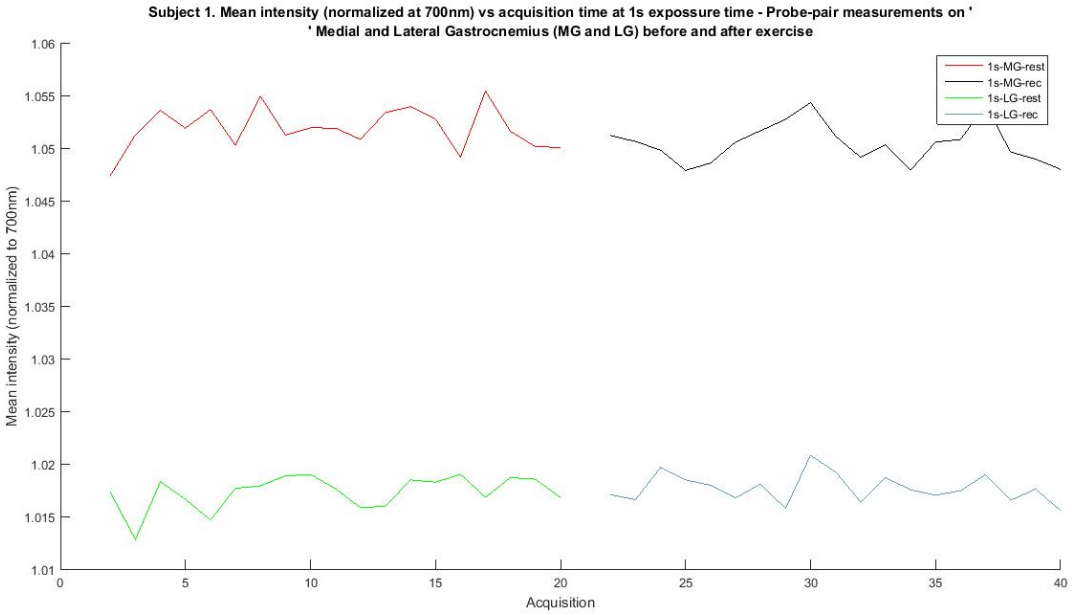

Figure 27. Mean pixel intensity (total=20 images) vs. image acquisition order in the MG and LG at rest and in recovery condition (1s exposure time). Images were acquired every 8s. A clear change from the rest curves was not found for these curves.

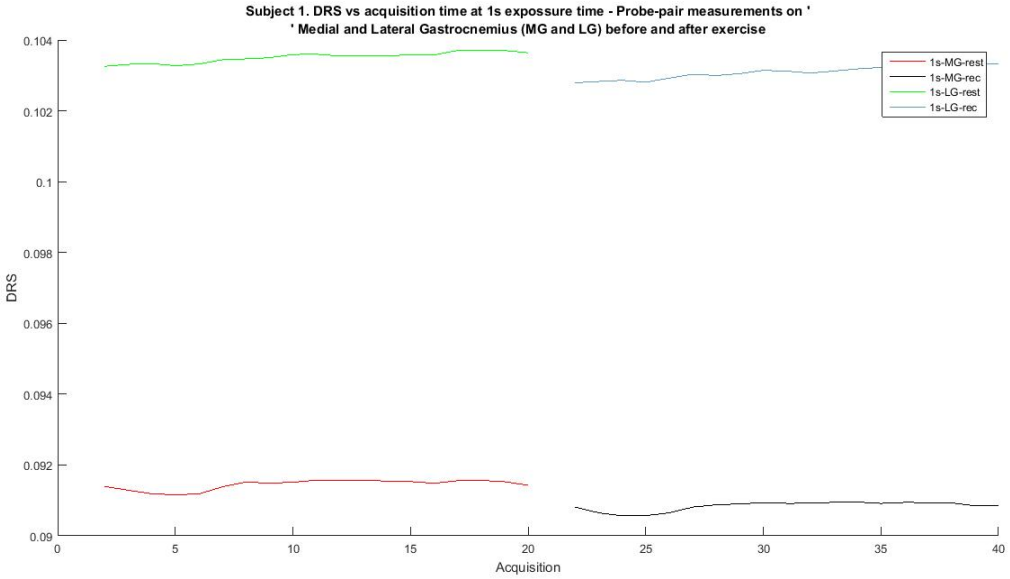

Figure 28. Reflectance signal vs. image acquisition order in the MG and LG at rest and in recovery condition (1s exposure time). Images were acquired every 8s. A clear change from the rest curves was not found for these curves.

2. Results using a single measurement probe

Figure 29 shows the mean intensity spectral measurements for the MG and LG at rest and in recovery condition. Differences in the morphology and mean intensity for the MG and LG spectra are apparent in this figure. Table 5 shows the relative mean pixel intensity changes at 750, 800, 808 and 850 nm between the recovery and the rest condition for the MG, whereas Table 6 shows the relative changes for the LG. Relative changes from the rest condition are ~1 to 4% in magnitude between experimental conditions and exhibit an increase at the MG position and a decrease at the LG position.

Table 5. Normalized mean pixel intensity values (n=20) and relative magnitude changes from the rest condition for MG positions (Single-probe arrangement).

Wavelength [nm]	**Rest**	**Recovery**	**Relative change**
750	0.82	0.84	0.02
800	0.82	0.85	0.04
808	0.79	0.81	0.03
850	0.74	0.77	0.04

Table 6. Normalized mean pixel intensity values (n=20) and relative magnitude changes from the rest condition for LG positions (Single-probe arrangement).

Wavelength [nm]	Rest	Recovery	Relative change
750	0.75	0.73	-0.03
800	1	0.99	-0.01
808	0.88	0.87	-0.01
850	0.91	0.87	-0.04

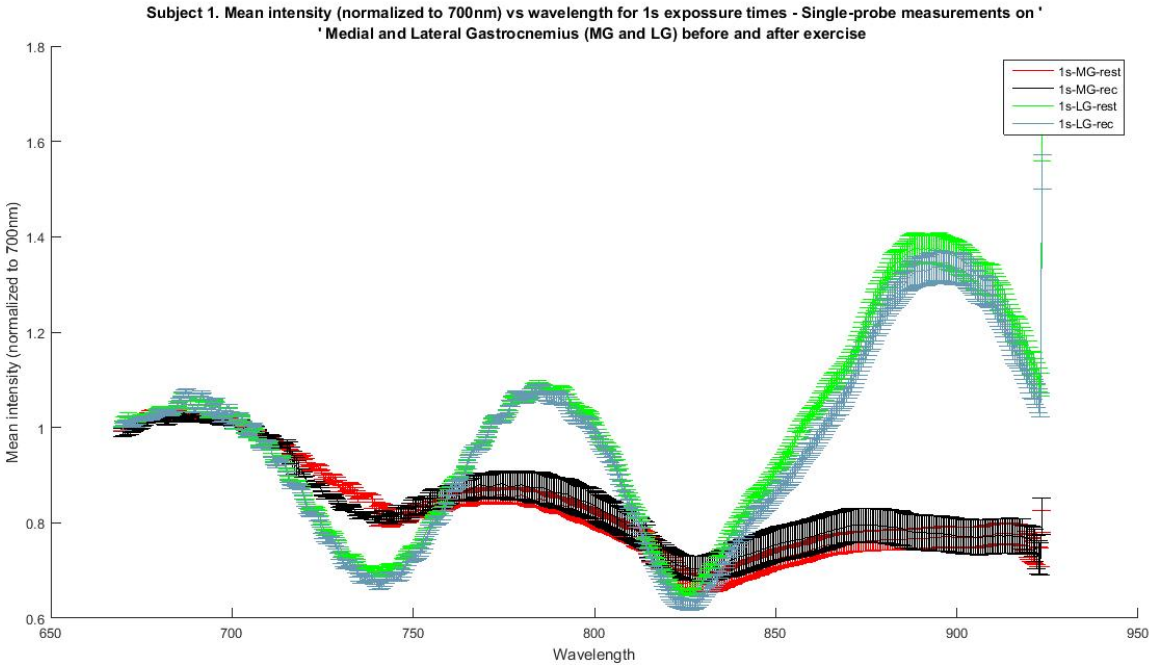

Figure 29. Mean pixel intensity (total=20 images) across wavelength (nm) for detectors located in the MG and LG at rest and recovery conditions (1s exposure time). Measurements were done with a single probe (inter-fiber separation of 80 µm).

Differences in the morphology and mean intensity for the MG and LG spectra are apparent in this figure.

The normalization of the mean intensity measurement and the standard spectra (see Figure 25) is shown in Figure 30, while Table 7 and Table 8 show the values for particular wavelengths. Differences of several order of magnitude were found when comparing these curves and values with the magnitudes measured with a pair of probes (see Figure 28). This suggests the need to further improve and validate the measurements using the standard spectralon in order to calculate the reflectance values.

Table 7. Reflectance values (n=20) and relative magnitude changes from the rest and recovery conditions for MG positions (Single-probe arrangement).

Wavelength [nm]	Rest	Recovery	Relative change
750	0.69	0.67	-0.02
800	0.72	0.7	-0.02
808	0.73	0.71	-0.02
850	0.68	0.68	0

Table 8. Reflectance values (n=20) and relative magnitude changes from the rest and recovery conditions for LG positions (Single-probe arrangement).

Wavelength [nm]	Rest	Recovery	Relative change
750	0.58	0.6	0.02
800	0.68	0.7	0.02
808	0.68	0.7	0.02
850	0.66	0.65	-0.01

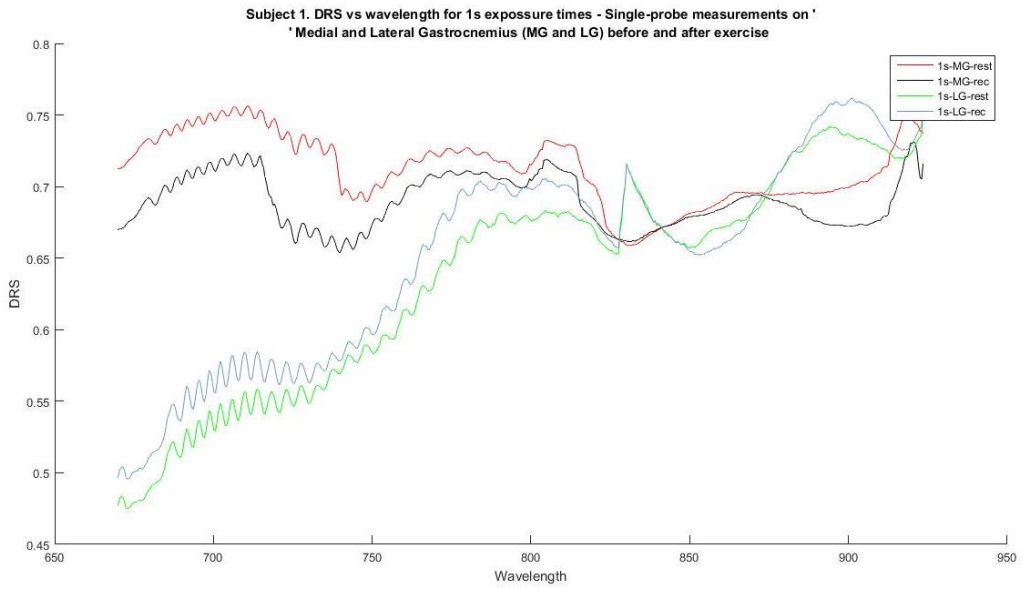

Figure 30. Reflectance signal across wavelength (nm) measured in the MG and LG at rest and under recovery condition (1s exposure time). Measurements were done with a single probe (inter-fiber separation of 80 µm). Differences of several orders of magnitude were found when comparing these curves with the reflectance magnitudes measured with a pair of probes (~50%) see Figure 28. This suggests the need to further improve and validate the measurements using the standard spectralon in order to calculate the reflectance values.

The time-series depiction of the mean signal intensity across wavelength is shown for each acquisition taken on the MG and LG using a single probe (see Figure 31). The overall spectral variation between the measurement conditions for both muscle groups is 0-2% across all wavelengths.

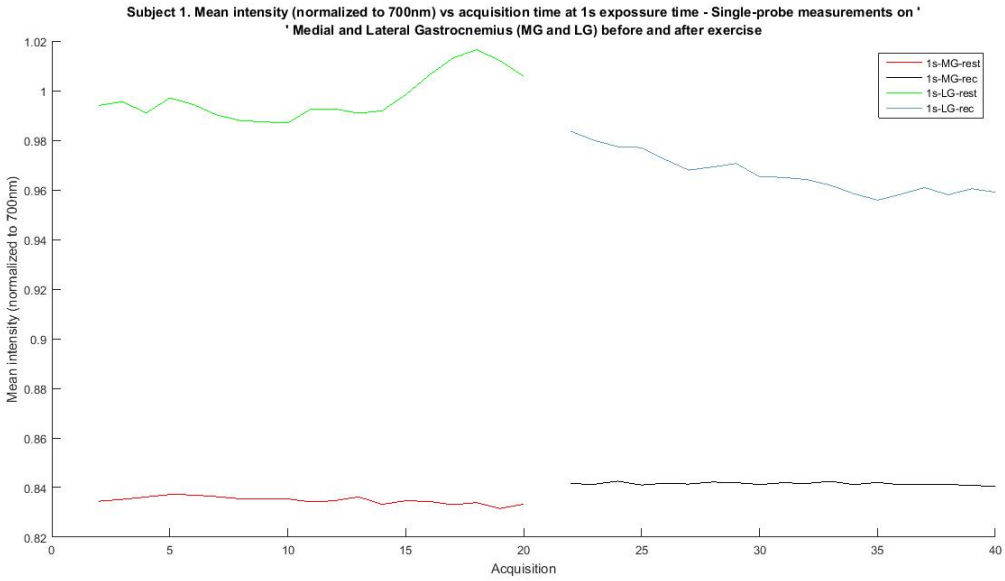

Figure 31. Mean pixel intensity (total=20 images) vs. image acquisition order in the MG and LG at rest and in recovery condition (1s exposure time, single-probe configuration). Images were acquired every 8s. Overall spectral variation between the measurement conditions for both muscle groups ranges between 0-2% across all wavelengths.

Changes in light attenuation (ΔA) can be related to changes in the chromophore concentrations from the baseline condition using the Modified Beer-Lambert law (equation 2), under the assumption that scattering and absorption are constant and excitation light is homogeneous [6].

Equation 1: $\Delta A = \log\left(\frac{I_0}{I}\right) = \alpha * \Delta\, c * L * DPF$,

where I is the light intensity transmitted through the medium, I_0 is the incident light intensity, α is the extinction coefficient of the chromophore, *c* is the chromophore concentration, *d* is the source-detector separation and *DPF* is the differential path length factor. Concentration changes from the baseline for two chromophores can be quantified using measurements at two wavelengths. The Modified Beer-Lambert law can then be stated as follows [6]:

Equation 3:

$$\Delta A^{750nm} = \log\left(\frac{I_O}{I}\right) = L * DPF * (\alpha_{HbO_2}^{750nm} * \Delta\, c_{HbO_2} + \alpha_{HbR}^{750nm} * \Delta\, c_{HbR})$$

Equation 4:

$$\Delta A^{850nm} = \log\left(\frac{I_O}{I}\right) = L * DPF * (\alpha_{HbO_2}^{850nm} * \Delta\, c_{HbO_2} + \alpha_{HbR}^{850nm} * \Delta$$

Rearranging terms, the equations can be written as [6].

Equation 5:

$$\Delta\, c_{HbR} = \frac{\alpha_{HbO_2}^{750nm}(\Delta A^{850nm}/(DPF * L)) - \alpha_{HbO_2}^{850nm}(\Delta A^{750nm}/(DPF * L))}{\alpha_{HbO_2}^{750nm} * \alpha_{HbR}^{850nm} - \alpha_{HbO_2}^{850nm} * \alpha_{HbR}^{750nm}}$$

Equation 6:

$$\Delta\, c_{HbO_2} = \frac{\alpha_{HbR}^{750nm}(\Delta A^{850nm}/(DPF * L)) - \alpha_{HbR}^{850nm}(\Delta A^{750nm}/(DPF * L))}{\alpha_{HbR}^{750nm} * \alpha_{HbO_2}^{850nm} - \alpha_{HbR}^{850nm} * \alpha_{HbO_2}^{750nm}}$$

Molar extinction coefficients of Hb can be found in Table 11. Essenpreis and colleagues published values for the differential path length factor (DPF) between 740 nm and 840 nm in several tissues including the calf muscle and the forearm. For the calf muscle, the DPF varies only about 15% from its measured value of 5.84 ±0.65 cm at 800 nm in males, and 10% from the value of 5.63 ±0.62 cm at 800 nm in females [25].

The reciprocal and logarithm of the reflectance values from Table 7 and Table 8 were calculated to estimate the term $\log\frac{I_0}{I}$ in equation 2. That implies that the intensity measured on the diffuse reflectance standard was used to estimate the initial excitation light intensity I_o, and the mean pixel intensities represented the light measured on the tissue, *I*. Results are shown in Table 9 and Table 10.

Table 9. Calculation of absorbance from reflectance values (n=20) and relative magnitude changes from the rest and recovery conditions for MG positions (Single-probe arrangement).

Wavelength [nm]	Rest	Recovery	Relative change
750	0.161	0.174	0.013
800	0.143	0.155	0.012
808	0.137	0.149	0.012
850	0.167	0.167	0.000

Table 10. Calculation of absorbance from reflectance values (n=20) and relative magnitude changes from the rest and recovery conditions for LG positions (Single-probe arrangement).

Wavelength [nm]	Rest	Recovery	Relative change
750	0.237	0.222	-0.015
800	0.167	0.155	-0.013
808	0.167	0.155	-0.013
850	0.180	0.187	0.007

Assuming that the excitation light intensity does not change during the whole experiment, information from Table 9, Table 10, Table 11 and equations 5 and 6 was then used to compute and compare the concentration changes of Hb, given in Table 12 and Table 13.

Table 11. Molar extinction coefficients for Hb in water based on [21].

Wavelength [nm]	Oxyhaemoglobin	Deoxyhaemoglobin
	cm^{-1}/M	**cm^{-1}/M**
700	290	1794.28
750	518	1405.24
800	816	761.72
808	856	723.52
850	1058	691.32

Table 12. Concentration changes of Hb measured at MG and LG (n=20) using a single probe (L=80 µm).

	Rest		**Recovery**	
Position	mean $\Delta\, c_{HbO_2}$ (M/cm)	mean $\Delta\, c_{HbR}$ (M/cm)	mean $\Delta\, c_{HbO_2}$ (M/cm)	mean $\Delta\, c_{HbR}$ (M/cm)
MG	-0.0002	0.0003	-0.0002	0.0003
LG	0.0004	-0.0004	0.0004	-0.0004

Table 13. Comparison of relative concentration changes for rest and recovery conditions measured at MG and LG (n=20) using a single probe (L=80 µm).

	Rest vs. recovery	
Position	$\Delta\, c_{HbO_2-REST}$ vs $\Delta\, c_{HbO_2-REC}$ (M/cm)	$\boldsymbol{\Delta\, c_{HbR-REST}}$ vs $\boldsymbol{\Delta\, c_{HbR-REC}}$ (M/cm)
MG	0.00	0.00
LG	0.00	0.00

Discussion

For single and probe-pair arrangements, the intensity reflected from the vessel area shows a reduced normalized mean pixel intensity at the wavelengths of interest and over the whole spectrum, when comparing to the reference tissue intensity. This may be related to a higher amount of chromophores at the vessel locations.

In contrast, only spectral differences in single-probe measurements in the lower leg experiments were found, showing a signal change of around 1-4% between the rest and the recovery condition at both muscle locations. At the particular wavelengths and overall, only LG measurements presented a signal decrease for the recovery condition, whereas MG showed the opposite trend.

In general, the results provided evidence of signal intensity changes at key wavelengths using a single-probe configuration, which lays the foundation for further studies of DRS along with BOLD fMRI measurements. Nevertheless, the range of the calculated concentration changes or reflectance values are/are not consistent with the experiments. Therefore, subsequent experimental validations are necessary to evaluate oxygenation assessment capabilities of this system.

Chapter 5. Combined Optical-MRI experiments on the lower leg

Objective

The purpose of this experiment is to measure simultaneous BOLD-fMRI and optical signals during a foot dorsiflexion protocol and compare time-series features.

Methods

A BOLD-fMRI sequence along with optical point-measurements were acquired in two subjects performing a leg-exercise protocol. The fiber bundle was located inside the magnet field of the MRI (3T magnet) and optical sensors were arranged as explained in chapter 4 (see Figure 17 and Figure 18). The exercise protocol consisted of 1 minute of foot dorsiflexion using an elastic band (Thera-Band, The Hygenic Corporation, Akron, Ohio) for resistance. Room lights were at a minimum level during these experiments.

The whole protocol was as follows:

A day before the experimental procedures:

- Install the optical components in the MRI control room
- Place the fiber bundle inside the examination room using the conduit connecting the control and examination rooms.
- Verify pixel calibration

- Illuminate the probes of interest and analyze the measured spectral images and compare the pixels of the recorded spectral lines with the reference values

Figure 32. Photographs showing the configuration of the optical setup in the MRI control room. The photograph in the left shows the MRI control room and the one in the right includes the arrangement on the DOS system in the MRI control room.

On the day of the experiment:

- Optical measurements on a diffuse reflectance standard during a BOLD sequence
  - Position excitation probes over the diffuse reflectance standard
  - Position the diffuse reflectance standard over an MRI leg phantom and fit it in the MRI leg coil
  - Acquire spectral images during a BOLD sequence

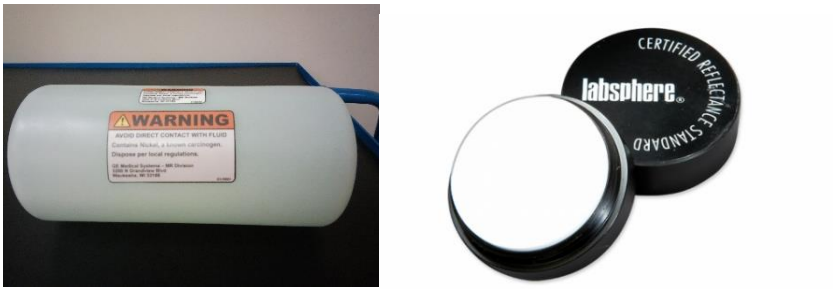

Figure 33. Photograph of the MRI leg phantom (left) and diffuse reflectance standard (right) to estimate the initial intensity delivered with the emitter probes. The measurements (total=20 images) were done along with a fragment of a BOLD-fMRI sequence to consider uniform experimental conditions. Emitter probes were secured on a diffuse reflectance standard using tape. The setup was then positioned on top of an MRI-leg coil to generate signal for the MRI and enable the sequence.

- Subject preparation
    - Explain the experimental procedure to the subject.
    - Prepare the measurement area by removing any hairs present on the area of interest using a razor.
    - Secure a set of two fiber probes (one excitation fiber with an attached fiducial marker[4], one detector fiber) on each measurement area (medial and lateral gastrocnemius positions) using skin tape.
    - Position the MRI leg coil by aligning the fiducial markers with the center of the coil and leaving the rest of the fiber probes besides the bed.

[4] Vitamin E pills (100 International Units, 67mg) were used as fiducial markers.

- Locate and secure the elastic band around the tip of the foot so that the subject can hold it with their hands.
- Provide ear plugs and hand alarm.

Figure 34. Photographs showing from the top-left to bottom right a) the MRI examination room, b) the MRI knee coil, c) the arrangement of the fiber bundle on the bed and d) the process of securing the measuring probes on the subject's leg.

- Combined optical-fMRI protocol upon foot dorsiflexion
    - Run the MRI protocol. Axial Proton Density fat saturation (PD FS) anatomical scan. FMRI study time: 6 minutes. 5 slices, Repetition time (TR)=250 ms for subject #1 (1440 volumes) and 1 s for subject #2 (360 volumes). Interleaved bottom-up slice acquisition.
    - Control the examination room lights to notify the subject of the beginning and the termination of the exercise period.
    - The optical camera acquisition (n=20 images, 1 s exposure time) was synchronized with the beginning of the rest and the recovery periods.

Results

Results using a pair of measurement probes.

1. Subject #1.

Figure 35 and Figure 36 show the normalized mean intensity spectral measurements across images as a function of wavelength for the MG and LG at rest and in recovery condition, respectively. Differences in the morphology for the MG and LG spectra are apparent, but changes between the rest and the recovery spectra within each muscle group are negligible or below the instrument's accuracy in this figure. A peak @750 was found in this results, which was not seen for the rest of the trials. Because of the aforementioned aspects, data does not provide the necessary information nor consistency to compute concentration changes for the obtained experimental data.

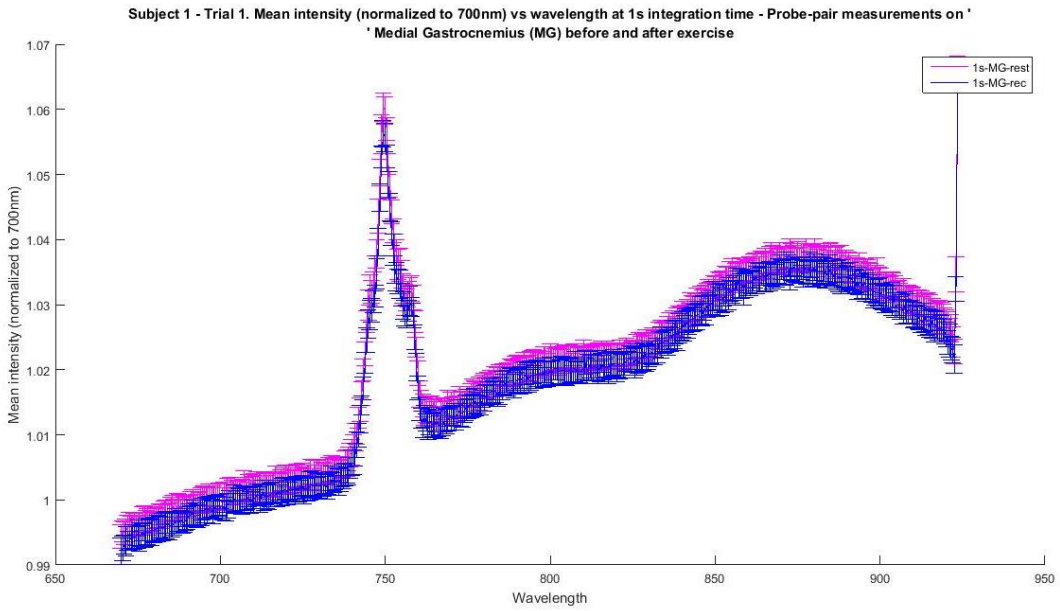

Figure 35. Mean pixel intensity (total=20 images) across wavelength (nm) for detectors located in the MG at rest and recovery conditions (1s exposure time). Measurements were done with a pair of probes (inter-fiber separation of 5 mm). Changes between the rest and the recovery spectra may be negligible or below the instrument's accuracy in this experiment. A peak @750 was found in this results, which was not seen for the rest of the trials.

The normalized mean intensity spectrum measured on the diffuse reflectance standard is shown in Figure 37 for the two excitation probes. The spectra show similar features than the previous standard measurements (see Figure 25). Differences in optodes were expected due to non-uniform excitation light transmitted from the fibers.

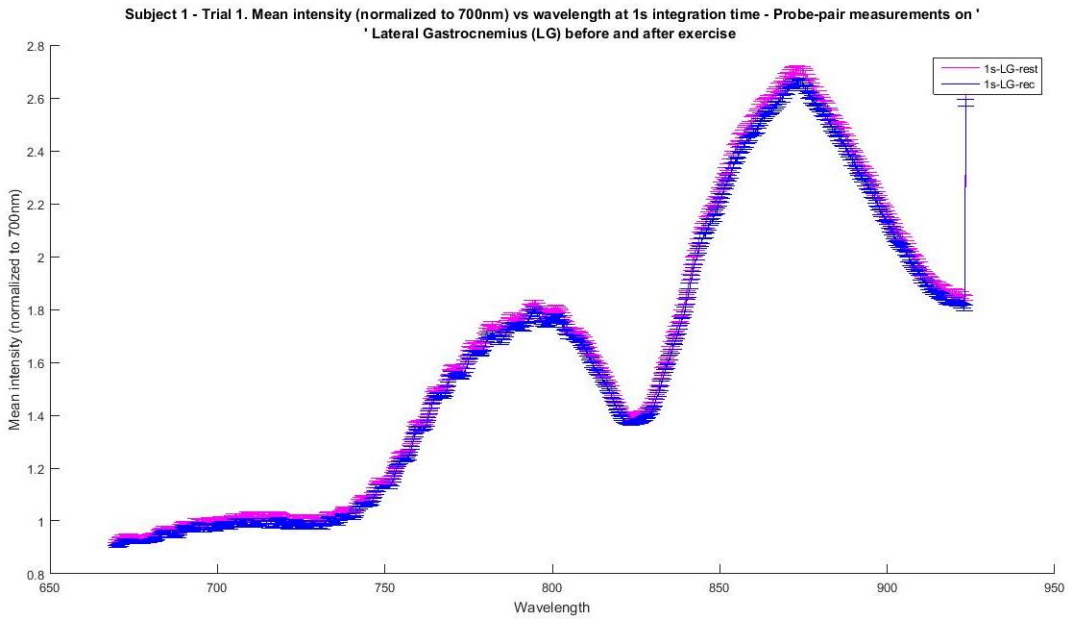

Figure 36. Mean pixel intensity (total=20 images) across wavelength (nm) for detectors located in the LG at rest and recovery conditions (1s exposure time). Measurements were done with a pair of probes (inter-fiber separation of 5 mm). Measurements were done with a pair of probes (inter-fiber separation of 5 mm). Changes between the rest and the recovery spectra may be negligible or below the instrument's accuracy in this experiment.

The normalization of the measurement and standard spectra is shown in Figure 38 and Figure 39. Significant differences were found when comparing these curves with the reflectance magnitudes measured in the previous experiment (see chapter 4, Figure 28 and Figure 30). This suggests the need to further improve and validate the measurements using the standard spectralon in order to calculate the reflectance values.

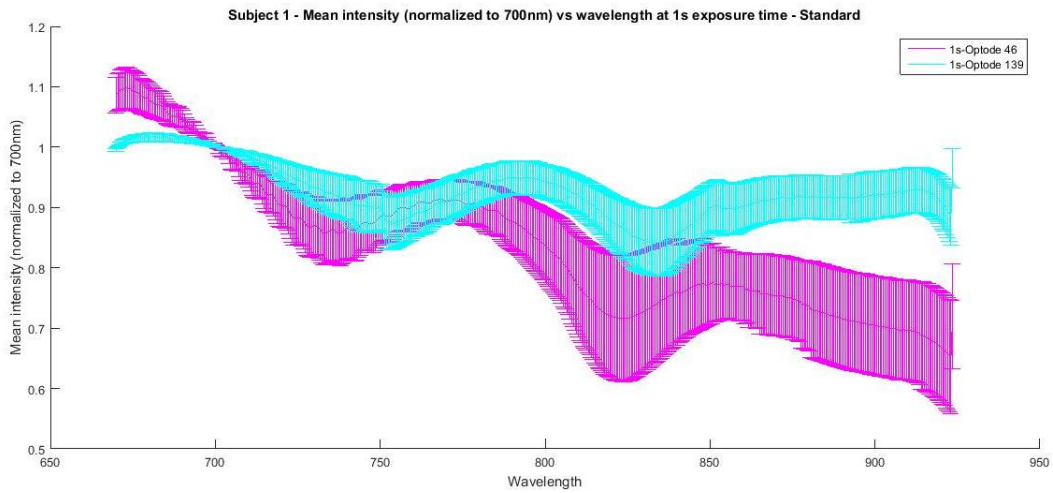

Figure 37. Mean pixel intensity (total=20 images) across wavelength (nm) measured on the diffuse reflectance standard with probe #46 – MG and #139 - LG position (1s exposure time). The normalized mean intensity spectrum was measured on a diffuse reflectance standard (standard spectralon®, Labsphere). The spectra show similar features than the previous standard measurements (see figure Figure 25). Differences in the curves were expected due to non-uniform excitation light transmitted from each of the excitation fibers.

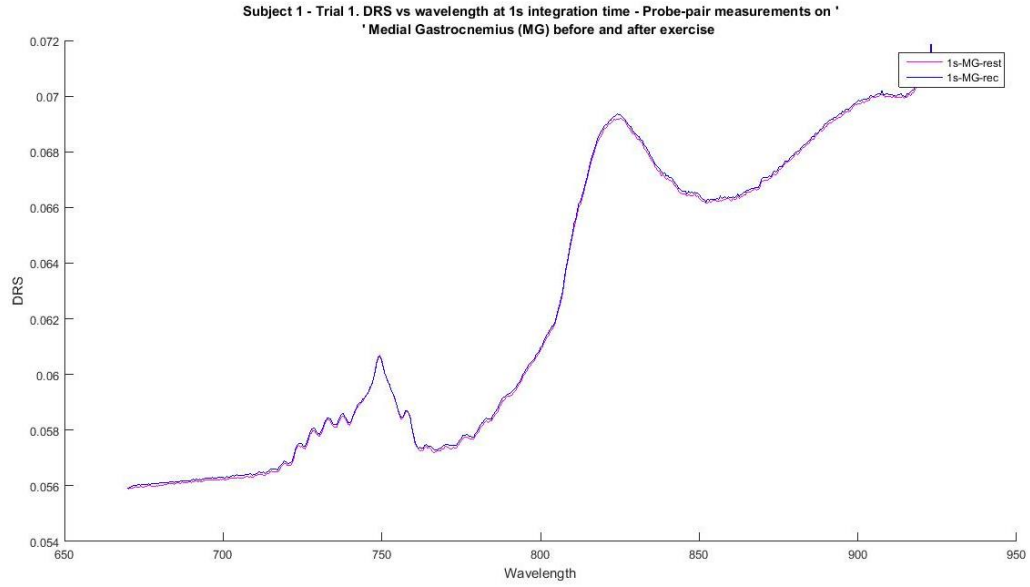

Figure 38. Reflectance signal across wavelength (nm) measured in the MG at rest and under recovery condition (1s exposure time). Measurements were done with a pair of

probes (inter-fiber separation of 5 mm). Significant differences were found when comparing these curves with the reflectance magnitudes measured in the previous experiment (see chapter 4, Figure 28 and Figure 30). This suggests the need to further improve and validate the measurements using the standard spectralon in order to calculate the reflectance values.

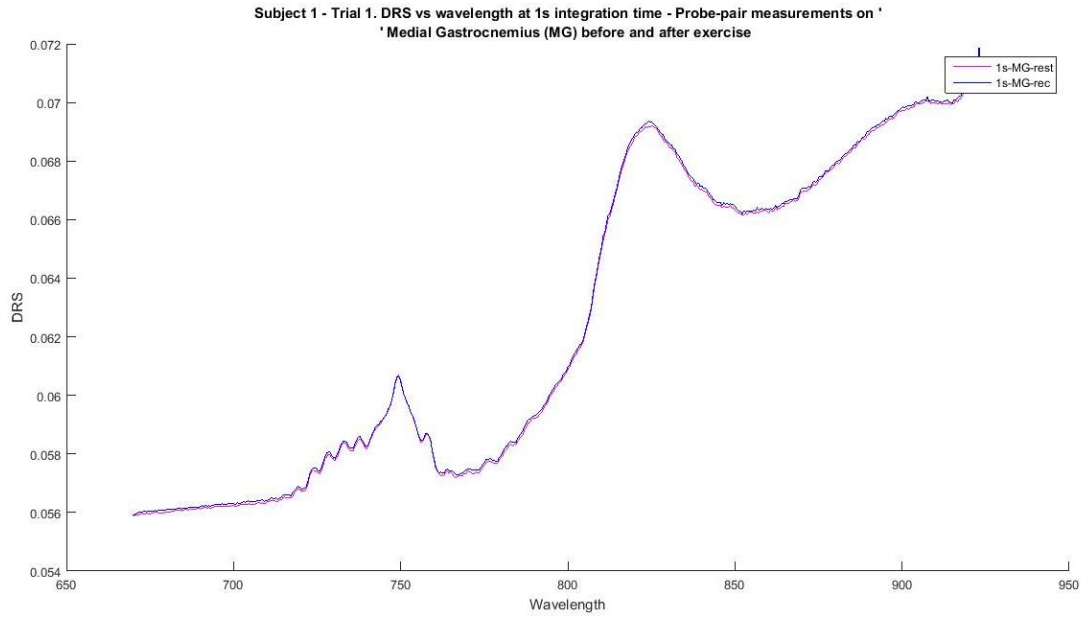

Figure 39. Reflectance signal across wavelength (nm) measured in the LG at rest and under recovery condition (1s exposure time). Measurements were done with a pair of probes (inter-fiber separation of 5 mm). Significant differences were found when comparing these curves with the reflectance magnitudes measured in the previous experiment (see chapter 4, Figure 28 and Figure 30). This suggests the need to further improve and validate the measurements using the standard spectralon in order to calculate the reflectance values.

The time-series depiction of the mean signal intensity across wavelength is shown for each acquisition taken on the MG and LG using the probe-pair arrangement

(see Figure 40). As shown in the figure, time series of the mean over the whole spectral range do not present a clear change from the rest signal.

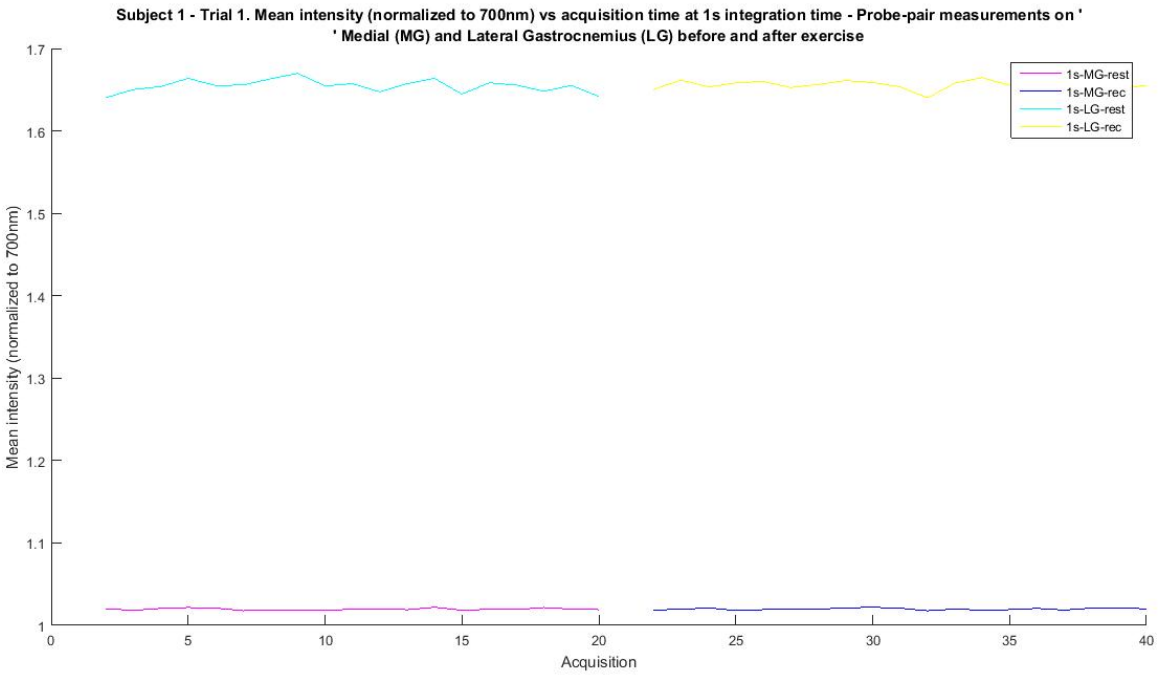

Figure 40. Mean pixel intensity (total=20 images) vs. image acquisition order in the MG and LG at rest and in recovery condition (1s exposure time). Time series of the mean recovery intensity over the whole spectral range do not present a clear change from the rest signals.

2. Subject #2

Figure 41 and Figure 42 shows the mean intensity spectral measurements for the MG and LG at rest and in recovery condition. A decrease in the recovery condition spectrum is apparent in these figures.

Table 14 shows the relative mean pixel intensity changes at 750, 800, 808 and 850 nm between the recovery and the rest condition for the MG, whereas Table 15 shows the relative changes for the LG. Relative changes from the rest condition are ~0.2-0.11% in magnitude and exhibit an increase at the MG position and a decrease at the LG position.

Table 14. Normalized mean pixel intensity values (n=20) and relative magnitude changes from the rest condition for MG positions (Probe-pair arrangement).

Wavelength [nm]	Rest	Recovery	Relative change
750	1.09	1.04	-0.05
800	1.26	1.22	-0.03
808	1.24	1.2	-0.03
850	1.33	1.28	-0.04

Table 15. Normalized mean pixel intensity values (n=20) and relative magnitude changes from the rest condition for LG positions (Probe-pair arrangement).

Wavelength [nm]	Rest	Recovery	Relative change
750	1.05	1.03	-0.02
800	1.64	1.52	-0.07
808	1.57	1.44	-0.08
850	1.85	1.64	-0.11

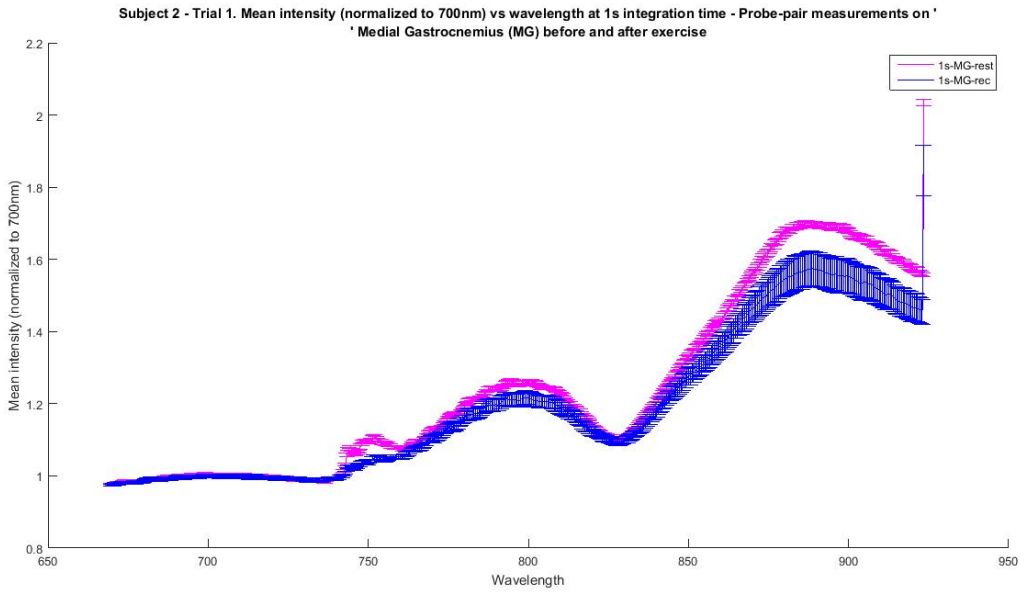

Figure 41. Mean pixel intensity (total=20 images) across wavelength (nm) for detectors located in the MG at rest and recovery conditions (1s exposure time). Measurements were done with a pair of probes (inter-fiber separation of 5 mm). Decrease in the recovery condition spectrum is apparent in this figure.

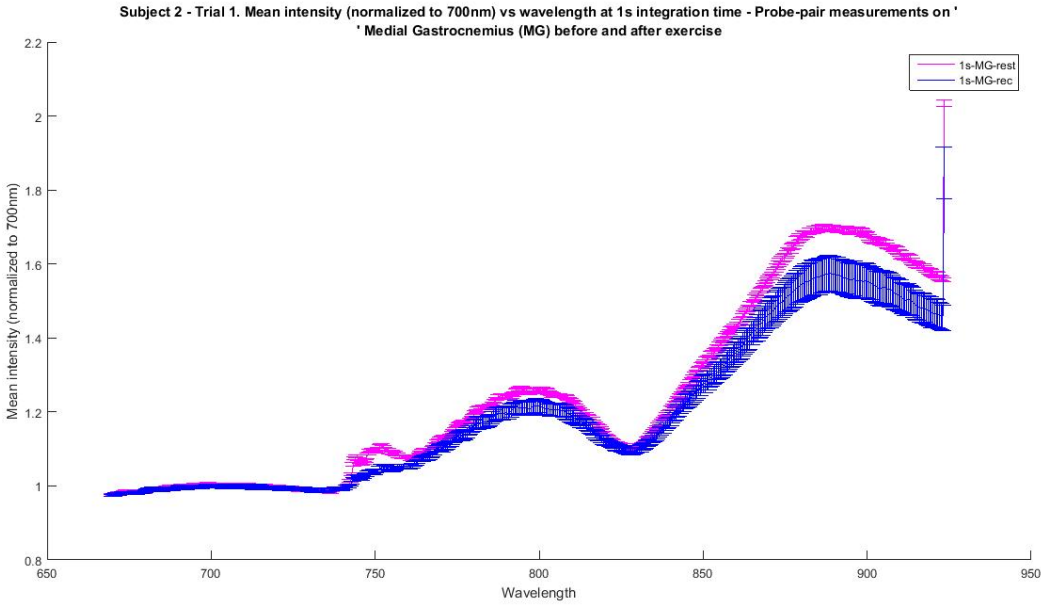

Figure 42. Mean pixel intensity (total=20 images) across wavelength (nm) for detectors located in the LG at rest and recovery conditions (1s exposure time). Measurements were

done with a pair of probes (inter-fiber separation of 5 mm). Decrease in the recovery condition spectrum is apparent in this figure.

The normalized mean intensity spectrum measured on the diffuse reflectance standard is shown in Figure 44 and Figure 45 for the two excitation probes. Reflectance magnitudes range in different orders of magnitude with respect to previous measurements (see Figure 28, Figure 30, Figure 39). Furthermore, reflectance values shown on Figure 45 have magnitudes greater than 1, which suggests lower intensity measurements due to defective fiber positioning on the standard's surface. This suggests the need to further improve and validate the measurements using the standard spectralon in order to calculate the reflectance values.

The mean pixel intensity across wavelength (nm) measured on the diffuse reflectance standard spectra is shown in Figure 43. Data corresponding to optode 53 show a particular peak at around 880 nm, which may be due to non-uniform plane of focus onto those pixels of the CCD sensor.

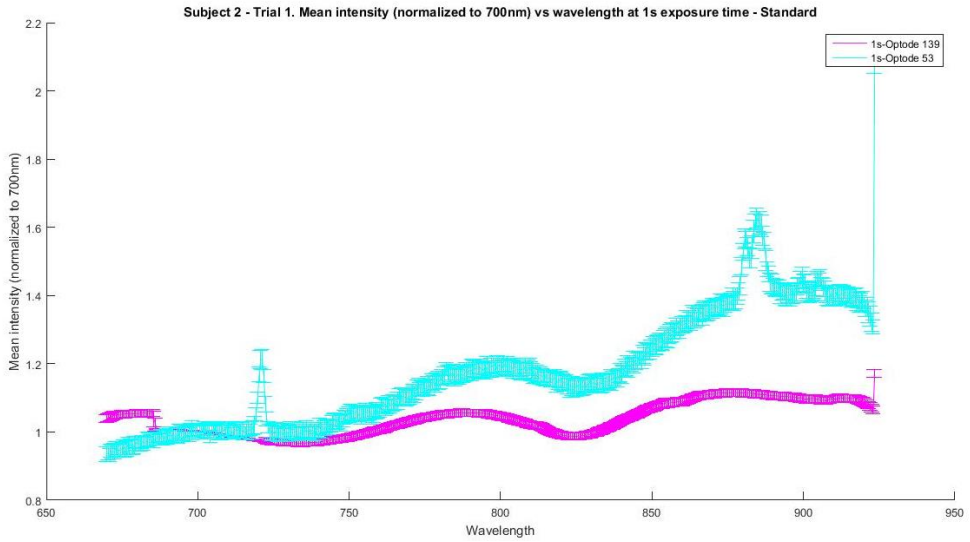

Figure 43. Mean pixel intensity (total=20 images) across wavelength (nm) measured on the diffuse reflectance standard with probe #139 – MG and #53 - LG position (250ms, 500ms and 1s exposure times). The normalized mean intensity spectrum was measured on a diffuse reflectance standard (standard spectralon®, Labsphere). Differences in the curves were expected due to non-uniform excitation light transmitted from the fibers.

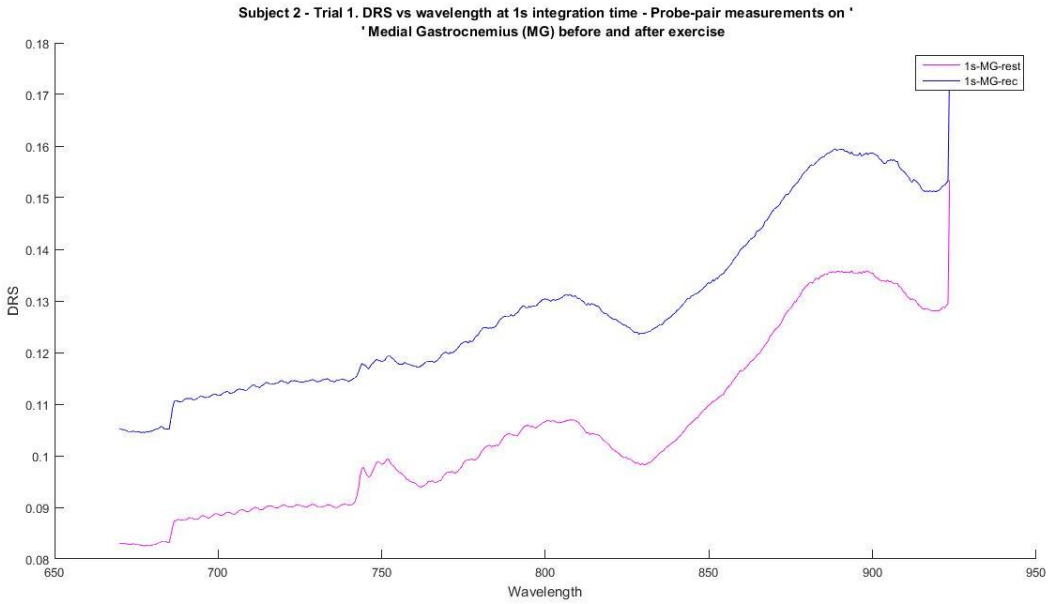

Figure 44. Reflectance signal across wavelength (nm) measured in the MG at rest and under recovery condition (1s exposure time). Measurements were done with a pair of

probes (inter-fiber separation of 5 mm). Differences of several orders of magnitude were found when comparing these curves with the reflectance magnitudes measured in the previous experiment (see Figure 28, Figure 30, Figure 39). This suggests the need to further improve and validate the measurements using the standard spectralon in order to calculate the reflectance values.

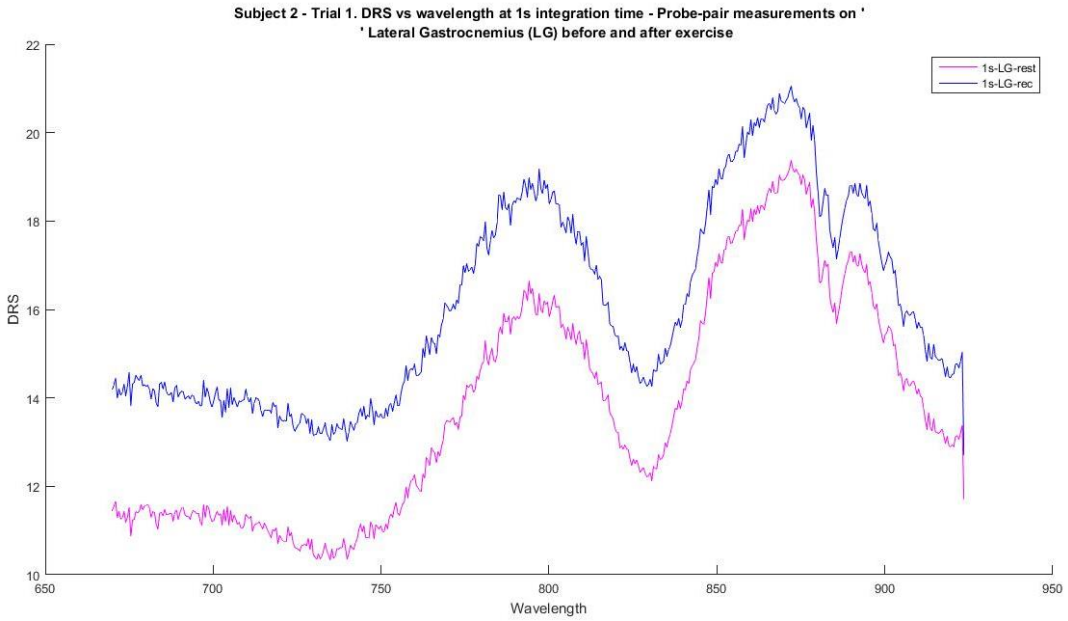

Figure 45. Reflectance signal across wavelength (nm) measured in the LG at rest and under recovery condition (1s exposure time). Measurements were done with a pair of probes (inter-fiber separation of 5 mm). Differences of several orders of magnitude were found when comparing these curves with the reflectance magnitudes measured in the previous experiment (see Figure 28, Figure 30, Figure 39). Furthermore, reflectance values resulting from this experiment have magnitudes greater than 1, which suggests lower intensity measurements due to defective fiber positioning on the standard's surface. This suggests the need to further improve and validate the measurements using the standard spectralon in order to calculate the reflectance values.

A time-series depiction of the mean intensity across wavelength is shown for each acquisition taken on the MG and LG using a probe-pair configuration (see Figure

46). The overall spectral variation between the measurement conditions for both muscle groups is 2-11% relative to the rest condition, across all wavelengths.

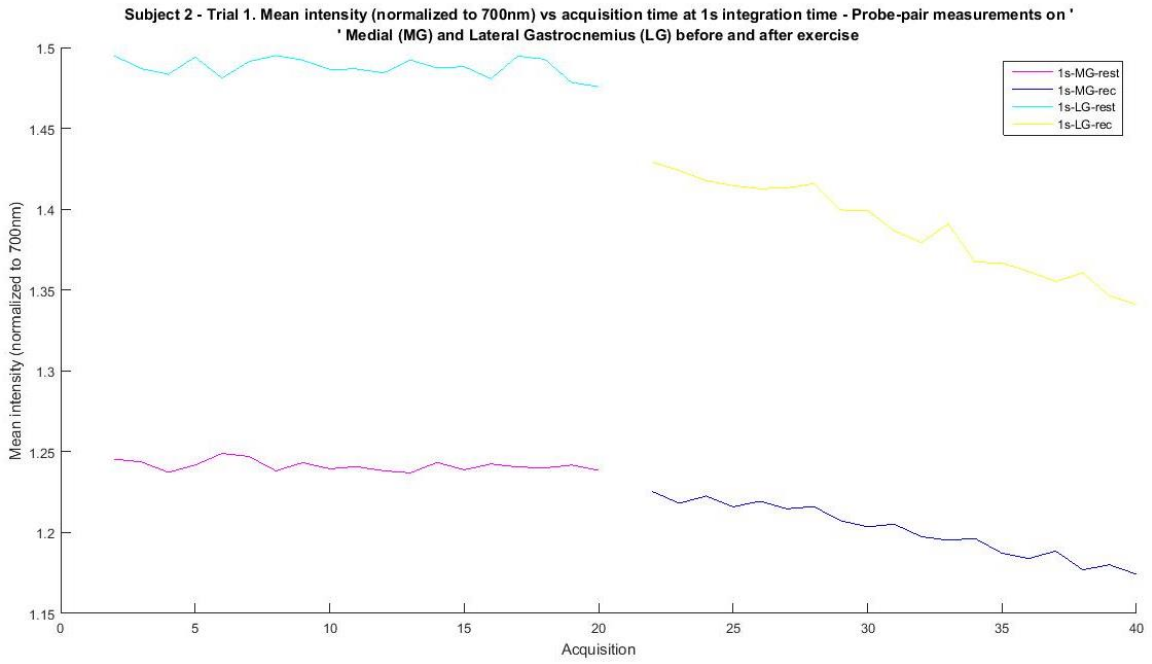

Figure 46. Mean pixel intensity (total=20 images) vs. image acquisition order in the MG and LG at rest and in recovery condition (1s exposure time). Images were acquired every 8s. Overall, the spectral variation between the measurement conditions for both muscle groups ranges between 2-11%, across all wavelengths.

Results using a single measurement probes.

1. Subject #1.

Figure 47 and Figure 48 shows the mean intensity spectral measurements for the MG and LG at rest and in recovery condition. A decrease in the recovery condition

spectrum is apparent in these figures. Also, error bars are comparatively larger than previous experiments, which may be due a loosening of the probe contact during this trial (see Figure 35, Figure 36, Figure 41 and Figure 42).

Table 16 shows the relative mean pixel intensity changes at 750, 800, 808 and 850 nm between the recovery and the rest condition for the MG, whereas Table 17 shows the relative changes for the LG. Relative change values from the rest condition range are ~1 to 20% in magnitude between experimental conditions and exhibit an increase at the MG position for 800, 808 and 850 nm and a decrease at the LG position at all of the studied wavelengths.

Table 16. Normalized mean pixel intensity values (n=20) and relative magnitude changes from the rest condition for MG positions (Single-probe arrangement).

Wavelength [nm]	Rest	Recovery	Relative change
750	0.94	0.96	0.02
800	1.38	1.12	-0.19
808	1.24	1.03	-0.17
850	1.32	1.06	-0.20

Table 17. Normalized mean pixel intensity values (n=20) and relative magnitude changes from the rest condition for LG positions (Single-probe arrangement).

Wavelength [nm]	Rest	Recovery	Relative change
750	0.88	0.87	-0.01
800	0.99	0.96	-0.03
808	0.96	0.94	-0.02
850	0.88	0.86	-0.02

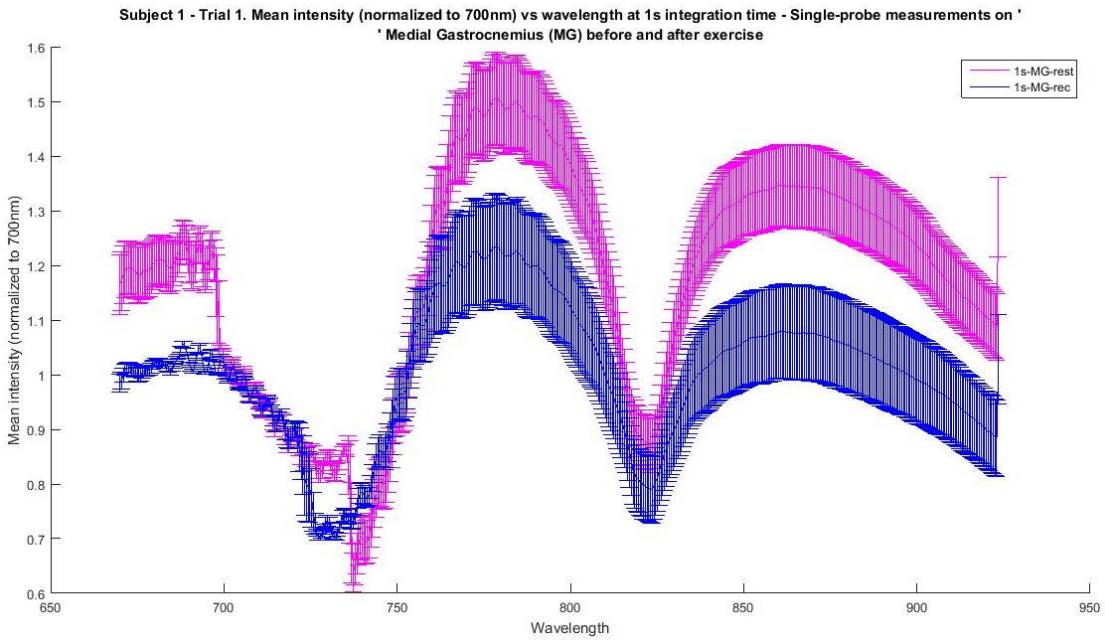

Figure 47. Mean pixel intensity (total=20 images) across wavelength (nm) for detectors located in the MG at rest and recovery conditions (1s exposure time). Measurements were done with a single probe (inter-fiber separation of 80 µm). A decrease in the recovery condition spectrum is apparent in these figures. Also, error bars are comparatively larger than previous experiments (see Figure 35, Figure 36, Figure 41 and Figure 42).

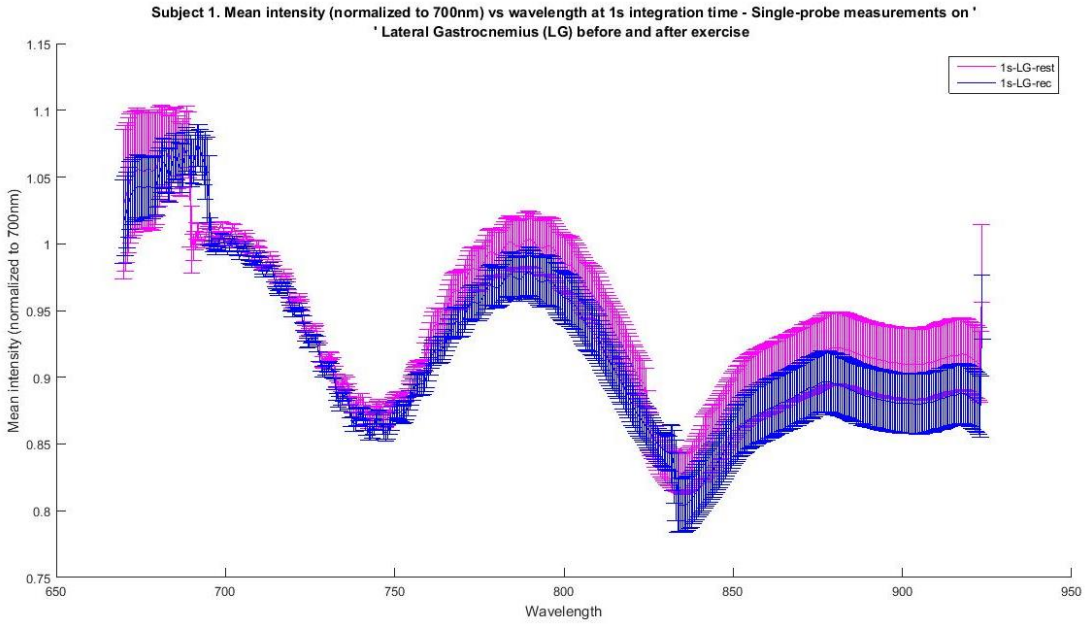

Figure 48. Mean pixel intensity (total=20 images) across wavelength (nm) for detectors located in the LG at rest and recovery conditions (1s exposure time). Measurements were done with a single probe (inter-fiber separation of 80 µm). A change in the overall recovery condition spectrum is apparent in this figure. Error bars are comparatively larger than previous experiments (see Figure 35, Figure 36, Figure 41 and Figure 42).

The normalized mean intensity spectrum measured on the diffuse reflectance standard is shown in Figure 37 for the two excitation probes. The normalization of the measurement and the standard spectra is shown in Figure 49 and Figure 50.

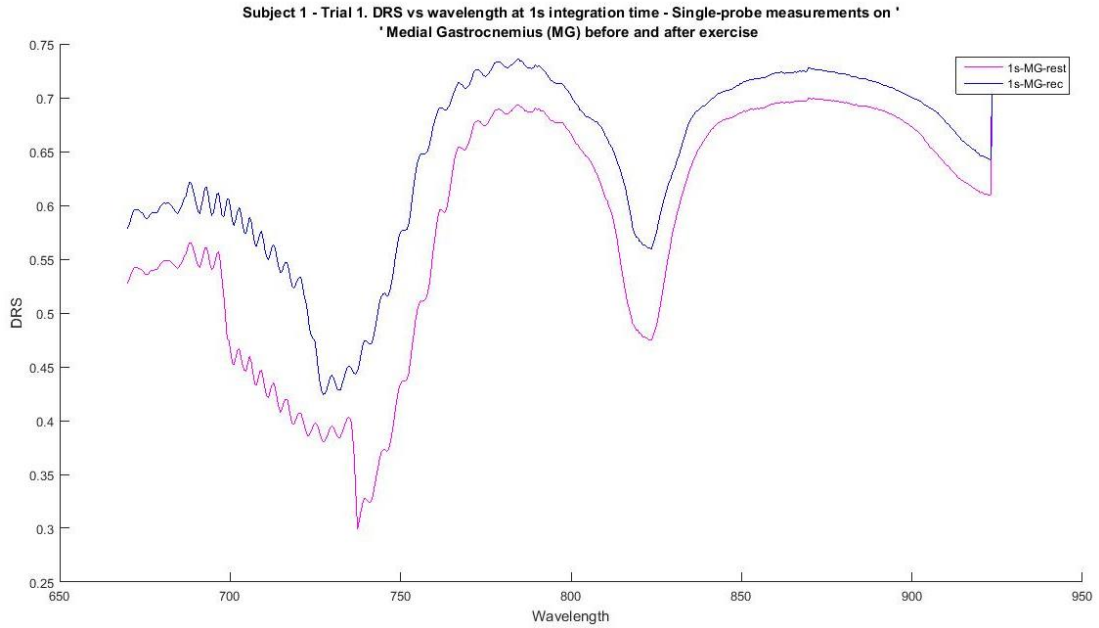

Figure 49. Reflectance signal across wavelength (nm) measured in the MG at rest and under recovery condition (1s exposure time). Measurements were done with a pair of probes (inter-fiber separation of 5 mm). Differences of several orders of magnitude were found when comparing these curves with the reflectance magnitudes measured in the previous experiment (see Figure 28, Figure 30, Figure 39, Figure 44 and Figure 45). This suggests the need to further improve and validate the measurements using the standard spectralon in order to calculate the reflectance values.

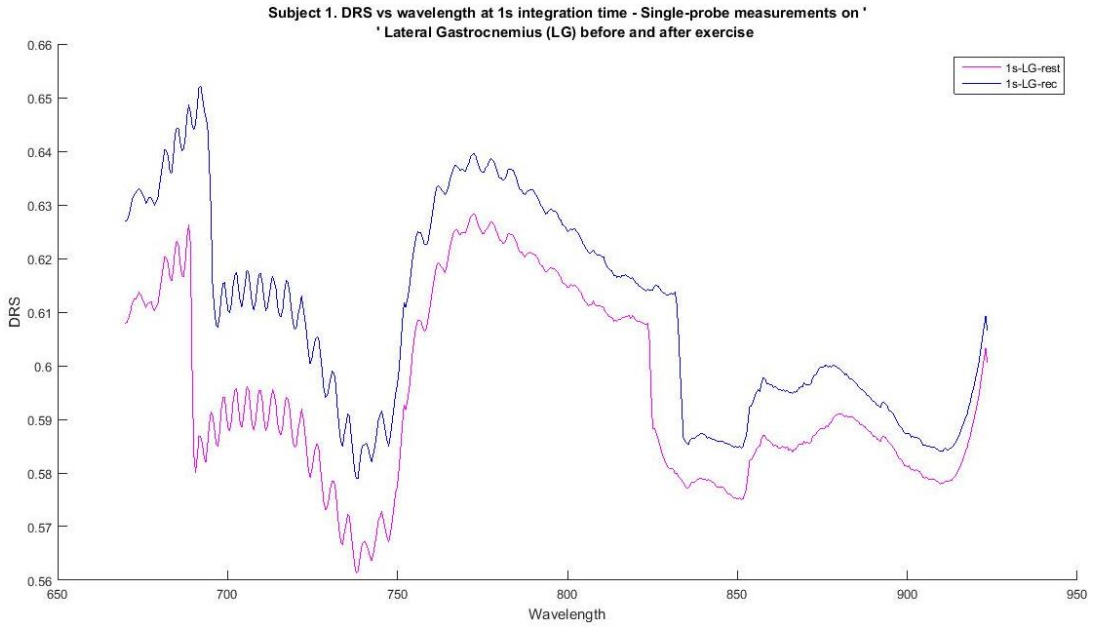

Figure 50. Reflectance signal across wavelength (nm) measured in the MG at rest and under recovery condition (1s exposure time). Measurements were done with a pair of probes (inter-fiber separation of 5 mm). As with Figure 49, differences of several orders of magnitude were found when comparing these curves with the reflectance magnitudes measured in the previous experiment (see Figure 28, Figure 30, Figure 39, Figure 44 and Figure 45). This suggests the need to further improve and validate the measurements using the standard spectralon in order to calculate the reflectance values.

A time-series depiction of the mean signal intensity across wavelength is shown for each acquisition taken on the MG and LG using a single probe (see Figure 51). The overall spectral variation between the measurement conditions for both muscle groups is 2-15% relative to the rest condition, across all wavelengths.

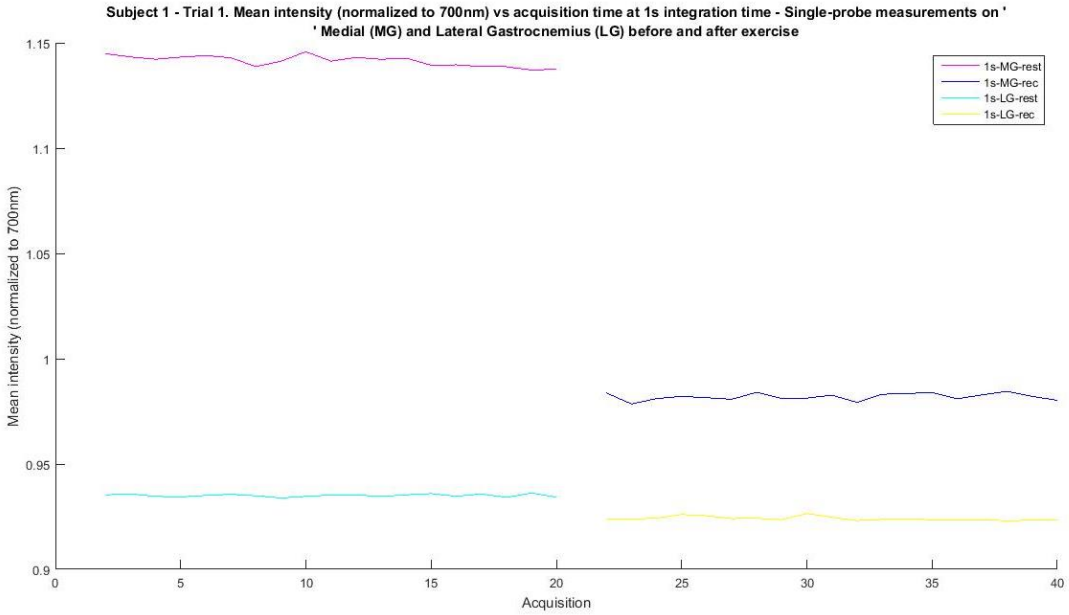

Figure 51. Mean pixel intensity (total=20 images) vs. image acquisition order in the MG and LG at rest and in recovery condition (1s exposure time). Images were acquired every 8s. Overall, the spectral variation between the measurement conditions for both muscle groups ranges between ~2-15%, across all wavelengths.

2. Subject #2

Figure 52 and Figure 53 shows the mean intensity spectral measurements for the MG and LG at rest and in recovery condition. A decrease in the recovery condition spectrum is apparent in these figures.

Table 18 shows the relative mean pixel intensity changes at 750, 800, 808 and 850 nm between the recovery and the rest condition for the MG, whereas Table 19 shows the relative changes for the LG. Relative change values from the rest

condition are ~0.1 to 3% in magnitude between experimental conditions and exhibit an increase at the MG position and a decrease at the LG position.

Table 18. Mean pixel intensity values (n=20) and relative magnitude changes from the rest and recovery conditions for MG positions (Single-probe arrangement).

Wavelength [nm]	Rest	Recovery	Relative change
750	0.91	0.91	0.00
800	0.87	0.86	-0.01
808	0.82	0.81	-0.01
850	0.79	0.77	-0.03

Table 19. Mean pixel intensity values (n=20) and relative magnitude changes from the rest and recovery conditions for LG positions (Single-probe arrangement).

Wavelength [nm]	Rest	Recovery	Relative change
750	1.02	1.01	-0.01
800	1.06	1.05	-0.01
808	1.06	1.05	-0.01
850	1.08	1.06	-0.02

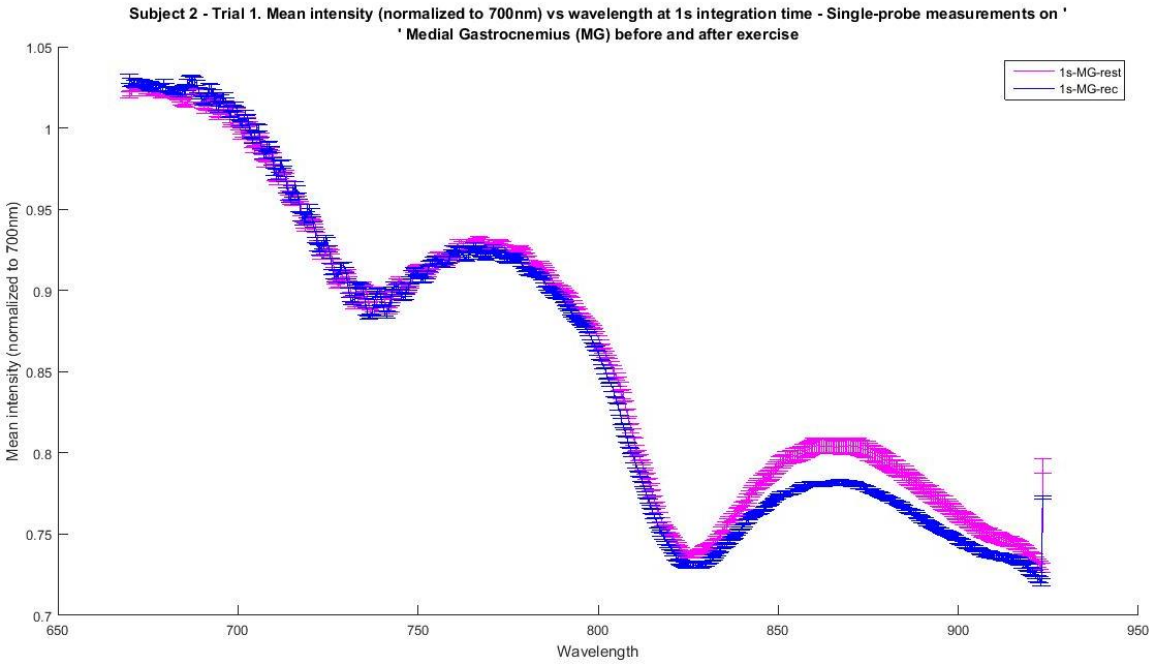

Figure 52. Mean pixel intensity (total=20 images) across wavelength (nm) for detectors located in the MG at rest and recovery conditions (1s exposure time). Measurements were done with a single probe (inter-fiber separation of 80 µm). Decrease in the recovery condition spectrum is apparent in this figure.

The normalized mean intensity spectrum measured on the diffuse reflectance standard is shown in Figure 43 for the two excitation probes. The normalization of the measurement and standard spectra provided values with magnitudes greater than 1, which suggests low level signal detection due to fiber rotation over the spectralon's surface (not shown). Changes in the reflectance data between the rest and the recovery condition show deviations in the same order of magnitude as for the mean spectral intensity.

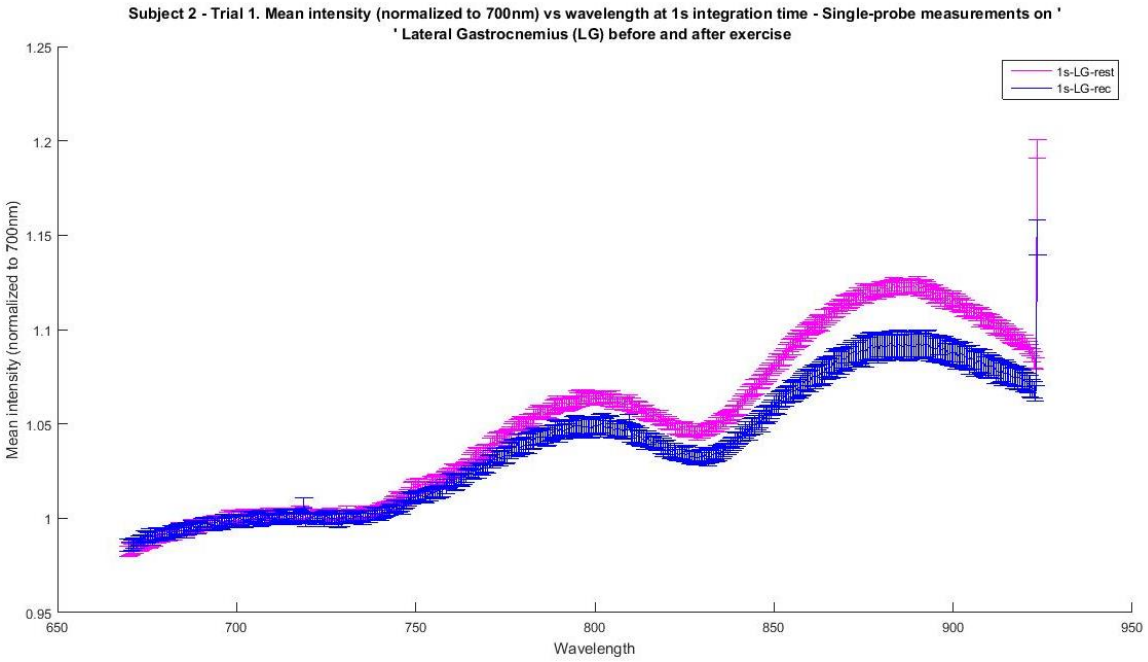

Figure 53. Measurements were done with a single probe (inter-fiber separation of 80 µm). Decrease in the recovery condition spectrum is apparent in this figure. An increasing trend with increasing wavelength was found for the LG, which opposes the general decreasing trend found in the previous results, e.g. in Figure 52.

The time-series depiction of the mean signal intensity across wavelength is shown for each acquisition taken on the MG and LG using a single probe (see Figure 54). The overall spectral variation between the measurement conditions for both muscle groups is only 0.1-2% relative to the rest condition, across all wavelengths.

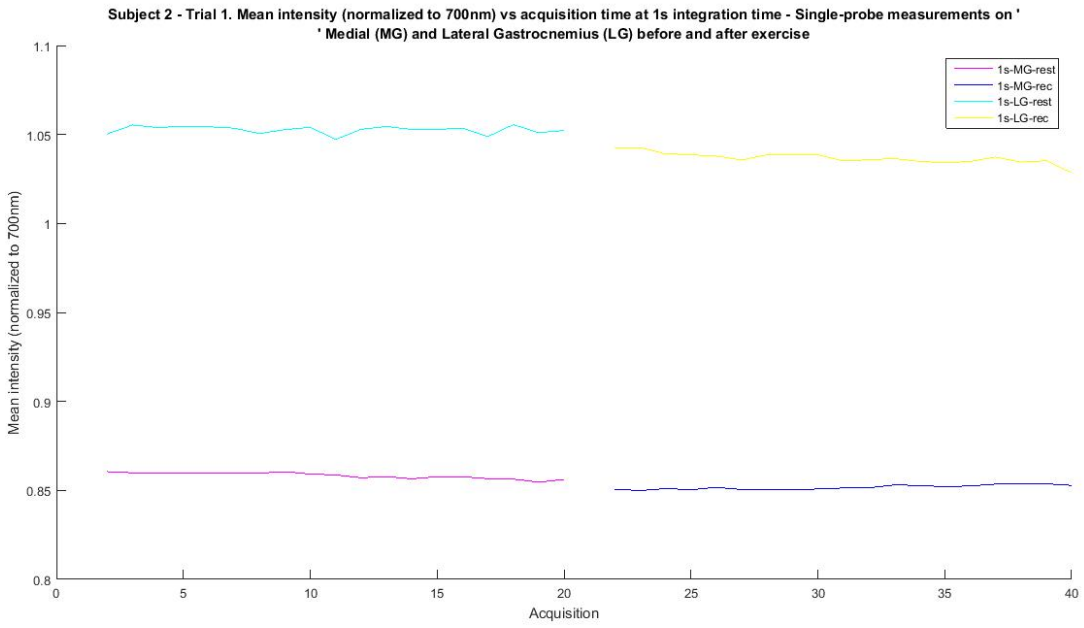

Figure 54. Mean pixel intensity (total=20 images) vs. image acquisition order in the MG and LG at rest and in recovery condition (1s exposure time). Images were acquired every 8s. Overall, the spectral variation between the measurement conditions for both muscle groups ranges between ~0.1-2%, across all wavelengths.

BOLD-fMRI analysis

In the following lines, a summary of the approach and results to study the fMRI time series is presented. As mentioned above, the study protocol consisted of 2 minutes of rest, 1 minute of exercise and 3 minutes of recovery. SPM12 (Statistical Parametric Mapping, FIL Methods group, http://www.fil.ion.ucl.ac.uk/spm/software/spm12/) was used for data analysis (compiled using the MATLAB Compiler).

After converting the anatomical and functional volumes from DICOM to NIfTI formats, slice timing correction and realignment routines were applied to the functional volumes, considering the imaging parameters mentioned at the beginning of this chapter. In a summary of the SPM output for motion correction is shown in Figure 55.

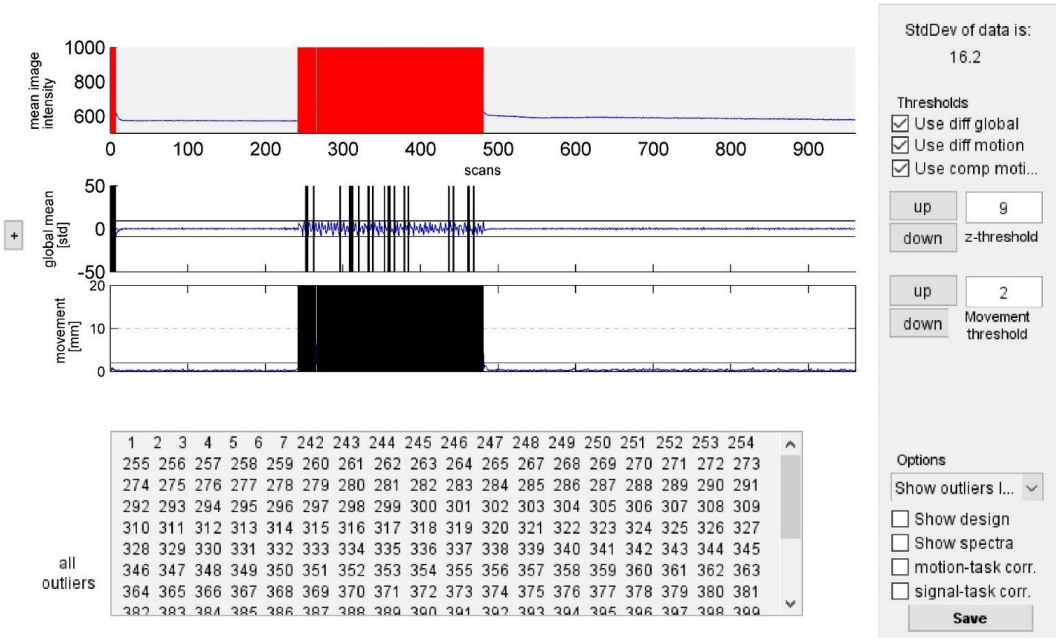

Figure 55. Results from motion correction routine using SPM12 (FIL Methods group). The study timing consisted of 2 minutes of rest, 1 minute of exercise and 3 minutes of recovery. A higher amount of motion can be observed during scans 250 to 450, which corresponds to the exercise period (volumes). Rest and recovery intervals show a slight-controlled motion. Most outlier correspond to the exercise section of the study.

Following motion correction, a first-level analysis was done by defining a canonical hemodynamic response function for parameter estimation. Figure 56 shows the contrasts computed from the parameter estimates.

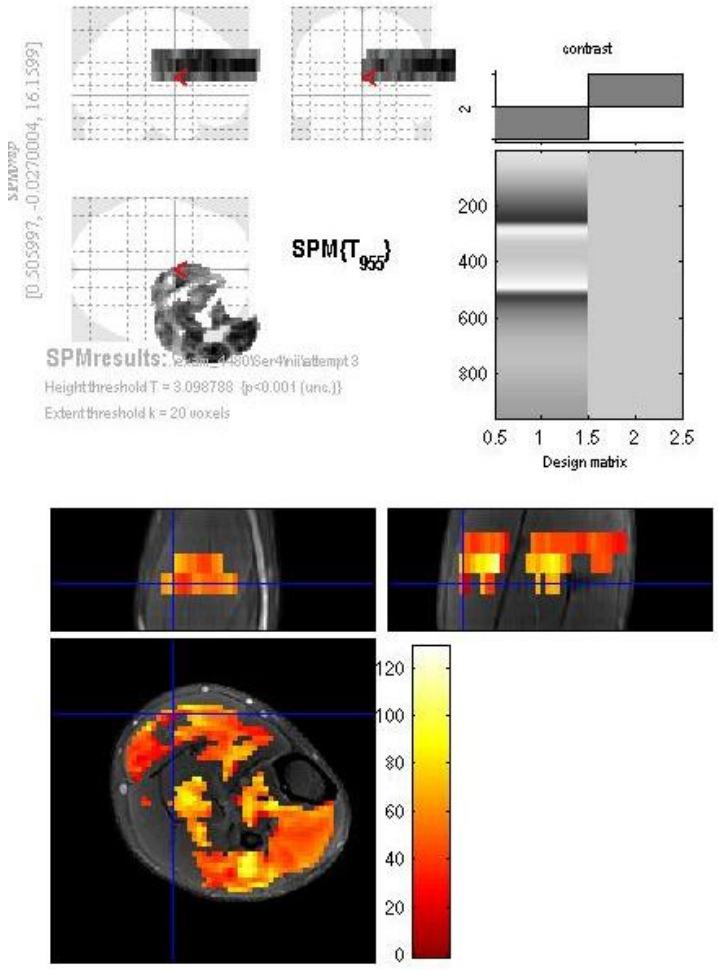

Figure 56. Contrasts generated from a first-level analysis for parameter estimation (B-estimates) using SPM12. A baseline intensity was compared with the BOLD signal intensity along the volumes (study time).

Subsequently, manual ROI determination was done by approximating a sphere along the MG and LG muscles locations (see Figure 57). Functional volumes along the ROI were selected for further analysis.

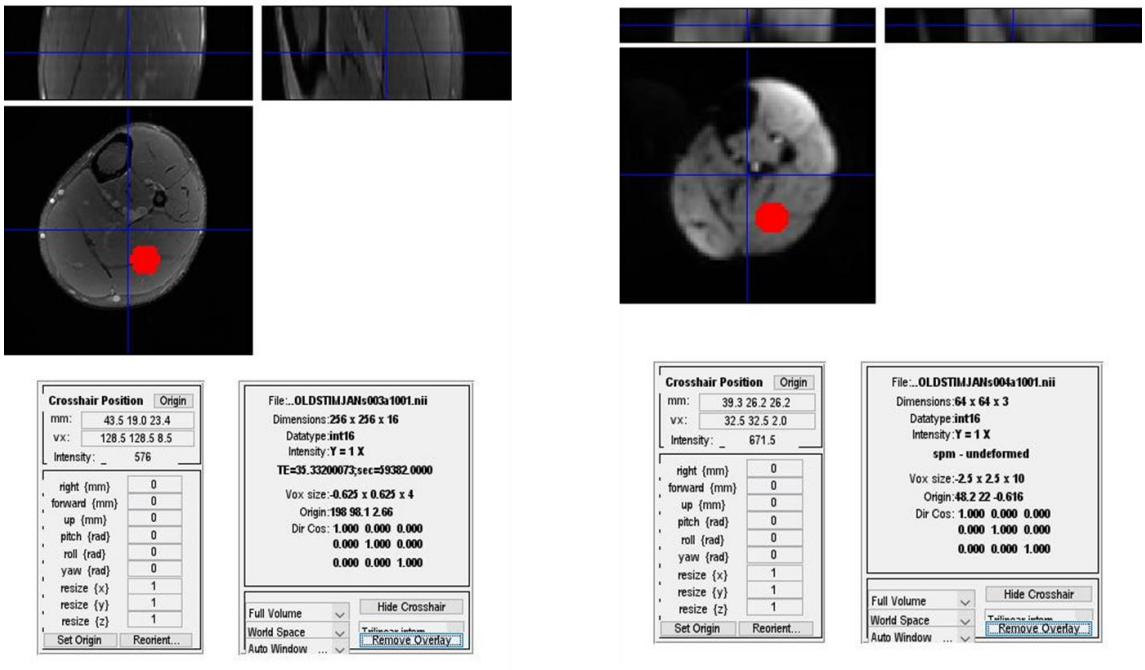

Figure 57. Manual ROI determination using SPM12. A red sphere was drawn near the deep muscles, including LG and soleus muscle. The figure on the left shows the ROI over the anatomical image, and figure on the right shows the ROI for the functional data (medium slice #3).

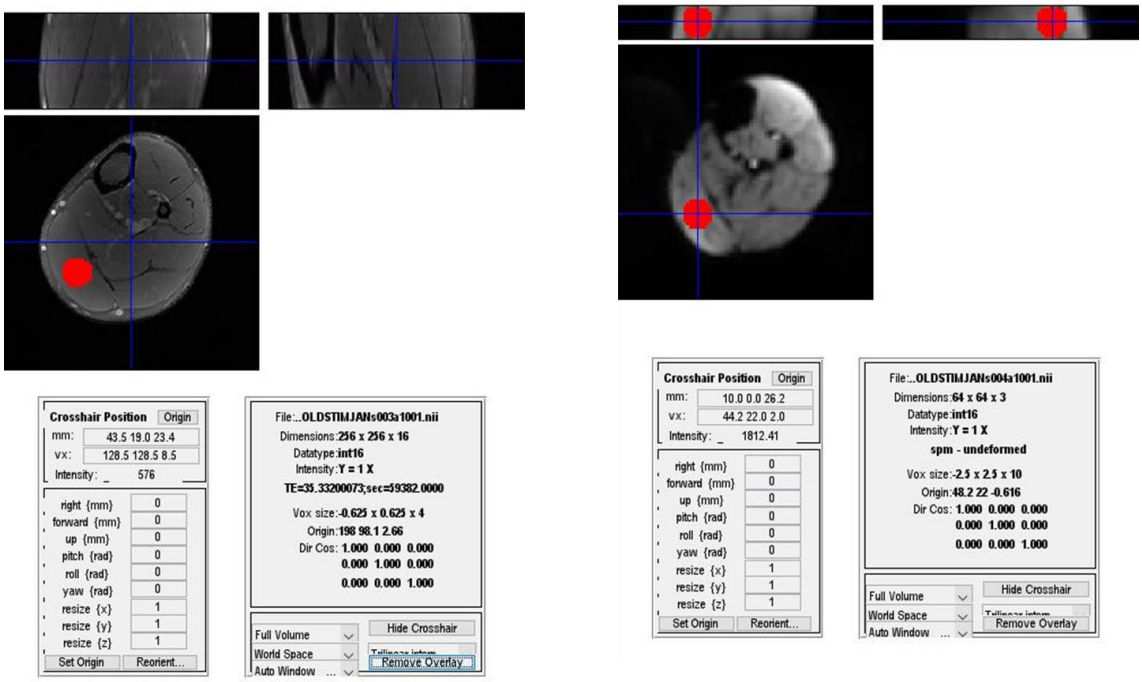

Figure 58. Manual ROI determination using SPM12. A red sphere was drawn near the deep MG. The figure on the left shows the ROI over the anatomical image, and figure on the right shows the ROI for the functional data (medium slice #3).

Finally, a plot of the parameter estimates (B-estimates) for the defined ROIs are presented in Figure 59 and Figure 60. According to the results, an increased intensity can be seen during recovery (after volume #500) compared to the rest period (first 200 volumes). For the ROI near the MG and soleus muscle, no signal increase was found during recovery (after volume #500) compared to the rest period (first 200 volumes).

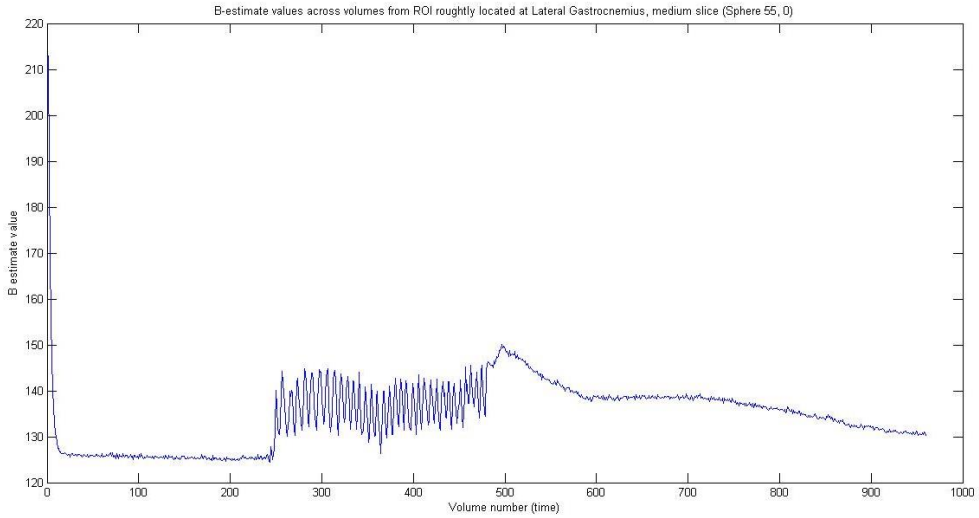

Figure 59. Plot of the parameter estimates (B-estimates) for the defined ROI near the LG. An increased magnitude can be seen during recovery (after volume #500) compared to the rest period (first 200 volumes).

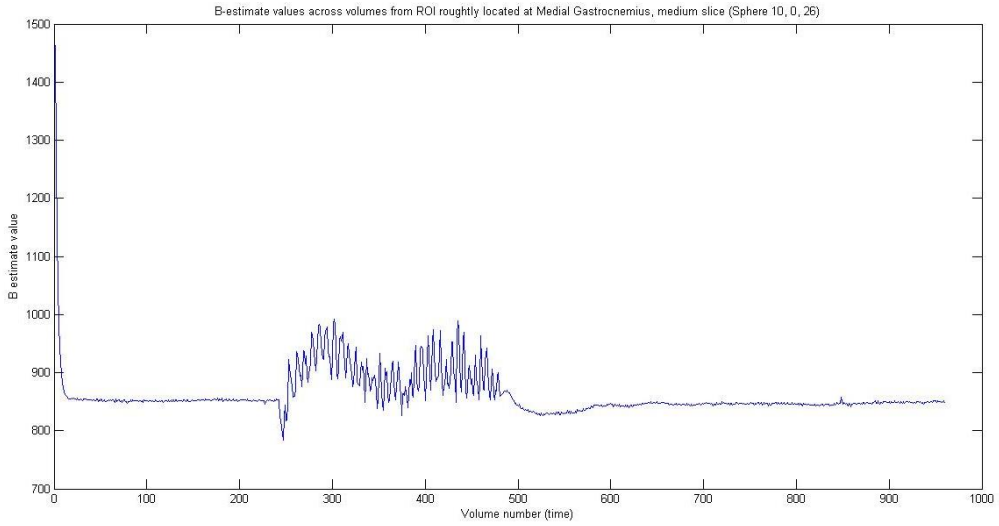

Figure 60. Plot of the parameter estimates (B-estimates) for the defined ROI near the MG and soleus muscle. In this case, no signal increase was found during recovery (after volume #500) compared to the rest period (first 200 volumes).

Discussion

Based on the results, a decrease for the mean signal intensity for the recovery condition (between ~0.1-20%) was found in three of four experimental trials of with reference to the rest condition at both muscle locations and probe configurations (for 800,808 and 850 nm). In general, this reduced intensity may be due to an increase in skin blood flow in the measurement sites after exercise. Nevertheless, further analysis need to be done to calculate concentration changes HbR and HbO_2. Regarding probe configuration, the probe-pair arrangement (5 mm inter-fiber separation) for subject 1 showed no relative differences, which suggests that further studies are necessary to identify that cause. Regarding the time-series analysis, a higher time resolution is necessary for the DOS system to better describe the progression of the recovery signals. Also, the time-series need to be analyzed for the wavelengths of interest. On the other hand, the BOLD signal measured in the LG after exercise showed a relatively increased magnitude level compared to the intensity for the rest condition. This may be due to an increase in blood flow after exercise for this muscle, which may correlate with the reduced signal intensity found with concurrent dermal DOS at the recovery condition, as found in [7],[32]. Nevertheless, further experiments and improvements need to be done to investigate the correlation between both techniques using this system. Also, the BOLD fMRI curves in the LG showed a hypointense signal after exercise, followed by sigmoidal-shaped signal recovery towards the baseline level. This trend was not found for the ROI located near the MG and soleus muscle, which

may be due to the inclusion of deeper muscle fibers in this ROI, showing the importance of the ROI determination process on the results.

Further validation needs to be done to compare the signal variations for different probe configurations and across the different optodes of the system. Regarding oximetry assessment capabilities, it is necessary to improve the fiber contact with the spectralon standard for repeatable reflectance calculations. Concurrent pulse-oxymetry measurements would be helpful to find correlates with DOS and fMRI at the skin and muscle levels. That way, concentration changes of Hb and HbO_2 in skin could be extracted and correlated with the BOLD signal progression.

Chapter 6. Conclusion

The experiments described along this project showed that the DOS system is capable to measure concurrent spectral-fMRI signals and to detect changes in the mean intensity spectral signals measured before and after exercise with this system. Subsequent validations and optimizations are necessary to evaluate the oxygenation assessment capabilities of this system.

Some challenges of using this system for DOS measurements rely on the following:

- Reduced optical core diameter: The optical fibers of this system have a diameter of 58 µm, which is relatively small compared to other systems to deliver and detect enough signal [17], [26].
- Variability of the pixel range determination for the channels: The pixel ranges relied on a manual ROI determination process. A comparable pixel intensity to the calibration data should be then maintained and verified for the experiments. Otherwise, a calibration should be done to determine the pixel range of each fiber of interest.
- Time resolution: Currently, data from full-CCD exposure is transferred at each acquisition. Therefore, it should be advantageous to incorporate a camera with hardware binning capabilities.

Future steps include increased optical power delivery, enhanced skin contact and fiber positioning, improved reflectance measurements, standardization of the exercise protocol and validation using suitable oximetry measurements.

List of References

[1] M. D. Noseworthy, D. P. Bulte, and J. Alfonsi, “BOLD magnetic resonance imaging of skeletal muscle.,” *Semin. Musculoskelet. Radiol.*, vol. 7, no. 4, pp. 307–315, 2003.

[2] M. D. Noseworthy, A. D. Davis, and A. H. Elzibak, “Advanced MR imaging techniques for skeletal muscle evaluation,” *Semin. Musculoskelet. Radiol.*, vol. 14, no. 2, pp. 257–268, 2010.

[3] a P. Gibson, J. C. Hebden, and S. R. Arridge, “Recent advances in diffuse optical imaging.,” *Phys. Med. Biol.*, vol. 50, no. 4, pp. R1–R43, 2005.

[4] H. Dehghani, S. Srinivasan, B. W. Pogue, and A. Gibson, “Numerical modelling and image reconstruction in diffuse optical tomography.,” *Philos. Trans. A. Math. Phys. Eng. Sci.*, vol. 367, no. 1900, pp. 3073–3093, 2009.

[5] S. R. Arridge, “Optical tomography in medical imaging,” *Inverse Probl.*, vol. 15, no. 2, pp. R41–R93, 1999.

[6] 22 Lloyd-Fox. (2010). Illuminating the developing brain: The past, present and future of functional near infrared spectroscopy. Neuroscience and Biobehavioral Reviews., vol. 34, issue 3, 269-284.

[7] Shadgan, B., et. Al. (2009). Wireless near-infrared spectroscopy of skeletal muscle oxygenation and hemodynamics during exercise and ischemia. Spectroscopy 23 (2009) 233–241 233. DOI 10.3233/SPE-2009-0391. IOS Press.

[8] Kek, K., et. Al. (2005). Imaging of Regional Differences of Muscle Oxygenation during Exercise Using Spatially Resolved NIRS. Proceedings of the 2005 IEEE. Engineering in Medicine and Biology 27th Annual Conference. Shanghai, China, September 1-4, 2005

[9] Zhongxing Zhang, et. al. (2010). Comparisons of muscle oxygenation changes between arm and leg muscles during incremental rowing exercise with near-infrared spectroscopy. Journal of Biomedical Optics 151, 017007. January/February 2010.

[10] Koga, S., et. al. (2007). Spatial heterogeneity of quadriceps muscle deoxygenation kinetics during cycle exercise. J Appl Physiol 103: 2049–2056, 2007. First published September 20, 2007; doi:10.1152/japplphysiol.00627.2007.

[11] a Siegel, J. J. Marota, and D. Boas, “Design and evaluation of a continuous-wave diffuse optical tomography system.,” Opt. Express, vol. 4, no. 8, pp. 287–298, 1999.

[12] M. a. Khalil, H. K. Kim, I.-K. Kim, M. Flexman, R. Dayal, G. Shrikhande, and A. H. Hielscher, “Dynamic diffuse optical tomography imaging of

peripheral arterial disease," Biomed. Opt. Express, vol. 3, no. 9, p. 2288, 2012.

[13] M. a. Khalil, J. Hoi, H. K. Kim, and a. H. Hielscher, "Dynamic contact-free continuous-wave diffuse optical tomography system for the detection of vascular dynamics within the foot," SPIE BiOS, vol. 8578, p. 85781H–85781H–7, 2013.

[14] H.-P. Ledermann, A.-C. Schulte, H.-G. Heidecker, M. Aschwanden, K. a Jäger, K. Scheffler, W. Steinbrich, and D. Bilecen, "Blood oxygenation level-dependent magnetic resonance imaging of the skeletal muscle in patients with peripheral arterial occlusive disease.," Circulation, vol. 113, no. 25, pp. 2929–2935, 2006.

[15] H. Hielscher, "Optical tomographic imaging of small animals," Curr. Opin. Biotechnol., vol. 16, no. 1 SPEC. ISS., pp. 79–88, 2005.

[16] H. Jiang, Diffuse Optical Tomography: Principles and applications, vol. 4242. 2001.

[17] Delpy, D. & Cope, M. (1997). Quantifcation in tissue near-infrared spectroscopy. Phil. Trans. R. Soc. Lond. B (1997) 352, 649±659 # 1997 The Royal Society.

[18] Damon, B., et. al. (2007). Dual Gradient-Echo MRI of Post-contraction Changes in Skeletal Muscle Blood Volume and Oxygenation. Magnetic Resonance in Medicine 57:670–679 (2007).

[19] D. a. Boas, D. H. Brooks, E. L. Miller, C. a. Dimarzio, M. Kilmer, R. J. Gaudette, and Q. Zhang, "Imaging the body with diffuse optical tomography," IEEE Signal Process. Mag., vol. 18, no. 6, pp. 57–75, 2001.

[20] InSeok, S., et. al. (2010). Simultaneous assessment of pulsating and total blood in inflammatory skin lesions using functional diffuse reflectance spectroscopy in the visible range. 2010 Society of Photo-Optical Instrumentation Engineers. [DOI: 10.1117/1.3524191]

[21] Prahl Scott (1999), Optical Absorption of Hemoglobin, Oregon Medical Laser Center, http://omlc.org/spectra/hemoglobin/

[22] Benaron, D., et. al. (2005). Design of a visible-light spectroscopy clinical tissue Oximeter. Journal of Biomedical Optics,044005, July/August 2005.

[23] Jakubowski, D., et. al. (2008). Chapter 13. Quantitative Absorption and Scattering Spectra in Thick Tissues Using Broadband Diffuse Optical Spectroscopy. Retrieved on Dec, 2016 from https://www.researchgate.net/publication/254102192

[24] Delpy, D. & Cope, M. (1997). Quantification in tissue near-infrared spectroscopy. Phil. Trans. R. Soc. Lond. B (1997) 352, 649±659 # 1997 The Royal Society.

[25] Shadgan, B., et. Al. (2009). Wireless near-infrared spectroscopy of skeletal muscle oxygenation and hemodynamics during exercise and

ischemia. Spectroscopy 23 (2009) 233–241 233. DOI 10.3233/SPE-2009-0391. IOS Press.

[26] Kek, K., et. Al. (2005). Imaging of Regional Differences of Muscle Oxygenation during Exercise Using Spatially Resolved NIRS. Proceedings of the 2005 IEEE. Engineering in Medicine and Biology 27th Annual Conference. Shanghai, China, September 1-4, 2005

[27] Koga, S., et. al. (2007). Spatial heterogeneity of quadriceps muscle deoxygenation kinetics during cycle exercise. Appl Physiol 103: 2049–2056, 2007. First published September 20, 2007; doi:10.1152/japplphysiol.00627.2007.

[28] Zhang, Z., et. al. (2010). Comparisons of muscle oxygenation changes between arm and leg muscles during incremental rowing exercise with near-infrared spectroscopy. Journal of Biomedical Optics, 017007. January/February 2010.

[29] V. a. Carr, J. Rissman, and A. D. Wagner, “Imaging the Human Medial Temporal Lobe with High-Resolution fMRI,” Neuron, vol. 65, no. 3, pp. 298–308, 2010.

[30] S. Partovi, H. von Tengg-Kobligk, N. Bhojwani, C. Karmonik, M. Maurer, and M. R. Robbin, “Advanced Noncontrast MR Imaging in Musculoskeletal Radiology,” Radiol. Clin. North Am., vol. 53, no. 3, pp. 549–567, 2015.

[31] P. M. Matthews and P. Jezzard, Functional magnetic resonance imaging., vol. 75, no. 1. 2004.

[32] Caterini, J., et. al. (2015). Characterizing blood oxygen level-dependent (BOLD) response following in-magnet quadriceps exercise. Magn Reson Mater Phy (2015) 28:271–278. DOI 10.1007/s10334-014-0461-4.

[33] R. a. Meyer, T. F. Towse, R. W. Reid, R. C. Jayaraman, R. W. Wiseman, and K. K. McCully, “BOLD MRI mapping of transient hyperemia in skeletal muscle after single contractions,” NMR Biomed., vol. 17, no. 6, pp. 392–398, 2004.

[34] T. F. Towse, J. M. Slade, and R. a Meyer, “Effect of physical activity on MRI-measured blood oxygen level-dependent transients in skeletal muscle after brief contractions.,” J. Appl. Physiol., vol. 99, no. 2, pp. 715–722, 2005.

[35] J. Damon, B., Hornberger, J., Wadington, M., Landsown, D. and Kent-Braun, “Dual Gradient-Echo MRI of Post-Contraction Changes in Skeletal Muscle Blood Volume and Oxygenation,” vol. 57, no. 4, pp. 670–679, 2015.

[36] Kumbhare, D., et. al. (2014). Advanced Skeletal Muscle MR Imaging Approaches in the Assessment of Muscular Dystrophies.Kumbhare et al., Int J Phys Med Rehabil 2014, 2:6

[37] Towse, T., et. al. (2011). Quantitative analysis of the postcontractile blood-oxygenation-level-dependent (BOLD) effect in skeletal muscle. J Appl Physiol

111: 27–39, 2011. First published February 17, 2011; doi:10.1152/japplphysiol.01054.2009.

[38] M. D. Noseworthy, A. D. Davis, and A. H. Elzibak, “Advanced MR imaging techniques for skeletal muscle evaluation,” Semin. Musculoskelet. Radiol., vol. 14, no. 2, pp. 257–268, 2010.

[39] M. M. Plichta, S. Heinzel, a. C. Ehlis, P. Pauli, and a. J. Fallgatter, “Model-based analysis of rapid event-related functional near-infrared spectroscopy (NIRS) data: A parametric validation study,” Neuroimage, vol. 35, no. 2, pp. 625–634, 2007.

[40] T. Eggebrecht, S. L. Ferradal, A. Robichaux-Viehoever, M. S. Hassanpour, H. Dehghani, A. Z. Snyder, T. Hershey, and J. P. Culver, “Mapping distributed brain function and networks with diffuse optical tomography,” Nat. Photonics, vol. 8, no. 6, pp. 448–454, 2014.

[41] T. F. Towse, J. M. Slade, and R. a Meyer, “Effect of physical activity on MRI-measured blood oxygen level-dependent transients in skeletal muscle after brief contractions.,” J. Appl. Physiol., vol. 99, no. 2, pp. 715–722, 2005.

[42] D. a. Boas, A. M. Dale, and M. A. Franceschini, “Diffuse optical imaging of brain activation: Approaches to optimizing image sensitivity, resolution, and accuracy,” Neuroimage, vol. 23, no. SUPPL. 1, 2004. disease,” Biomed. Opt. Express, vol. 3, no. 9, p. 2288, 2012.

[43] S. K. Biswas, R. Kanhirodan, R. M. Vasu, and E. T. Al, “Models and Algorithms for Diffuse Optical Tomographic System,” vol. 2013, no. December, pp. 489–496, 2013.

[44] M. a. Yücel, T. J. Huppert, D. a. Boas, and L. Gagnon, “Calibrating the BOLD signal during a motor task using an extended fusion model incorporating DOT, BOLD and ASL data,” Neuroimage, vol. 61, no. 4, pp. 1268–1276, 2012.

[45] D. Huppert, Theodore J., diamond, Solomon, Boas, “Direct estimation of evoked hemoglobin changes by multimodality fusion imaging,” Changes, vol. 29, no. 6, pp. 997–1003, 2012.

[46] Darmouth University. Optics in Medicine. Retrieved on Dec, 2016 from the web: http://sites.dartmouth.edu/optmed/research-projects/)

[47] Mastanduno, M. (2013). COMBINED MRI AND NEAR-INFRARED SPECTROSCOPY FOR INCREASED SPECIFICITY OF BREAST CANCER IMAGING. PhD. Thesis. Dartmouth College. Hanover, New Hampshire

[48] Ghussein, F. (2014). Design of a magnetic field compatible, high-performance optical breast imaging system for MRI-guided optical spectroscopy. PhD. Thesis. Dartmouth College. Hanover, New Hampshire

[49] Zhiqui, Li. (2011). HIGH-SPEED MRI-GUIDED NEAR-INFRARED TOMOGRAPHY SYSTEM TO MONITOR BREAST HEMODYNAMICS IN VIVO. PhD. Thesis. Dartmouth College. Hanover, New Hampshire

[50] University College London (UCL). Optical and Multimodal Imaging. Retrieved on Dec, 2016 from the web: http://www.ucl.ac.uk/medphys/research/borl/imaging.

Appendices

Appendix 1: Channel calibration database for the DOS system.

Optode Number	Pixel range
1	56 74;
2	84 110;
3	102 124;
4	125 156;
5	144 166;
6	180 202;
7	194 216;
8	208 221;
9	213 226;
10	217 244;
11	227 253;
12	245 272;
13	259 285;
14	268 299;
15	291 322;
16	309 331;
17	319 345;
18	332 359;
19	351 368;
20	365 376;
21	374 396;
22	383 405;
23	392 419;
24	406 433;
25	415 446;
26	429 465;
27	447 474;
28	466 472
29	470 497;
30	484 506;
31	498 515;
32	516 534;
33	521 552;

34	535 561;
35	544 571;
36	564 575;
37	572 598;
38	581 607;
39	694 617;
40	608 635;
41	664 686;
42	632 658;
43	645 672;
44	659 681;
45	673 700;
46	687 709;
47	701 723;
48	710 736;
49	724 746;
50	737 759;
51	751 778;
52	765 787;
53	784 796;
54	788 815;
55	808 819;
56	816 838;
57	833 847;
58	844 861;
59	852 870;
60	866 884;
61	875 902;
62	889 911;
63	908 925;
64	919 939;
65	933 950;
66	947 964;
67	961 974
68	972 992;
69	982 999;
70	1000 1017;
71	1014 1031;
72	1025 1045;

73	1039 1056;
74	1046 1067;
75	1060 1081;
76	1075 1091;
77	1089 1105;
78	1099 1116;
79	1114 1130;
80	1010 1013;
81	1138 1159;
82	1130 1139;
83	1163 1177;
84	1174 1191;
85	1193 1210;
86	1206 1226;
87	1226 1239;
88	1234 1251;
89	1248 1265;
90	1262 1273;
91	1290 1297;
92	1287 1297;
93	1300 1314;
94	1316 1336;
95	1329 1344;
96	1341 1357;
97	1355 1370;
98	1365 1385;
99	1379 1396;
100	1390 1407;
101	1404 1424;
102	1418 1435;
103	1429 1446;
104	1443 1463;
105	1454 1474;
106	1468 1485;
107	1479 1499;
108	1489 1506;
109	1507 1524;
110	1514 1538;
111	1525 1548;

	112	1542 1559;
	113	1549 1570;
	114	1564 1580;
	115	1574 1594;
	116	1588 1605;
	117	1642 1662;
	118	1613 1630;
	119	1627 1641;
	120	1645 1662;
	121	1652 1672;
	122	1670 1687;
	123	1698 1715;
	124	1716 1736;
	125	1737 1757;
	126	1751 1772;
	127	1762 1786;
	128	1776 1793;
	129	1790 1804;
	130	1805 1825;
	131	1812 1832;
	132	1822 1839;
	133	1836 1850;
	134	1840 1860;
	135	1858 1874;
	136	1868 1889;
	137	1881 1901;
	138	1893 1913;
	139	1914 1920;
	140	1914 1931;
	141	1932 1949;
	142	1943 1959;
	143	1953 1977;
	144	1964 1988;

Appendix 2. Matlab code routines for spectral analysis

Main file

```
fclose('all')

close all

amount_fibers=2;

amount_sources=0;

%source_positions=[12];

background=1;

background_s=1;

fiber_numbers=  [139 53]; % to be manually determined

lightning_conditions=0;

images_per_condition=0;

spectralon_captions=20;

spectralon=1;

lightning_condition=0;

wave=1:508;

hp=668.93+0.504*wave-0.00000652*wave.^2+0.00000000194*wave.^3; %spectral
calibration curve


fclose('all')

close all


[CM,CE,SM,SEf]=fiber_horizontal_analysis(amount_fibers,  amount_sources,
source_positions,background,background_s,fiber_numbers,lightning_conditi
ons,images_per_condition,spectralon,spectralon_captions);
```

Function fiber_horizontal_analysis

```
function    [CM,CE,SM,SE,    f]=fiber_horizontal_analysis(amount_fibers,
amount_sources,                source_positions,background,background_s,
fiber_numbers,lightning_conditions,images_per_condition,spectralon,spect
ralon_captions)

i=0;
```

```
     for i=1:amount_sources
     fibers_channel(i,1:2)=[channels(i) channels(i+1)];
     sum_fibers_channel(i,1:channels(i)+channels(i+1)+1)=0;
     end


[CM,CE,SM,SE,DRS]=fiber_selection(fiber_numbers,images_per_condition,lig
htning_conditions,background,amount_fibers,source_positions);


 f=1:amount_fibers;
```

Function fiber_selection (Example for analysis of spectral data)

```
function
[CM,CE,SM,SE,DRS]=fiber_selection(fiber_numbers,images_per_condition,lig
htning_conditions,background,amount_fibers,source_positions)
wave=2:508;


hp=668.93+0.504*wave-0.00000652*wave.^2+0.00000000194*wave.^3;
t1=[2:20];
t2=[22:40];
im_s_62_MG_mean=0;
im_s_143_LG_mean=0;
channel_range;
 channel_ranges=ranges(fiber_numbers,:);


 for s=1:2 % number of subjects


for t=3:3 %integration times considered (1=250ms, 2=500ms, 3=1s)
     if background==1
     if t==1
  File_bkd=sprintf('Background_1.raw');
```

```
 bkd=fopen(File_bkd);
 sum_b=fread(bkd,[2048 508],'*uint16');
 fclose('all')
for b=5:20
 File_bkd=sprintf('Background_%d.raw',b);
 bkd=fopen(File_bkd);
 sum_b=sum_b+fread(bkd,[2048 508],'*uint16');
 fclose('all')
end
 bkd=sum_b/16;
  fclose('all')
    else

File_bkd=sprintf('Background_1.raw');
bkd=fopen(File_bkd);
sum_b=fread(bkd,[2048 508],'*uint16');
fclose('all')
for b=2:20
 File_bkd=sprintf('Background_%d.raw',b);
 bkd=fopen(File_bkd);
 sum_b=sum_b+fread(bkd,[2048 508],'*uint16');
 fclose('all')
end
 bkd=sum_b/20;
fclose('all')
end


end


 for g=1:20 % number of images acquired  if g==1
 im_rest = sprintf('Nov30_Rest_%d.raw',g); % files read as .raw
```

```
  im_rest= fopen(im_rest);
  im_rest = fread(im_rest,[2048 508],'*uint16');
  fclose('all')
  if background==1
  im=im_rest-bkd;
  im_rest_mean=im;
  end
  else
  im_rest = sprintf('Nov30_Rest_%d.raw',g);
  im_rest= fopen(im_rest);
  im_rest = fread(im_rest,[2048 508],'*uint16');
  fclose('all')
  if background==1
  im=im_rest-bkd;
  im_rest_mean=im_rest_mean+im;
  end

  end

if g==1
  im_rec = sprintf('Nov30_Rec_%d.raw',g);
  im_rec= fopen(im_rec);
  im_rec = fread(im_rec,[2048 508],'*uint16');
  fclose('all')
  if background==1
  im=im_rec-bkd;
  im_rec_mean=im;
  end
 else
  im_rec = sprintf('Nov30_Rec_%d.raw',g);
  im_rec= fopen(im_rec);
```

```
  im_rec = fread(im_rec,[2048 508],'*uint16');
  fclose('all')
  if background==1
  im=im_rec-bkd;
  im_rec_mean=im_rec_mean+im;
  end

 end

if g==1
  im_rest_2 = sprintf('Nov30_Rest_t2_%d.raw',g);
  im_rest_2= fopen(im_rest_2);
  im_rest_2 = fread(im_rest_2,[2048 508],'*uint16');
  fclose('all')
  if background==1
  im_2=im_rest_2-bkd;
  im_rest_mean_2=im_2;
  end
  else
  im_rest_2 = sprintf('Nov30_Rest_t2_%d.raw',g);
  im_rest_2= fopen(im_rest_2);
  im_rest_2 = fread(im_rest_2,[2048 508],'*uint16');
  fclose('all')
  if background==1
  im_2=im_rest_2-bkd;
  im_rest_mean_2=im_rest_mean_2+im_2;
  end
  end

 if g==1
  im_rec_2 = sprintf('Nov30_Rec_t2_%d.raw',g);
```

```
 im_rec_2= fopen(im_rec_2);
 im_rec_2 = fread(im_rec_2,[2048 508],'*uint16');
 fclose('all')
 if background==1
 im_2=im_rec_2-bkd;
 im_rec_mean_2=im_2;
 end
else
 im_rec_2 = sprintf('Nov30_Rec_t2_%d.raw',g);
 im_rec_2= fopen(im_rec_2);
 im_rec_2 = fread(im_rec_2,[2048 508],'*uint16');
 fclose('all')
 if background==1
 im_2=im_rec_2-bkd;
 im_rec_mean_2=im_rec_mean_2+im_2;
 end
 end

 im_s_62_MG = sprintf('Spc_1s_%d.raw',g);
 im_s_62_MG= fopen(im_s_62_MG);
 im_s_62_MG = fread(im_s_62_MG,[2048 508],'*uint16');
 fclose('all')

 if background==1
 im_s_62_MG=im_s_62_MG-bkd;
 im_s_62_MG_mean=im_s_62_MG_mean+im_s_62_MG;

 end
 fclose('all')
 im_s_143_LG = sprintf('Spc_1s_%d.raw',g);
 im_s_143_LG= fopen(im_s_143_LG);
```

```
  im_s_143_LG = fread(im_s_143_LG,[2048 508],'*uint16');
  fclose('all')

  if background==1
 im_s_143_LG=im_s_143_LG-bkd;
 im_s_143_LG_mean=im_s_143_LG_mean+im_s_143_LG;

  end
  fclose('all')
for c=1:2  % amount of fibers in the vector "fiber_numbers", defined in
the main function

    if c==1
    for w=2:508

eval(sprintf('mean_spectral_s_%d(g,c,w)=mean(im_s_62_MG([1904:1920],w));
', t));

eval(sprintf('std_spectral_s_%d(g,c,w)=std(double(im_s_62_MG([1904:1920]
,w)),1);', t));

    end
    else
    for w=2:508

eval(sprintf('mean_spectral_s_%d(g,c,w)=mean(im_s_143_LG([784:796],w));'
, t));

eval(sprintf('std_spectral_s_%d(g,c,w)=std(double(im_s_143_LG([784:796],
w)),1);', t));

 end
 end

  for w=2:508
```

```
eval(sprintf('mean_spectral_rest_%d(g,c,w)=mean(im_rest([channel_ranges(
c,1):channel_ranges(c,2)],w));', t));

eval(sprintf('mean_spectral_rec_%d(g,c,w)=mean(im_rec([channel_ranges(c,
1):channel_ranges(c,2)],w));', t));

eval(sprintf('std_spectral_rest_%d(g,c,w)=std(double(im_rest([channel_ra
nges(c,1):channel_ranges(c,2)],w)),1);', t));

eval(sprintf('std_spectral_rec_%d(g,c,w)=std(double(im_rec([channel_rang
es(c,1):channel_ranges(c,2)],w)),1);', t));

eval(sprintf('mean_spectral_rest_2_%d(g,c,w)=mean(im_rest_2([channel_ran
ges(c,1):channel_ranges(c,2)],w));', t));

eval(sprintf('mean_spectral_rec_2_%d(g,c,w)=mean(im_rec_2([channel_range
s(c,1):channel_ranges(c,2)],w));', t));

eval(sprintf('std_spectral_rest_2_%d(g,c,w)=std(double(im_rest_2([channe
l_ranges(c,1):channel_ranges(c,2)],w)),1);', t));

eval(sprintf('std_spectral_rec_2_%d(g,c,w)=std(double(im_rec_2([channel_
ranges(c,1):channel_ranges(c,2)],w)),1);', t));


  end
  end
  end


  im_s_62_MG_mean=im_s_62_MG_mean/20;
  im_s_143_LG_mean=im_s_143_LG_mean/20;
  im_rest_mean=im_rest_mean/20;
  im_rec_mean=im_rec_mean/20;


if t==3
    figure
    imagesc(im_s_62_MG_mean,[0 65535]);
    colormap(gray);
```

```
    ylabel('Y pixel')
    xlabel('X pixel')
    name = sprintf('Standard__Fiber62__mean__t%d',t);
    title(name);
    figure
    imagesc(im_s_143_LG_mean,[0 65535]);
    colormap(gray);
    ylabel('Y pixel')
    xlabel('X pixel')
    name = sprintf('Standard__Fiber143__mean__t%d',t);
    title(name);
   end
   end


for t=3:3
for c=1:2
for g=1:20
eval(sprintf('mean_spectral_rest_norm_%d(g,c,[2:508])=mean_spectral_rest
_%d(g,c,[2:508])./mean_spectral_rest_%d(g,c,62);', t,t,t));
eval(sprintf('mean_spectral_rec_norm_%d(g,c,[2:508])=mean_spectral_rec_%
d(g,c,[2:508])./mean_spectral_rec_%d(g,c,62);', t,t,t));
eval(sprintf('mean_spectral_s_norm_%d(g,c,[2:508])=mean_spectral_s_%d(g,
c,[2:508])./mean_spectral_s_%d(g,c,62);', t,t,t));
eval(sprintf('mean_spectral_rest_norm_2_%d(g,c,[2:508])=mean_spectral_re
st_2_%d(g,c,[2:508])./mean_spectral_rest_2_%d(g,c,62);', t,t,t));
eval(sprintf('mean_spectral_rec_norm_2_%d(g,c,[2:508])=mean_spectral_rec
_2_%d(g,c,[2:508])./mean_spectral_rec_2_%d(g,c,62);', t,t,t));
eval(sprintf('mean_spectral_s_norm_%d(g,c,[2:508])=mean_spectral_s_%d(g,
c,[2:508])./mean_spectral_s_%d(g,c,62);', t,t,t));


end
end
end
```

```
  for t=3:3
  for c=1:2


eval(sprintf('CM_rest_%d(s,c,:)=mean(mean_spectral_rest_%d(1:20,c,[2:508
]));', t,t));
eval(sprintf('CE_rest_%d(s,c,:)=std(mean_spectral_rest_%d(1:20,c,[2:508]
,1));', t,t));
eval(sprintf('CM_rec_%d(s,c,:)=mean(mean_spectral_rec_%d(1:20,c,[2:508])
);', t,t));
eval(sprintf('CE_rec_%d(s,c,:)=std(mean_spectral_rec_%d(1:20,c,[2:508]),
1);', t,t));
eval(sprintf('SM_%d(s,c,:)=mean(mean_spectral_s_%d(1:20,c,[2:508]));',
t,t));
 eval(sprintf('SE_%d(s,c,:)=std(mean_spectral_s_%d(1:20,c,[2:508]),1);',
t,t));


eval(sprintf('DRS_rest_%d(s,c,:)=CM_rest_%d(s,c,:)./SM_%d(s,c,:);',t,t,t
));
 eval(sprintf('DRS_rec_%d(s,c,:)=CM_rec_%d(s,c,:)./SM_%d(s,c,:);',
t,t,t));


eval(sprintf('CM_rest_2_%d(s,c,:)=mean(mean_spectral_rest_2_%d(1:20,c,[2
:508]));', t,t));


eval(sprintf('CE_rest_2_%d(s,c,:)=std(mean_spectral_rest_2_%d(1:20,c,[2:
508],1));', t,t));



eval(sprintf('CM_rec_2_%d(s,c,:)=mean(mean_spectral_rec_2_%d(1:20,c,[2:5
08]));', t,t));


eval(sprintf('CE_rec_2_%d(s,c,:)=std(mean_spectral_rec_2_%d(1:20,c,[2:50
8]),1);', t,t));


eval(sprintf('DRS_rest_2_%d(s,c,:)=CM_rest_2_%d(s,c,:)./SM_%d(s,c,:);',t
,t,t));
 eval(sprintf('DRS_rec_2_%d(s,c,:)=CM_rec_2_%d(s,c,:)./SM_%d(s,c,:);',
t,t,t));
```

```
  end
  end

  for t=3:3
  for c=1:2

eval(sprintf('CM_rest_norm_%d(s,c,:)=CM_rest_%d(s,c,:)./CM_rest_%d(s,c,62);', t,t,t));
eval(sprintf('CE_rest_norm_%d(s,c,:)=std(mean_spectral_rest_norm_%d(1:20,c,[2:508]),1);', t,t));

eval(sprintf('CM_rec_norm_%d(s,c,:)=CM_rec_%d(s,c,:)./CM_rec_%d(s,c,72);', t,t,t));
eval(sprintf('CE_rec_norm_%d(s,c,:)=std(mean_spectral_rec_norm_%d(1:20,c,[2:508]),1);', t,t));

 eval(sprintf('SM_norm_%d(s,c,:)=SM_%d(s,c,:)./SM_%d(s,c,62);', t,t,t));
eval(sprintf('SE_norm_%d(s,c,:)=std(mean_spectral_s_norm_%d(1:20,c,[2:508]),1);', t,t));

eval(sprintf('CM_rest_norm_2_%d(s,c,:)=CM_rest_2_%d(s,c,:)./CM_rest_2_%d(s,c,62);', t,t,t));
eval(sprintf('CE_rest_norm_2_%d(s,c,:)=std(mean_spectral_rest_norm_2_%d(1:20,c,[2:508]),1);', t,t));
eval(sprintf('CM_rec_norm_2_%d(s,c,:)=CM_rec_2_%d(s,c,:)./CM_rec_2_%d(s,c,72);', t,t,t));
eval(sprintf('CE_rec_norm_2_%d(s,c,:)=std(mean_spectral_rec_norm_2_%d(1:20,c,[2:508]),1);', t,t));

 eval(sprintf('SM_norm_%d(s,c,:)=SM_%d(s,c,:)./SM_%d(s,c,62);', t,t,t));
eval(sprintf('SE_norm_%d(s,c,:)=std(mean_spectral_s_norm_%d(1:20,c,[2:508]),1);', t,t));

  end
  end
```

```
 fig=figure('units','normalized','outerposition',[0 0 1 1])
 q=1;

for t=3:3
for c=1:1

% % colors is an 9 by 3 array of your custom colors.
colors =[ 1 0 1;
          0 1 1;
          1 0 0;
          0 1 0;
          0 0 1;
          1 1 0;
          0 0 0;
          0.4 0.6 0.7;
          0.2 0.8 0.3;
          1 0.5 1;
          1 0.5 0;
          0.4 0.1 0.9];

eval(sprintf('errorbar(hp,CM_rest_norm_%d(s,c,:),CE_rest_norm_%d(s,c,:),
''Color'',colors(%d,:))',t,t,q))
eval(sprintf('errorbar(hp,CM_rec_norm_%d(s,c,:),CE_rec_norm_%d(s,c,:),''
Color'',colors(%d+4,:))',t,t,q))
q=q+1;

end
   if t==3
        xlabel('Wavelength')
        ylabel('Mean intensity (normalized to 750nm)')
```

```
        tit=sprintf('Subject 2 - Trial 1. Mean intensity (normalized to
750nm) vs wavelength at different integration times - Single-probe
measurements on \n Medial Gastrocnemius (MG) before and after exercise
',s);

        title (tit);

         legend  ('250ms-MG-rest','250ms-MG-rec','500ms-MG-rest','500ms-
MG-rec','1s-MG-rest','1s-MG-rec')

    end

end

hold off


  fig=figure('units','normalized','outerposition',[0 0 1 1])

   hold on

   q=1;

for t=3:3

for c=1:1

eval(sprintf('errorbar(hp,CM_rest_norm_%d(s,c,:),CE_rest_norm_%d(s,c,:),
''Color'',colors(%d,:))',t,t,q))

eval(sprintf('errorbar(hp,CM_rec_norm_%d(s,c,:),CE_rec_norm_%d(s,c,:),''
Color'',colors(%d+4,:))',t,t,q))

q=q+1;

end

   if t==3

        xlabel('Wavelength')

        ylabel('Mean intensity (normalized to 700nm)')

        tit=sprintf('{{Subject 2 - Trial 1. Mean intensity (normalized to
700nm) vs wavelength at 1s integration time - Single-probe measurements
on ''\n'' Medial Gastrocnemius (MG) before and after exercise}}',s);

       % filename='{Intensity_W_SP_MG}';

        title ({tit});

         legend ('1s-MG-rest','1s-MG-rec')

    end

    end

hold off
```

```
  fig=figure('units','normalized','outerposition',[0 0 1 1])
   hold on
   q2=1;


for t=3:3
for c=2:2
eval(sprintf('errorbar(hp,CM_rest_norm_%d(s,c,:),CE_rest_norm_%d(s,c,:),
''Color'',colors(%d,:))',t,t,q2))
eval(sprintf('errorbar(hp,CM_rec_norm_%d(s,c,:),CE_rec_norm_%d(s,c,:),''
Color'',colors(%d+4,:))',t,t,q2))
q2=q2+1;


end
   if t==3
        xlabel('Wavelength')
        ylabel('Mean intensity (normalized to 700nm)')
        tit=sprintf('Subject 2 - Trial 1. Mean intensity (normalized to
700nm) vs wavelength at 1s integration time - Single-probe measurements
on ''\n'' Lateral Gastrocnemius (LG) before and after exercise ',s);


        %filename='{Intensity_W_SP_LG}';
        title ({tit});
         legend ('1s-LG-rest','1s-LG-rec')
    end
    end


hold off
```

---- Code for plotting additional figures is omitted.